January 2017

Mapping Groundwater Discharge Along Lake Margins Using Satellite And UAV Thermal Imagery

Kelsey A. Forward

MAPPING GROUNDWATER DISCHARGE ALONG LAKE MARGINS USING SATELLITE AND UAV THERMAL IMAGERY

by

Kelsey Ann Forward

Bachelor of Science, North Dakota State University, 2012

A Thesis

Submitted to the Graduate Faculty

of the

University of North Dakota

In partial fulfillment of the requirements

For the degree of

Master of Science Geology

Grand Forks, North Dakota

December

2017

This thesis, submitted by Kelsey A. Forward in partial fulfillment of the requirements for the Degree of Master of Science from the University of North Dakota, has been read by the Faculty Advisory Committee under whom the work has been done and is hereby approved.

Dr. Philip Gerla, Chairperson

Dr. Taufique Mahmood

Dr. Bradley Rundquist

This thesis is being submitted by the appointed advisory committee as having met all of the requirements of the School of Graduate Studies at the University of North Dakota and is hereby approved.

Grant McGimpsey

Dean of the School of Graduate Studies

November 29, 2017

Date

PERMISSION

Title Mapping Groundwater Discharge Along Lake Margins Using Satellite and UAV Thermal Imagery

Department Geology and Geological Engineering

Degree Master of Science

In presenting this thesis in partial fulfillment of the requirements for a graduate degree from the University of North Dakota, I agree that the library of this University shall make it freely available for inspection. I further agree that permission for extensive copying for scholarly purposes may be granted by the professor who supervised my thesis work or, in his absence, by the Chairperson of the department or the Dean of the School of Graduate Studies. It is understood that any copying or publication or other use of this thesis or part thereof for financial gain shall not be allowed without my written permission. It is also understood that due recognition shall be given to me and to the University of North Dakota in any scholarly use which may be made of any material in my thesis.

Kelsey Ann Forward
December 7, 2017

TABLE OF CONTENTS

LIST OF FIGURES viii

LIST OF TABLES x

ACKNOWLEDGMENTS xi

ABSTRACT xii

CHAPTER

I. INTRODUCTION 1

Research Objective 3

Background 4

Groundwater and Surface Water Connectivity 4

Littoral Zone Groundwater Seepage 5

Generating Groundwater Contribution Using Numerical Modeling and DEM 6

Heat as a Groundwater Tracer 6

Mapping Recharge and Discharge Using Remote Sensing 7

Research Contribution of this Study 8

II. METHODS 9
Study Site 9
Methodology 12
GIS Modeling 13
Thermal Infrared Remote Sensing 23
Ground Calibration 25
TIR Image Processing 27
Limitations and Assumptions 29
III. RESULTS 32
Empirical Modeling 32
Water Table Elevation Estimation 32
Cell-by-cell Groundwater Balance 35
Satellite Imagery 38
Locations of Interest 38
UAV Imagery 44
Locations of Interest 44
Ground Calibration 54
IV. DISCUSSION 56
Water Table Estimation and Darcy Flow Model 56

Satellite Imagery Analysis 57

UAV Imagery Analysis 58

Influencing Factors for All Thermal Imagery..... 60

Geologic factors 60

Hydrologic factors..... 60

Weather factors 61

Ecological factors 61

V. CONCLUSIONS AND RECOMMENDATIONS..... 62

APPENDICES 64

Appendix A 65

Data Collection

Appendix B 66

Water Table Interpolation

Appendix C 69

ASTER TIR Instrument Characteristics

Appendix D 70

ASTER TIR Processing

Appendix E 72

Historical Lake Water Levels

Appendix F 77

Ground Calibration Temperature Plots

Appendix G 84

Ground Calibration Thermistor Locations on UAV Imagery

REFERENCES 105

LIST OF FIGURES

Figure Page

1. Generalized conceptual groundwater flow diagram. 5
2. Study area location within Minnesota and the Pelican River Watershed District. 11
3. Surficial geology of the study area. 12
4. 10 m spatial resolution digital elevation model of study area. 15
5. Conceptual diagram showing a cross-sectional view of the recharge and discharge mapping method. 19
6. Conceptual diagram of map view of the recharge and discharge mapping method 20
7. Location of ground calibration thermistors. 26
8. Estimated water table elevation 33
9. Estimated water table gradients 33
10. Hydric soils used for error analysis of estimated water table elevations.. 34
11. Hydric soil and water table error analysis results 35
12. Groundwater recharge and discharge. 36
13. Areas of distinct shoreline groundwater discharge patterns. 37
14. Relative surface water temperatures, July 2006 (ASTER). 40

15. Relative surface water temperatures, August 2006 (ASTER). 42

16. Relative surface water temperatures, September 2015 (ASTER). 43

17. Potential springs or seeps on Fox Lake. 46

18. Seep on Dart Lake. 48

19. Surface water drainage from wetland adjacent to Fox Lake. 49

20. Spring emerging from pipe near shoreline on Johnson Lake. 50

21. Sucker Creek entering Detroit Lake 51

22. Spring or culvert entering Detroit Lake 52

23. Floating bog on Johnson Lake 53

24. Comparison of surface water temperatures recorded by thermistors and UAV imagery at each thermistor location. 55

25. Lake boundaries and relative lake surface temperature (ASTER) 58

LIST OF TABLES

Table Page

Table 1. Characteristics of thermal survey lakes. 25

ACKNOWLEDGMENTS

I wish to express my sincere appreciation to the members of my advisory committee for their guidance and support during my time in the master's program at the University of North Dakota. Thank you to Tera Guetter and Brent Alcott of the Pelican River Watershed District, and SkySkopes for their assistance in collecting field data. I would also to thank Emily Sundell, Logan Peterson, and Jeff Gendreau for their assistance in developing flight planning and image processing procedures for my thesis as part of the UAS in Engineering Design and Applications course. Thank you to David Dvorak of Field of View, LLC for his insights regarding thermal imagery analysis. Funding for this project was provided by the North Dakota View Scholarship and the Harold Hamm School of Geology and Geological Engineering. Thank you to my family and friends, who have provided unwavering support throughout my academic pursuits.

ABSTRACT

Effective watershed management decisions depend on understanding groundwater-surface water interactions. Traditional hydrogeological investigations are invasive, time-consuming, and expensive; therefore, regions that lack accessibility or agency funding need other ways of evaluating groundwater-lake interactions. Heat has long been known to be an effective groundwater tracer. Groundwater is insulated from most solar radiation, and its temperature does not fluctuate greatly from the annual average air temperature year-round in higher latitudes. In contrast, lakes are directly exposed to solar radiation, and water temperature fluctuates greatly both seasonally and diurnally. The winter and summer seasons produce the greatest contrast between groundwater and surface water temperatures. An empirical groundwater flow model of the water table near Detroit Lakes, Minnesota, was created using digital elevation model data and GIS analysis tools. This model estimates the distribution of potential groundwater discharge zones for further investigation with thermal imagery. Thermal remote sensing data acquired by satellite (ASTER) are freely available, non-invasive, and may serve as an effective means to identify potential areal groundwater recharge and discharge. Higher resolution thermal data were collected by using a DJI Matrice 600 UAV fitted with a FLIR Zenmuse XT thermal imaging sensor, which provides a potentially fast, minimally invasive, and cost-effective method for identifying possible groundwater discharge points within waterbodies at regional scales. Results suggest that large, well-defined springs and seeps can be identified with UAS imagery, but that slower groundwater seepage in

shoreline areas is obscured by land cover, weather conditions, emergent vegetation, sediment characteristics, and other factors. The large scale of imagery coupled with local thermal heterogeneity leads to limited information on groundwater discharge from satellite imagery.

CHAPTER I

INTRODUCTION

Effective watershed management decisions depend on understanding groundwater-surface water interactions. Surface water bodies are connected to groundwater in most landscapes, and therefore are components of groundwater flow systems (Winter 1999). This interconnectivity illustrates the importance of protecting both sources from contamination that could negatively impact environmental and human health. Areas of focused groundwater seepage can transform into pollution point-sources capable of discharging substantial chemical mass-flux into surface water when a local shallow aquifer is polluted (Hare et al. 2015). Mapping groundwater seeps and springs can help water resource managers better understand groundwater flow patterns and potential sources of contamination (Winter et al. 1998). With this information, managers can promote land use that is not detrimental to watershed health in susceptible recharge areas. Using recent advances in technology, this study will explore the effectiveness of using Unmanned Aerial Vehicle (UAV) collected thermal imagery to locate and identify springs and seeps along lake shores.

Traditional hydrogeological investigations are invasive, time-consuming, and expensive; therefore, regions that lack accessibility or agency funding need other ways of evaluating groundwater-lake interactions. Groundwater modeling at the watershed scale is typically

of coarse scale, as increasing complexity and resolution comes at the cost of increasing time and expense. To obtain finer-scale groundwater–surface water interaction, other techniques may practically be used.

Heat has long been known to be an effective groundwater tracer (Anderson 2005). Groundwater is insulated from most solar radiation, and its temperature does not fluctuate greatly from the annual average air temperature year-round in higher latitudes (Moore 1982). In contrast, lakes are exposed to solar radiation and water temperature fluctuates greatly both seasonally and diurnally. The winter and summer seasons produce the greatest contrast between groundwater and surface water temperatures. Thermal infra-red imagery acquired by satellite (ASTER) is freely available, non-invasive, and has served as an effective means to identify areal groundwater discharge into fresh water bodies in various environments (Rundquist et al. 1985; Banks et al. 1996; Tcherepanov et al. 2005).

Minnesota is known as the “Land of 10,000 Lakes”, and therefore groundwater and surface water interact extensively in many areas. According to monitoring data gathered by the Minnesota Pollution Control Agency, however, it is likely that approximately 40% of all surface waterbodies in the state have impaired water quality (Minnesota Pollution Control Agency 2017), suggesting that groundwater quality may be diminished in many areas.

The Upper Pelican River watershed, centered around the city of Detroit Lakes, Minnesota, is no exception. This city and the surrounding area is powered by greatly by tourism tied to water-related activities such as boating, fishing, and swimming. Hundreds of predominantly seasonal homes surround several of the region’s lakes resulting in heavily

developed shorelines, where manicured lawns treated with pesticides, herbicides, and fertilizer are common. A study confirmed the presence of groundwater-borne septic tank nutrients in Lake Sallie (Lee 1972). Septic nutrients contribute to algal blooms, a decrease in available oxygen, and decreased water clarity. Currently, a program put in place by Becker County encourages homeowners to replace failing septic systems to improve water quality. Other pollutants of concern are chemicals and fertilizers used in agriculture and lawncare, and sediment (PRWD 2005). By mapping groundwater discharge into lakes, we can identify potential sources of pollutants and act to mitigate further contamination. Gaining a better understanding of groundwater-surface water interaction in this region highly susceptible to water source contamination has potential to further improve water quality through appropriate land management practices.

Research Objective

GIS analysis and thermal imagery may provide a fast, minimally invasive, and cost-effective method for mapping of groundwater discharge along developed lake margins in heterogenous glacial outwash deposits.

There are three broad parts of the work presented in this report. The first part of the study involves creating a numerical groundwater flow model using a digital elevation model (DEM) data and analysis tools in the commercial software ArcMap 10.3 (Environmental Systems Research Institute, Redlands, CA). This will determine potential groundwater discharge zones for further investigation with thermal imagery. The second part attempts to use large-scale satellite-collected thermal imagery to identify areas of potential groundwater discharge within

waterbodies. Finally, part three involves collecting high resolution (<1 m) thermal imagery of select waterbodies with UAV to identify potential groundwater discharge at a finer scale.

The goal of the study will be to show the effectiveness of this remote sensing approach in minimizing the cost and effort to characterize groundwater–surface water interaction along lake margins using the Detroit Lakes region as a case study. If successful, this method could provide a valuable tool to assist watershed and land managers in making sound decisions about land use and zoning. Higher-resolution thermal data collected by UAV may increase the accuracy of maps created with satellite data, at a much smaller cost when compared to traditional hydrogeological investigations.

Background

This section provides a brief overview of the basic principles and existing literature that provide the basis for the research presented in this report. It concludes with a description of the gap in current knowledge that this project aims to fill.

Groundwater and Surface Water Connectivity

In most terrain types, surface water is connected to groundwater (Figure 1). Therefore, surface water bodies are fundamental components of groundwater flow systems. Water resource development or contamination of one often affects the other due to the exchange of water between these two components (Winter 1999). Interactions between surface water and groundwater are challenging to observe and measure, and often are disregarded in water resource management plans. These interactions can be affected by several different natural processes and human activities such as withdrawal from shallow aquifers for domestic water supply, irrigation, and industrial uses. Groundwater seepage into one side of a lake and out the

other side often occurs in waterbodies existing in glacial and dune landscapes composed of deposits with high permeability (Winter et al. 1998).

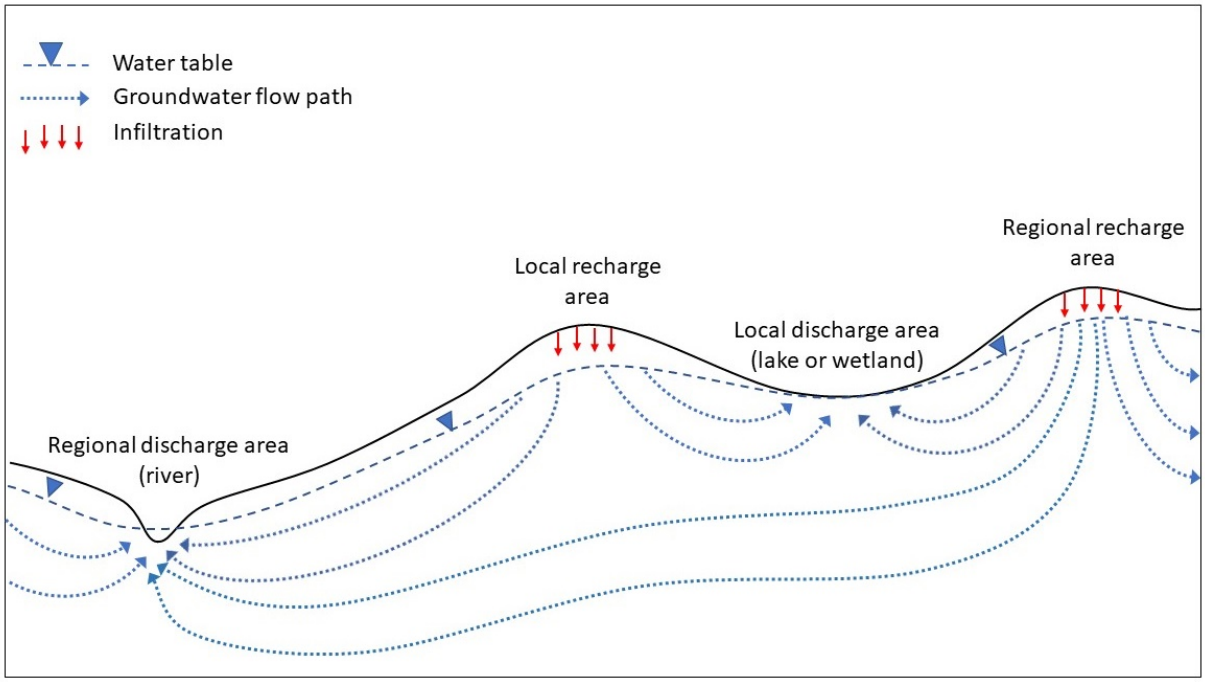

Figure 1. Generalized conceptual groundwater flow diagram. Groundwater recharge occurs at topographic highs, and discharge occurs at topographic lows. Shorter groundwater flow path lines indicate local recharge and discharge. Long flow path lines indicate regional recharge and discharge. Lakes, wetlands, and rivers occur where the water table intersects the landscape surface (Modified from Fleming 1994).

Littoral Zone Groundwater Seepage

Many studies using both analytical and numerical modeling have established that groundwater generally seeps into a lake through the littoral zone and surface (lake) water seeps out into the groundwater system through deep parts of the lake (John and Lock 1977; Lee 1977; Pfannkuch and Winter 1984; Winter and Pfannkuch 1984). This trend can be attributed to, in

part, shallow perimeters where fine-grained sediments may be removed by wave-action (Winter et al. 1998).

Generating Groundwater Contribution Using Numerical Modeling and DEM

Stoertz and Bradbury (1989) developed a numerical modeling method to produce maps of recharge and discharge patterns across the landscape. Their method uses the mass-balance equation, water table elevation data, hydraulic conductivity, and aquifer thickness data to calculate groundwater recharge rates. Water balance is obtained for each water table cell by calculating fluxes between the water table cell and its four adjacent cells. Stoertz and Bradbury achieved good agreement between the modeled recharge and discharge map and a recharge map based on field observations. Gerla (1999) suggested that digital terrain analysis can provide groundwater contribution estimates when coupled with Stoertz and Bradbury's numerical modeling method. Digital elevation models (DEMs) can provide water table elevations at surface water bodies, which can then be used to interpret the water table elevation for the surrounding area. The resulting estimated water table elevations can then be introduced into the Stoertz and Bradbury model to map recharge and discharge across the landscape. The MN DNR has also used DEM data to create water table elevation estimation maps using ArcGIS; however, detailed information about the methods used have not been published (MN DNR 2016).

Heat as a Groundwater Tracer

Heat has been recognized as an effective groundwater tracer since 1905. Beginning in the 1960s, several researchers published the basics of using heat as a groundwater tracer (Anderson 2005). Slichter (1905) was one of the initial workers that identify the value of heat as

a groundwater tracer, observing that comparatively high groundwater temperatures signaled induced infiltration from a pond in Long Island, New York. Later, Lee (1985) used heat to locate groundwater seeps to lakes.

Mapping Recharge and Discharge Using Remote Sensing

Satellite imagery has been frequently used to assist hydrogeologic interpretation. A majority of these uses have focused on mapping bedrock geology for groundwater resource evaluation (Waters et al. 1990). In recent times, satellite measurements of topography, soil moisture, temperature, vegetation characteristics, and gravity have been used to assemble information about the occurrence of groundwater(Becker 2006). Human activities that alter the soil moisture and vegetation within the area of interest for this study make those methods unsuitable. Gravity measurements can be suitable for determining depth to groundwater, but only after the influence of vegetation has been removed (Becker 2006). The significant temperature difference between surface water and groundwater observed in the study area during the late summer months suggests that thermal remote sensing is a suitable method for identifying springs and seeps in and adjacent to surface waters.

One of the early efforts to map groundwater pathways using thermal remote sensing involved the use of an airborne Thermal Infrared Multispectral Scanner (TIMS) to identify flow-through lakes in the Nebraska Sandhills (Rundquist et al. 1985). TIMS has also been used to locate and describe the extent of groundwater discharge in coastal waters (e.g. Banks et al. 1996; Tamborski et al. 2015). Satellite thermal imagery can identify groundwater discharge in sparsely vegetated shallow groundwater-dominated lakes underlain by relatively homogeneous

sediments (Tcherepanov et al. 2005). For these past studies, temperature regimes seen in satellite imagery were verified using direct water temperature and chemistry measurements.

With the advent of UAVs, and sensors small enough to be mounted on them, wide availability and new regulations allow flights and data collection to occur relatively cheaply, quickly, and legally. This technology has been used to get higher resolution imagery to study groundwater discharge. Aicardi et al. (2016) demonstrated a methodology for acquiring and processing thermal UAV imagery to aid in subfluvial springs mapping.

Research Contribution of this Study

This research will add to the existing body of work by exploring the visibility of groundwater discharge along lake margins in a new geologic substrate (heterogeneous glacial outwash), and by comparing the visibility of groundwater discharge in thermal imagery collected at two different scales. Large-scale satellite imagery will be examined for potential groundwater signatures. Small-scale thermal imagery will be used to examine a subset of waterbodies for potential groundwater signatures at finer resolution. In addition, a new method using readily available UAV technology will be tested. Unlike previous studies using airborne TIR imagery to map seeps and springs (Rundquist et al. 1985; Banks et al. 1996; Tcherepanov et al. 2005; Tamborski et al. 2015; Aicardi et al. 2016), this study area's natural groundwater flow patterns have been heavily influenced by the installation of hundreds of water supply wells, and drain tiling on and in the vicinity of the shorelines of these lakes. Much of the shoreline in the study area has been developed for residential and agricultural use. This study may provide insights into how human activities can influence the effectiveness of remote sensing methods in identifying groundwater seepage.

CHAPTER II

METHODS

Study Site

The upper Pelican River watershed is in northwest central Minnesota (Figure 2), located almost entirely within Becker County, and has an area of approximately 310 km^2. The Pelican River flows south to join the Ottertail River, which empties into the Red River of the North. Receiving an annual average of 610 mm of precipitation, the watershed has 144 lakes (PRWD 2005). Average annual air temperature for Detroit Lakes is 5^o C (41^o F) for 2007-2016 (Midwest Regional Climate Center). A set of subwatersheds, with a total area of 124.5 km^2, containing some of the most densely developed lakes were chosen within the upper Pelican River watershed for this study (Figure 2).

Land use types include agricultural, residential, recreational, and industrial. The city of Detroit Lakes is the largest city in the watershed, as well as the county seat of Becker County. Located at the center of the watershed, the city's population is approximately 9,000 (US Census 2010), with an unofficial summer population of an estimated 13,000. Tourism is a significant economic driver in the region. Activities such as swimming, fishing, hunting, boating, and watersports draw thousands of people to the watershed throughout the year.

Many of the larger lakes within the watershed are ringed by seasonal lake cabins, with significantly fewer of them serving as year-round homes. Most of the lake cabins that fall

outside of the Detroit Lakes municipality have private septic systems, many of which are older and prone to failure. A study completed in 1971 confirmed the presence of groundwater-borne septic tank nutrients in Lake Sallie (Lee 1972). Septic nutrients contribute to algal blooms, a decrease in available oxygen, and decreased water clarity. Currently, a program put in place by Becker County encourages homeowners to replace failing septic systems to improve water quality. Other pollutants of concern are chemicals and fertilizers used in agriculture and lawn care, and sediment (Pelican River Watershed District 2005).

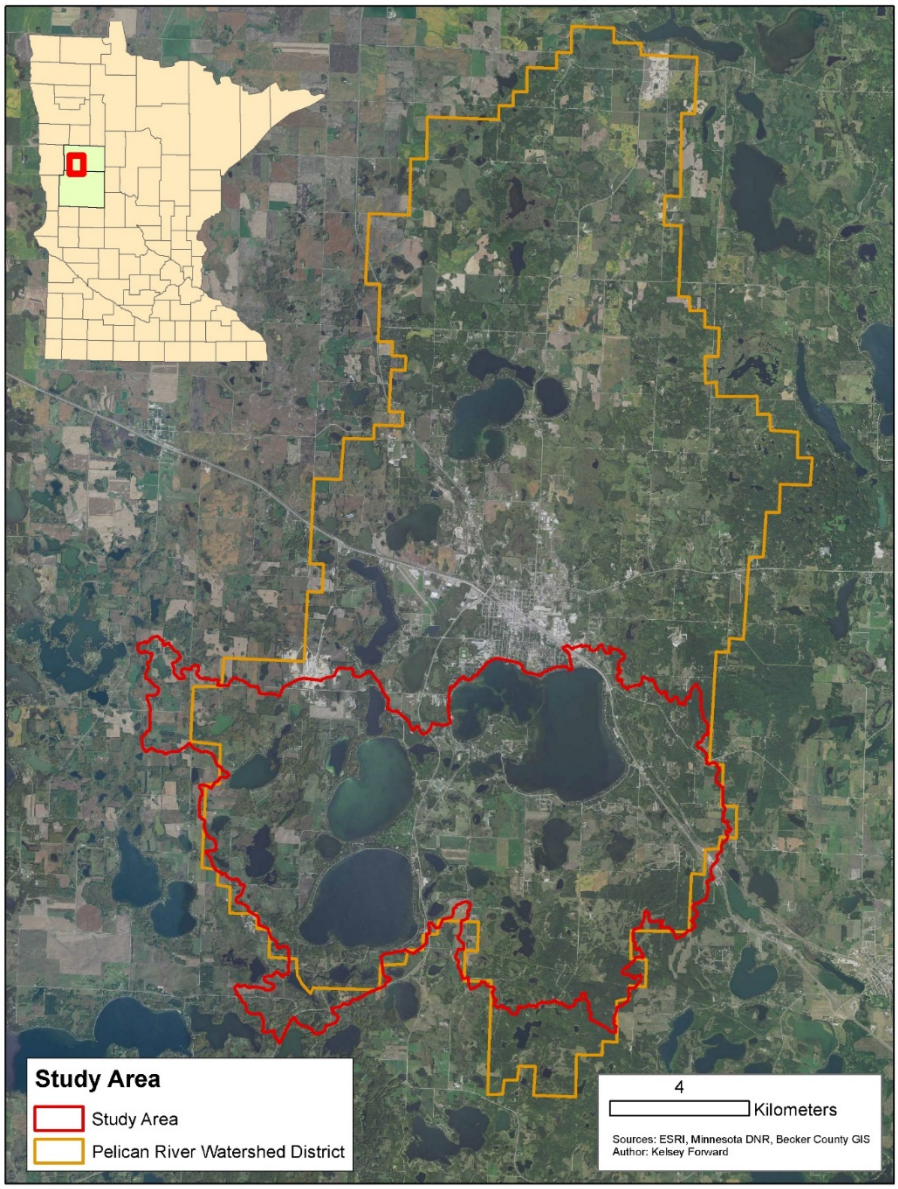

Figure 2. Study area location within Minnesota (insert) and the Pelican River Watershed District.

The surficial geology underlying the watershed is dominated by Quaternary till and outwash sediment (Figure 3). Poorly to moderately sorted sand and gravel outwash comprises most of the Pelican River sand-plain aquifer and the central portion of the watershed. Clayey

loam till surrounds the margins of the watershed. These sediments were deposited along the ice margin and collapsed after the ice retreated (Lusardi 2005).

The Pelican River sand-plain aquifer is composed of two outwash units: an upper unconfined unit (water table) and a lower confined unit. A layer of till serves as the confining layer between the two (Miller 1981).

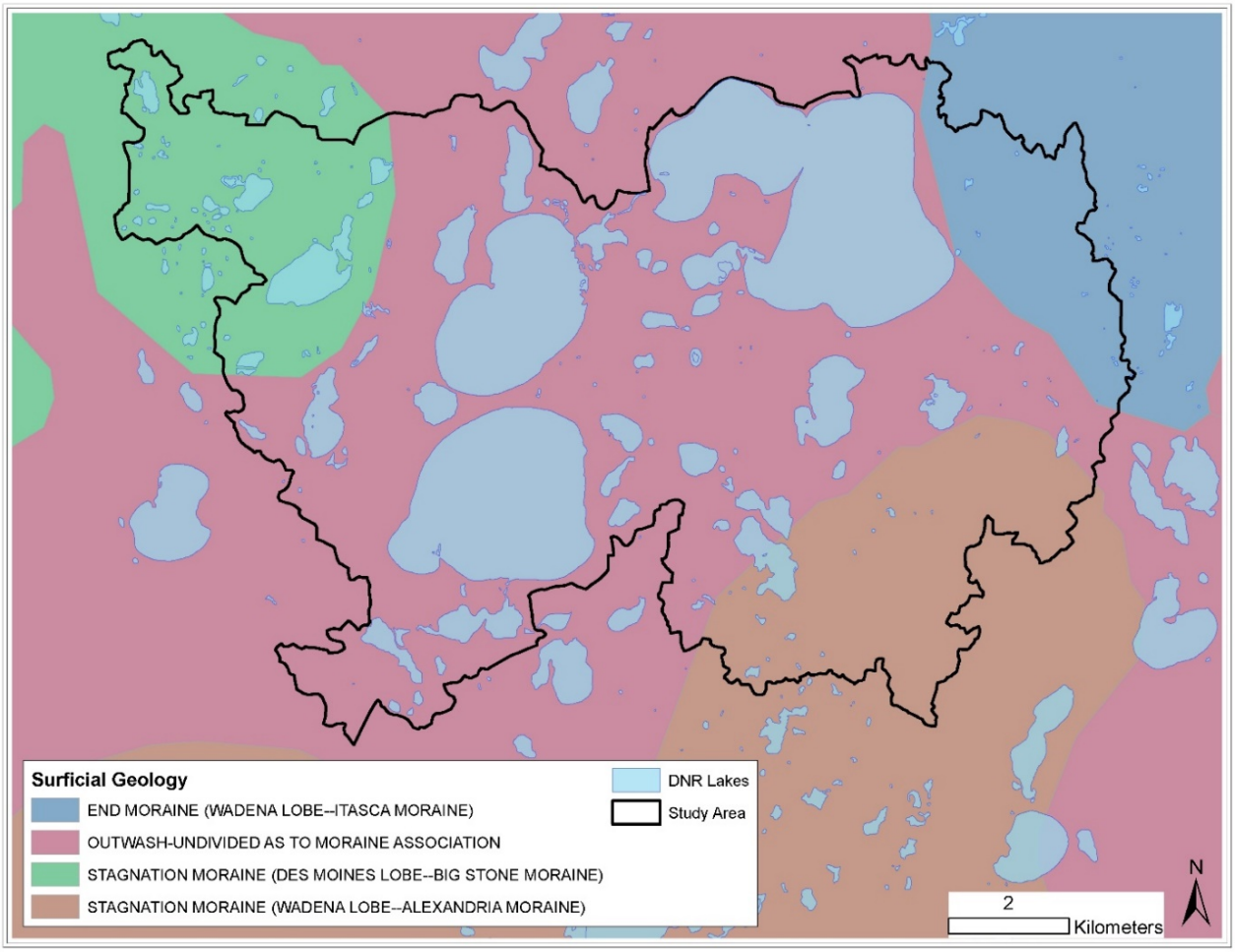

Figure 3. Surficial geology of the study area.

Methodology

To predict where recharge and discharge are likely occurring across the landscape, and therefore which waterbodies should be surveyed with TIR, a cell-by-cell groundwater budget

was created. In GIS, the cell-by-cell groundwater budget can be calculated using the parameters of water table elevation, porosity, aquifer thickness, and hydraulic conductivity. Since water table elevation data are not available for the study area, water table elevations were estimated from a DEM, and an error analysis performed on the results. The estimated water table elevation, together with other parameters, was then used to calculate the cell-by-cell water budget. Satellite and UAV imagery was then collected and reviewed for potential groundwater discharge within waterbodies in the study area. A description of the methods used for each of these steps is described below in the following order: modeling and error analysis in ArcGIS, thermal satellite imagery processing, ground calibration, and UAV imagery processing.

GIS Modeling

Background. An empirical groundwater flow model of the Pelican River aquifer near Detroit Lakes, Minnesota, was created using a digital elevation model (DEM) data and GIS analysis tools. This model was created to understand the basic groundwater system, and used to estimate the distribution of potential groundwater discharge zones for further investigation with thermal imagery. Specifically, the groundwater model provides: 1) an estimate of groundwater elevation in the study area, and 2) the pattern to predict areas of recharge and discharge across the study area.

To create a model of a complex and continuous natural system, the system must be discretized, broken down into distinct, separate pieces, to enable quantification of groundwater processes. This system was discretized by breaking the three-dimensional (3D) system down into a 100 m finite-difference (FD) grid oriented in the north-south direction, parallel to the known flow of groundwater in the region. This means the grid is 100 m wide in the X (east to

west) and Y (north to south) directions. The Z direction of each cell is the hydraulic head, which is measured relative to a mean sea level datum. Boundaries conditions at the edges of the model are constant head and the heads are assumed to be steady state. Each cell is permitted to act as a source or sink. Although the system is unconfined, in this analysis it is treated as confined. The discrepancy between confined and unconfined is likely small because of the large thickness of the aquifer and small groundwater slopes.

Data Sources. Data for the water table model was obtained from various sources (Appendix A). Stream and lake data were obtained from the National Hydrography Database. Additional stream and lake data, as well as the hydrological watershed boundaries, were obtained from the Minnesota Department of Natural Resources via Minnesota Geospatial Commons. Soils data created by the NRCS was obtained from Becker County GIS. The district provided the political boundary of the Pelican River Watershed District. The 10 m DEM was obtained from the U.S. Geological Survey (USGS) via National Map Viewer. Aerial photography used for reference in ArcMap was provided by MnGeo WMS service. All files were converted into to the NAD 1983 UTM Zone 15N coordinate system for analysis.

Interpolating the Water Table. Average water table elevations throughout the study area are not available and had to be estimated. Since lakes are typically an expression of the water table at the surface (Winter et al. 1998), it was assumed that lake elevations could be used as control points for interpolating the water table elevation in the area. A 10 m DEM created from Light Detection and Ranging (LiDAR) data collected over two consecutive days provide relatively accurate and coherent water table elevations via surface water bodies (Figure 4). These elevation data provided the basis for the interpolation. Higher resolution DEMs (1 m,

3 m and 5 m) are available for the study area; however, in test runs the data took a large amount of time to process and did not produce reasonable results. Lower resolution DEMs (30 m) would have obscured finer landscape features, and may not have provided reasonable results. Using a 10 m resolution allowed reasonable processing times and sufficient landscape detail.

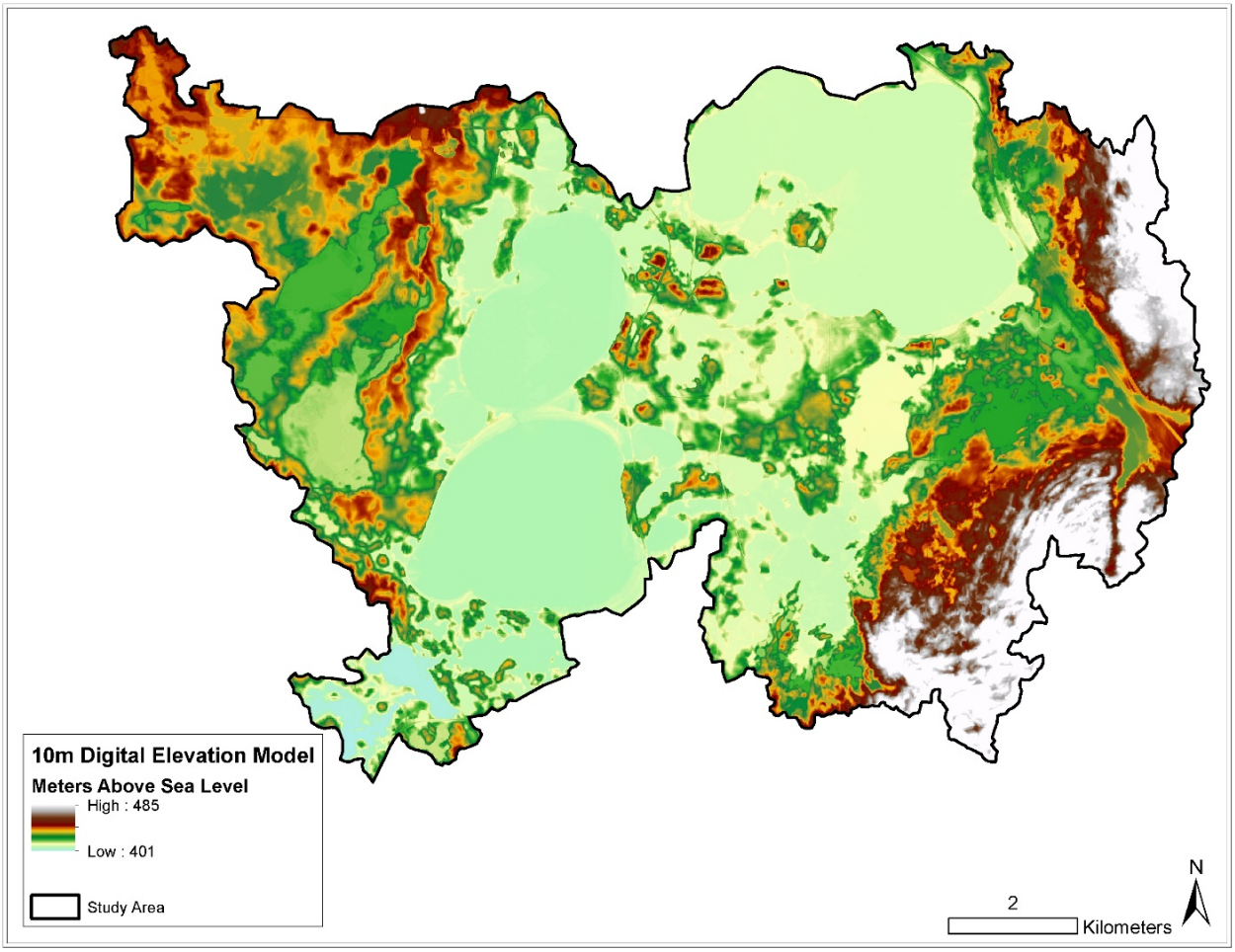

Figure 4. 10 m spatial resolution digital elevation model of study area.

The water table elevation was interpolated using the following generalized steps in ArcMap:

1. Download the 10 m DEM and NHD lakes and streams coverage in UTM Zone 15 N projection.
2. Load the data into ArcMap and export the lakes and streams data from the gdb and into projected shape files.
3. Use the Feature2Point tool to convert polygons (lakes) and lines (streams) to points, turn on the Inside option (checked) so that the point falls within the lake polygon. For streams, choose Feature2Point.
4. Using the DEM, run the Extract Values2Points tool to find the elevations of the points for both files created in the previous step.
5. Join the lakes polygon file to the elevations associated with its point. This creates an elevation field for the lake features. Export or otherwise save the attribute file with the new elevation information.
6. Create a nominal grid with the desired cell size using the Create Constant Raster tool. I chose a 100 m cell size and chose the bounding x-y coordinates in whole integral values to the nearest 100 m with a buffer of at least one subwatershed on each side.
7. Populate cells of this raster with the best-fit value for the water table elevation. Do this by the following:
    a. Set the environment so that the output extent and snap raster are set to your nominal grid (step 6).
    b. Use the lake points file, and stream points files that include the elevation field to find the best-fit elevation for each cell. Use null for empty cells, which should be done automatically by ArcMap.

c. Do this by using the Polygon2Raster and Point2Raster tools. Set the environment to match the nominal grid.

d. Use the Mosaic2NewRaster tool to combine the two rasters created in step 7c.

8. Convert the mosaic grid into a point shape file so it can be interpolated. Use the Raster2Point tool.
9. Edit the output to eliminate any points that appear inconsistent, such as unusually high points along stream cells or isolated locations where water table appears locally high, suggesting that the water table may be perched.
10. Use the points to interpolate into a grid using the nominal grid's properties. Natural Neighbor is the easiest to use and is designed for clustered data (ESRI 2017). This interpolation method locates the nearest subset of input samples to a query point, then "applies weights to them based on proportionate areas to interpolate a value" (ESRI).

A full description of the water table interpolation method is available in Appendix A.

This water table elevation grid was then used to conduct a cell-by-cell water budget analysis.

Cell-by-cell water budget analysis for mapping recharge and discharge. Total hydraulic head gradients cause groundwater to flow. Darcy's Law describes the flow of water through a porous medium in one dimension, and may take the one-dimensional form of:

$$Q = -KA(\frac{h_A - h_B}{L})$$

where K = hydraulic conductivity (length/time), A = area (length^2), Q = discharge (length^3/time), h = hydraulic head, and L = distance along the flow path between h_A and h_b (length) (Fetter 1999).

Provided that the variation of hydraulic heads along a flow path is known, cell-by-cell flow can be computed and tabulated. For example, Figure 4 shows how flow in one dimension can be determined for each cell along a flow path. In a one-dimensional model, Q can be calculated for two cell faces (Figure 5). For example, cell B loses more water to cell C than it gains from cell A. Because there is no mass deficit for cell B, according to Darcy's Law and conservation of mass, recharge must make up the rest of the water to preserve the observed head. Likewise, the mass surplus in cell F will be counteracted by discharge.

The concept and extension to Darcy's Law in two-dimensions can, therefore, provide a cell-by-cell water budget across a surface of known hydraulic heads, which in this analysis is the water table estimated for this section of the Pelican River watershed.

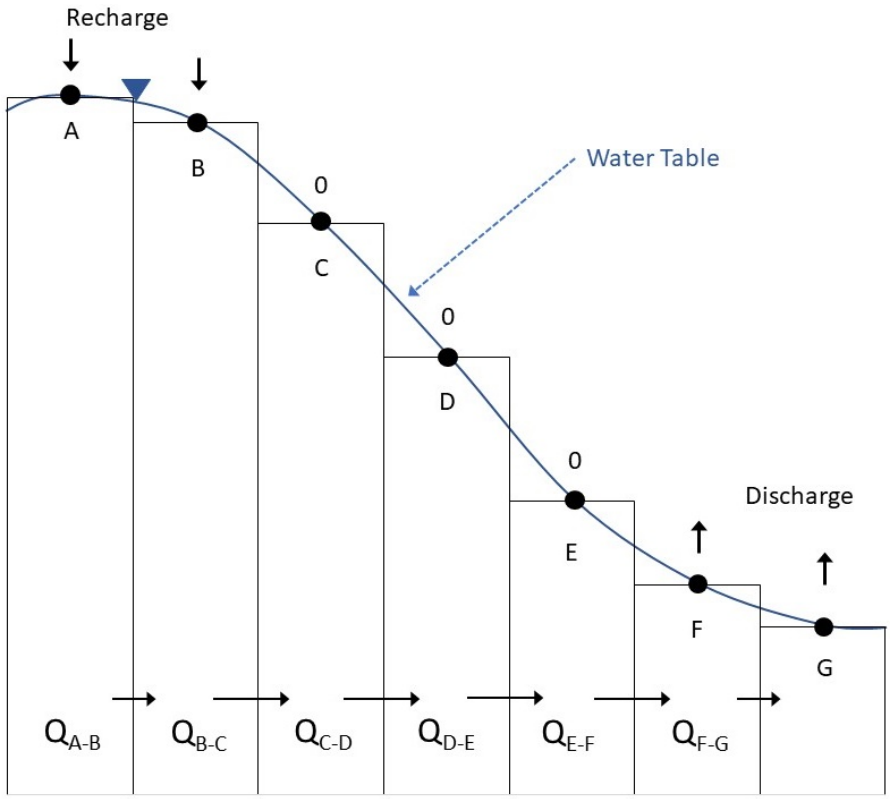

Figure 5. Conceptual diagram showing a cross-sectional view of the recharge and discharge mapping method. Each column represents a grid column, and each dot represents a grid node. Modified from Gerla (1999) and Stoertz and Bradbury (1989).

Moving to the map view (Figure 6), the second dimension can be incorporated by using the heads of the four neighboring cells to calculate the mass balance.

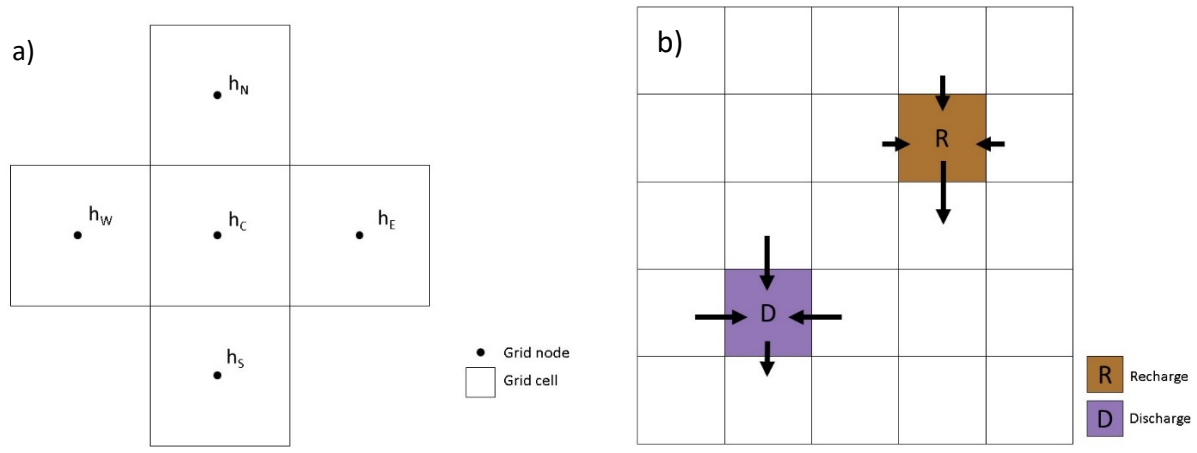

Figure 6. Conceptual diagram of map view of the recharge and discharge mapping method. Figure 6a. Each square represents a grid column, and each point represents a grid node. Figure 6b. Each square represents a grid column, with the arrows representing flow vectors. The length of the arrows indicates the quantity and direction of flow between cells through the four cell walls. Cells that have more water flowing out than flowing in are recharge cells. Cells that have more water flowing in than flowing out are discharge cells.

In ArcGIS, the Darcy Flow analysis tool is designed to be used to test the consistency of groundwater datasets and to generate raster of groundwater flow vectors. However, in this study the Darcy Flow tool was used together with the water table elevation map to estimate groundwater deficits and surpluses, simulating areas of recharge and discharge across the study area. The default output raster gives the difference between the flow of water into and out of each cell, and is called the groundwater volume balance residual raster (ESRI 2017). Within each cell, Darcy Flow tool calculates the volume balance, which is typically small if sources or sinks, such as wells, infiltration and recharge, or leakage and discharge, are not present. Volume balance residual is calculated by:

$$R_{vol} = Q_S - Q_N + Q_W - Q_E$$

A balance between flow into and out of the cell is indicated by a zero-volume balance residual. Negative or positive residual values indicate recharge or discharge, respectively, at the location represented by the cell (Figures 5 and 6).

Inputs to the Darcy Flow tool were as follows:

1) Water table elevation (computed)
2) Porosity = 1 (unused in the Darcy Flow tool)
3) Saturated thickness = 18.3 m (Miller 1982)
4) Transmissivity = 1 (assumed homogeneous).

The output of the Darcy Flow tool was the grid with residual values for each cell (the difference between inflow and outflow). Note that there was little information available on the hydraulic conductivity and transmissivity (product of hydraulic conductivity and saturated thickness). In this case, simply a qualitative, relative estimate of the recharge and discharge was needed to guide the plans for acquiring remote sensing imagery. Additional effort at including heterogeneity and more appropriate analysis of flow by considering unconfined conditions (e.g., Haitjema and Mitchell-Bruker 2005; Anderson et al. 2015) may provide more quantitative results for the flow residuals, and hence, more accurate recharge and discharge rates. Instead, this simpler approach used here provides a qualitative map of recharge and discharge across the landscape.

Error Analysis. Error analysis was performed in this study to test goodness of fit by comparing the elevations of the interpolated water table to the elevations of select hydric soils within the study area. The goal was to obtain a 75% or greater match of the interpolated water

table elevation to the elevations of hydric soils (assumed to be at or near the water table), that had also been extracted from the same 10 m DEM. Hydric soils described as muck or peat (saturated) were extracted from the Becker County soils data. These hydric soil polygons were then converted to a 100-m raster if hydric soils covered a minimum of 50% of the cell area. Using this 100-m hydric soil raster as a mask, elevations for the soils were extracted from the 10 m DEM. The 100 m hydric soils raster was then used to extract cells from the interpolated water table elevation raster. The water table elevation hydric soil raster was then subtracted from the hydric soil raster. The difference raster was then reclassified with varying tolerances to evaluate the quantity of matching cells.

Quantitative summary statistics describe the goodness of fit. These statistics include measures such as mean error (ME), mean absolute error (MAE), root mean square error (RMSE), and scaled root mean square error (SRMSE) for steady state models, and are ideally minimized (Anderson 2005; Barnett et al. 2012). As an alternative measure the goodness of fit of the estimated water table elevation to the elevation of hydric soils, RMSE and SRMSE were used to evaluate the residuals between the two rasters. The equation for RMSE is as follows:

$$RMSE = \left[\frac{1}{n}\sum_{i=1}^{n}(h_h - h_w)_i^2\right]^{0.5}$$

where h_h is the elevation of hydric soils and h_w is the estimated water table elevation. Scaled root mean square error (SRMSE) takes into account the range of measured values and is expressed as a percentage (Barnett et al. 2012). SRMSE is calculated by dividing the RMSE by the range of measured hydric soil elevations, and is shown by the following formula:

$$SRMSE = \frac{100}{\Delta H}\left[\frac{1}{n}\sum_{i=1}^{n}(h_h - h_w)_i^2\right]^{0.5}$$

where ΔH is the range of measured hydric soil elevation values.

It is important to note that while quantitative summary statistics are often provided with a model, there are no established guidelines by the groundwater modeling community. This is likely because different models have different objectives, and the reasonableness of a model is often best determined by subjective judgment (Anderson et al. 2015).

Thermal Infrared Remote Sensing

Satellite. Archived thermal satellite imagery is available for free from the Advanced Spaceborne Thermal Emission and Reflection Radiometer (ASTER). The thermal infrared (TIR) system aboard ASTER uses "a single, fixed-position, nadir-looking telescope with a resolution of 90 m" (NASA Jet Propulsion Laboratory 2004) to collect 5 TIR bands. Additional information about ASTER is listed in Appendix B. Landsat 8 Thermal Infrared Sensor (TIRS) imagery is also free and has greater temporal resolution than ASTER; however, the spatial and spectral resolutions are lower.

Winter or summer data are most suitable for this type of analysis, as the difference in surface and groundwater temperature is greatest during these seasons. Minnesota's cold winters cause the lakes to freeze over completely most years, making winter imagery unsuitable for analysis. Open water that may appear in the winter could potentially be attributed to warmer groundwater discharging; however, lake aerators also produce the same

result. The cause of the open water cannot be differentiated by satellite imagery; therefore, summer imagery was used.

Past studies have found that minimizing the effects of solar radiation during the daytime help eliminate atmospheric interference, leading to more accurate results. Few night images were available for the study area, and those were obscured by cloud cover or collected in the wrong season. As the focus of this study is not to find the absolute temperature of the surface waterbodies, but to identify relative differences, it was decided that daytime imagery would be sufficient.

Daytime ASTER imagery was downloaded from the USGS Global Visualization Viewer (GloVis), an online search and order tool for selected satellite data, with the search parameters of less than 10% cloud cover and ranging from June 31st to September 30th of any given year. Three images from July, August, and September were selected based on these requirements, one from each respective month.

UAV. Higher resolution thermal data were collected by using a multirotor UAV (DJI Matrice 600) fitted with an uncooled VOx microbolometer thermal camera (FLIR Zenmuse XT with a 9mm lens) and a red-green-blue (RGB) camera (Sony A6000 with a 30mm lens). Both cameras collected images by pointing straight down, perpendicular to the Earth's surface (nadir). The thermal camera records a single spectral band with wavelengths ranging from 7.5-13.5 µm. Temperatures recorded can be accurate to 10℃. The camera provides radiometric geotagged .jpg files. The RGB camera was fitted with a Field of View Geosnap geotagging device

to allow for easy georeferencing. Collected digital imagery will be stored by Dr. Phil Gerla at the University of North Dakota.

Surveys were conducted of eleven lakes (Table 1) during daylight hours July 26th and 27th, 2017. The UAV was deployed from land, docks, and a 16-foot fishing boat, as required by field conditions. Images were collected to achieve the desired fore lap of 90%, which was recommended by sensor expert David Dvorak (Field of View, LLC) to increase the ability of image stitching software to stitch the thermal images. The UAV was flown at an altitude of approximately 110 m (360 ft) above ground level (AGL), providing a spatial resolution of 23.6 cm/pixel for thermal imagery and 1.4 cm/pixel for RGB imagery.

Table 1. Characteristics of thermal survey lakes (Minnesota Department of Natural Resources).

Lake Name	Surface Area (km^2)	Max. Depth (m)
Detroit	12.79	25.0
Sallie	5.08	15.2
Fox	0.53	7.3
Munson	0.52	7.9
Loon	0.63	Unknown
Reeves	0.34	13.1
Johnson	0.69	9.1
Pearl	1.04	16.5
Little Pearl	0.04	Unknown
Mud	0.36	Unknown
Dart	0.11	1.5

Ground Calibration

Thermistors (HOBO pendant temperature data logger - Onset HOBO Miniature, Waterproof Temperature Recorder) recording surface water temperature every 15 minutes were attached to buoys, and two thermistors were placed in the shallow margins of each lake.

The thermistors were placed several days before the surveys and retrieved the day after all thermal surveys were complete to ensure that temperatures were collected during the time of the thermal surveys. Three thermistors were placed in shaded sites within the study area to obtain ambient air temperature. Locations (Figure 7) were recorded using a hand-held GPS unit (Trimble GeoXT – 6000 series).

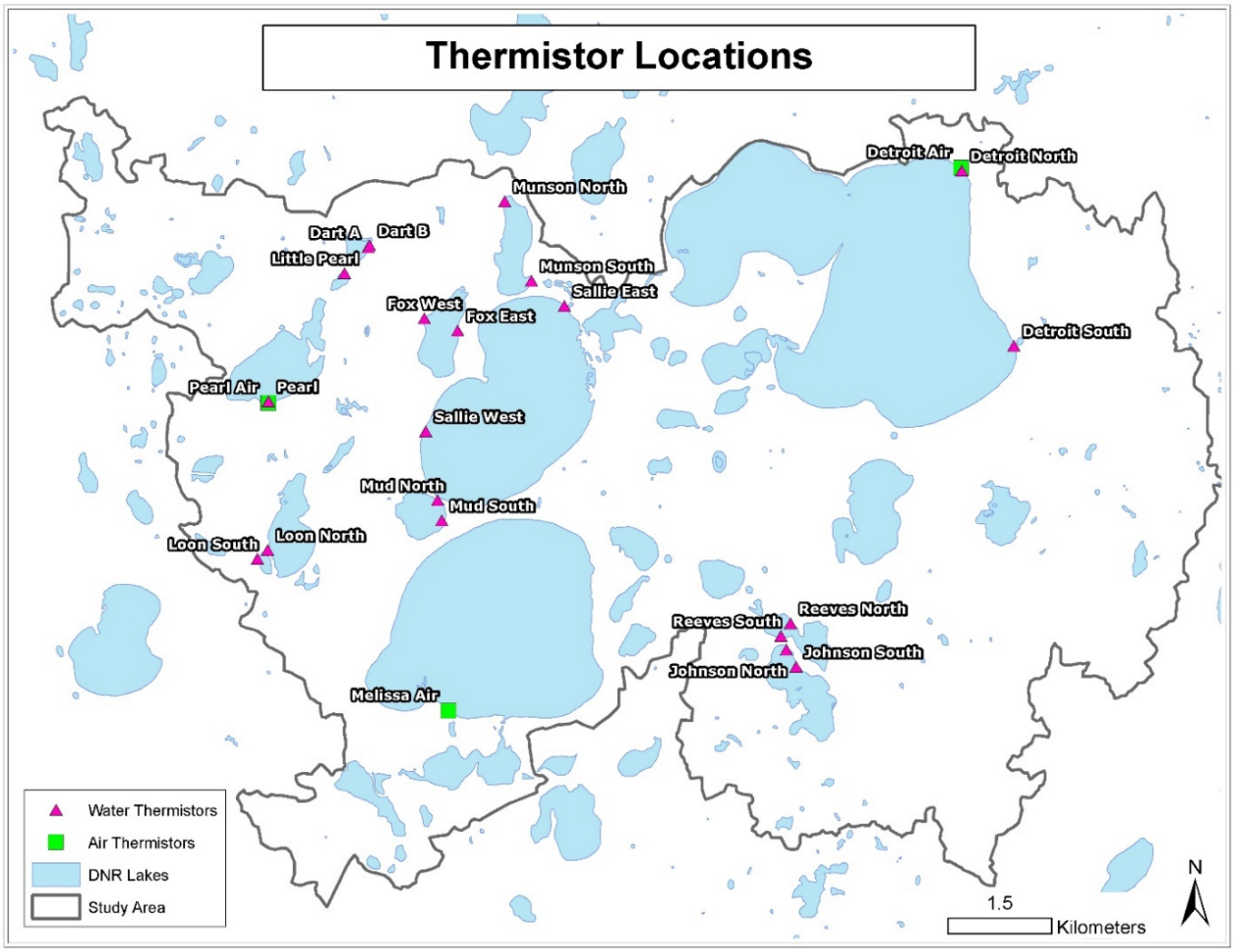

Figure 7. Location of ground calibration thermistors.

TIR Image Processing

Satellite Imagery. Each of the three scenes was processed separately in ENVI (Harris Geospatial Solutions, Melbourne, FL), an image analysis software platform. The selected images originate from ASTER AST_L1T datasets, which ENVI opens with "byte values" (binary sequence that records the brightness sensed for each band of the sensor (Campbell and Wynne 2011)). The recorded brightness is relative to the brightness within that single image, and is not calibrated (Campbell and Wynne 2011). The byte values must be converted to floating-point radiance values before being converted to radiance (Yale University 2016). Radiance is the true or calibrated brightness of an object. Once converted to radiance, atmospheric correction can be applied to approximate and remove the atmospheric contributions caused by dust, particles, and moisture. The algorithm used by ENVI (ISAC) assumes that the atmosphere is uniform over the entire scene. Then, "The algorithm first determines the wavelength that most often exhibits the maximum brightness temperature. This wavelength is then used as the reference wavelength. Only spectra that have their brightest temperature at this wavelength are used to calculate the atmospheric compensation. At this point, for each wavelength, the reference blackbody radiance values are plotted against the measured radiances. A line is fitted to the highest points in these plotted data and the fit is weighted to assign more weight to regions with denser sampling. The compensation for this band is then applied as the slope and offset derived from the linear regression of these data with their computed blackbody radiances at the reference wavelength" (Harris Geospatial 2017). Once the radiance values have been atmospherically corrected, the data can be converted into its two parts: emissivity and temperature. This is referred to as emissivity normalization. Emissivity is the ratio between the

emittance (the amount of solar radiation an object absorbs and reemits) of a given object and that of a blackbody at the same temperature. A blackbody is a hypothetical source of energy (does not exist in nature) that absorbs all radiation and reflects none (Campbell and Wynne 2011). The surface's composition is accounted for in the emissivity value. "The highest temperature for each pixel is used to calculate the emissivity values using the Planck function." (Harris Geospatial, 2016). Planck's constant (h) relates frequency (v) to radiant energy (Q).

$$Q = hv$$

Raw TIR imagery was then converted into Kelvin. Once the Kelvin temperature file was created for the entire image, the DNR 24k lakes polygons were used to create a mask to block out the land surface, allowing the focus and scaling to be exclusively on the waterbodies. Detailed instructions for ASTER TIR processing can be found in Appendix C.

UAV. Thermal UAV imagery was examined frame-by-frame in FLIR Tools (FLIR Systems, Wilsonville, Oregon), looking for noticeable cold streaks or spots. RGB imagery was viewed simultaneously to assist with feature identification and to ensure that cold signatures were not attributable to shadowing or vegetation near the shoreline. The color ramp was manually adjusted to bring out temperature differences in the water. This was best accomplished by increasing the contrast by reducing the range of temperatures displayed by the color ramp (approximately 10-20°C). Initial plans were to stitch the thermal images together in Photoscan (Agisoft LLC, St. Petersburg, Russia) to get a single model of each individual lake for temperature comparison. For reasons presented in the Results and Discussion sections, the frame-by-frame method of analysis was used instead.

Limitations and Assumptions

For each of the three parts of this research, the water table model, recharge, and discharge distribution across the watershed landscape, and the application of thermal band remotely sensed data, there are important limitations and assumptions.

As a simplification of reality, a model can never represent the entirety of the natural world's complexity (Anderson et al. 2015). The interpolated water table elevation and empirical groundwater flow model are both subject to this constraint. This study does not attempt to precisely quantify groundwater balance volumes – recharge and discharge – only to predict the location of subaqueous discharge along shorelines.

Wells were not used to model the water table, as sorting through well logs to determine which wells are completed in the aquifer of interest would be time-consuming and of little value for defining the elevation of the water table. Typically, the well logs are for deeper aquifers and the static water levels, if reported at all, do not reflect the long-term conditions in the shallow, unconfined aquifer.

Three major assumptions were made in recharge and discharge mapping using the cell-by-cell water balance method. First, the model assumes uniform saturated thickness (b) of the unconfined aquifer. Second, the model assumed homogeneous hydraulic conductivity (K) across the study area. Third, the aquifer is assumed to be isotropic, meaning the hydraulic conductivity is the same in all three principal directions (Fetter 1999). These assumptions were determined acceptable, as the intent of the model is not to quantify flow.

The remotely sensed thermal data collected for this study needed to be acquired at a time when the contrast between air temperature and groundwater temperature are as large as possible. The larger the temperature difference, the more readily visible the groundwater discharge will be in the thermal images.

Groundwater in the study area remains near the average annual air temperature of 5℃. Surface water in the study area typically freezes over in the winter and often accumulates snow, preventing the temperature to be accurately read using remote thermal sensing. At the end of the summer, surface water temperatures can reach >20℃ (PRWD Water Quality Database), providing excellent thermal contrast. For this reason, collection of thermal imagery was limited to the end of the summer (July or August).

Ideally, thermal imagery would be collected at night, when there is no interference from the sun, typically less wind, and less boat traffic. However, due to current FAA regulations and the safety concerns of the UND UAS Research Ethics and Compliance Committee, it was decided to collect imagery during the day to maintain visual line of sight as well as assist in collision avoidance with stationary objects and wildlife. In addition, time and funding constraints only allowed for two days of thermal imagery collection. The subset of lakes to be surveyed were chosen based primarily on empirical model results and geographic location. Geographic location was important for two reasons: 1) To get representative waterbodies underlain by the two types of surficial geology (outwash and till) in the watershed, and 2) To reduce travel time between the waterbodies, thereby maximizing available flight time for surveying.

Varying cloud cover, wind-caused mixing, vegetation, as well as the type and quality of available sensors all influenced the ability of the thermal imagery to accurately read surface

skin temperature of the waterbodies. RGB imagery taken concurrently with the thermal imagery allowed some of these factors to be subjectively included and considered in the imagery analysis process.

CHAPTER III

RESULTS

Results for each portion of the study are presented in the same order as in the previous section: empirical modeling and error analysis, satellite thermal imagery analysis, UAV imagery analysis, and ground calibration.

Empirical Modeling

Water Table Elevation Estimation

The estimated water table elevation map indicates, as expected, that the water table elevation decreases toward the center of the study area where the largest lakes are located. Water table elevation also decreases toward the southwest, following known regional flow patterns (Figure 8).

Gradients (equal to the slope) of the water table (Figure 9) were relatively high in two large areas. The northeast margin of the study area and just east of Reeves and Johnson lakes have water table slopes of greater than 0.9 degrees. Another relatively high slope area is west of Fox Lake, where slopes are greater than 0.7 degrees. Comparing the 10 m DEM to the estimated water table, the greatest depth to water table is approximately 65 m. This occurs in the southeast portion of the study area, where the topographic highs are the greatest.

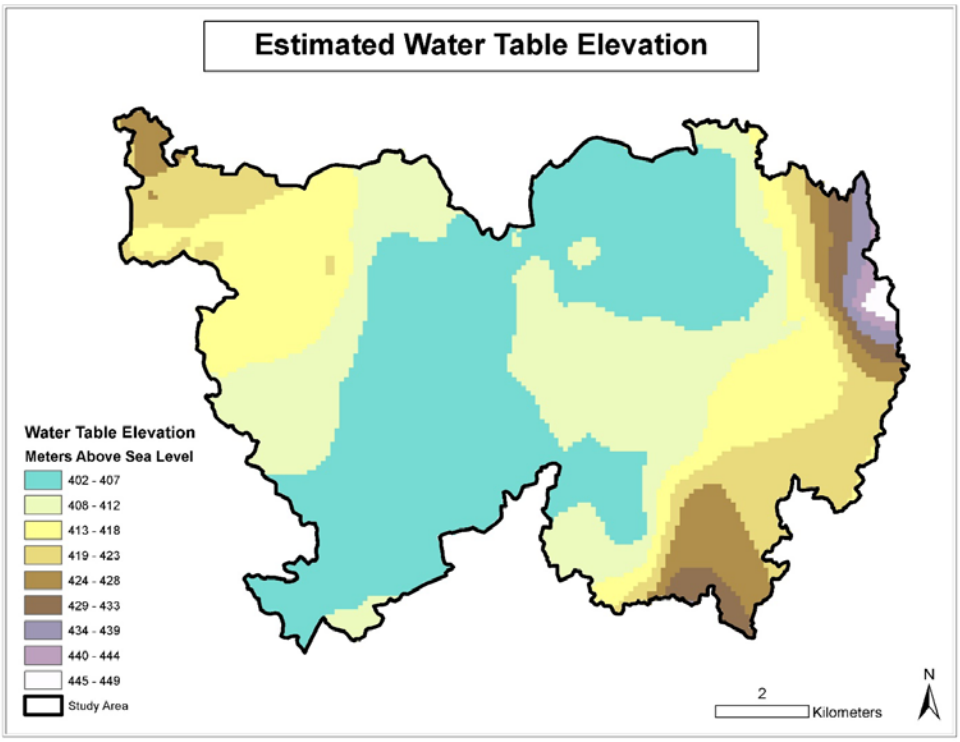

Figure 8. Estimated water table elevation.

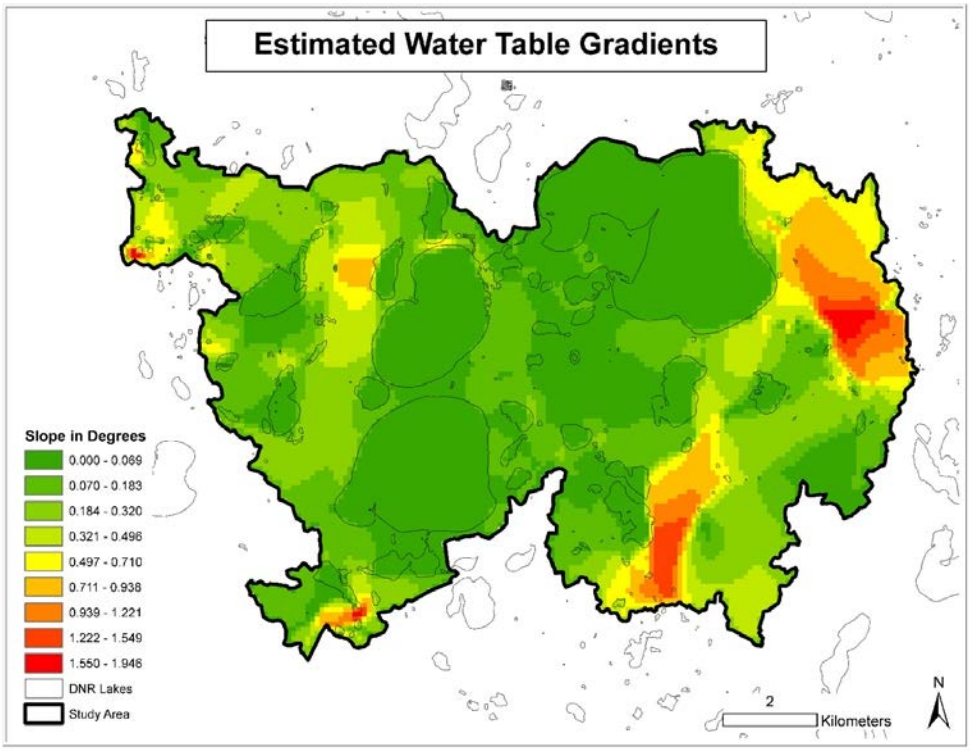

Figure 9. Estimated water table gradients. The greatest slope calculated for each cell from the estimated water table elevation raster is shown in degrees.

Error Analysis. 850 hydric soil cells with a resolution of 100 m were selected for comparison (Figure 10). Error analysis showed 74.9% of modeled water table elevations within ± 1 m of hydric soil elevations (Figure 11). Historical lake levels show a maximum lake fluctuation of approximately 1 m (Appendix E), therefore a fluctuation of this magnitude was considered an acceptable margin of error. Summary statistics calculated by the traditional methods of RMSE and SRMSE were 1.44 m and 72%, respectively.

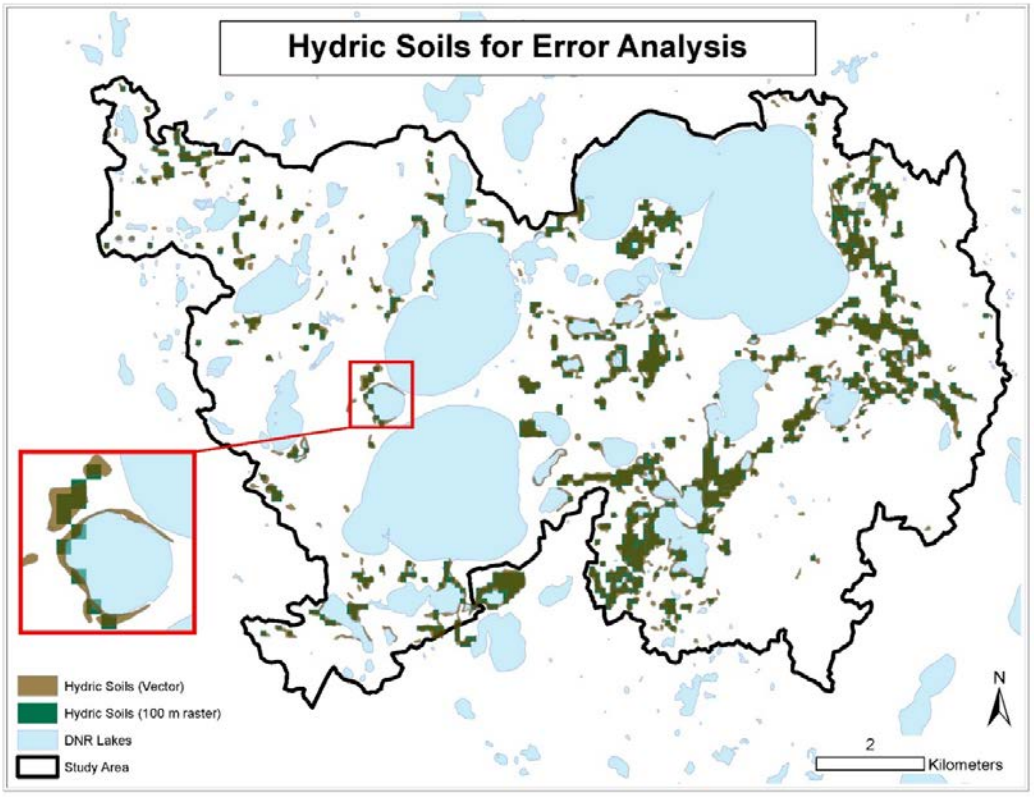

Figure 10. Hydric soils used for error analysis of estimated water table elevations. Brown polygons show hydric soils as mapped by the NRCS in vector format. The green cells indicate the location and extent of the gridded and resampled hydric soils at 100m spatial resolution.

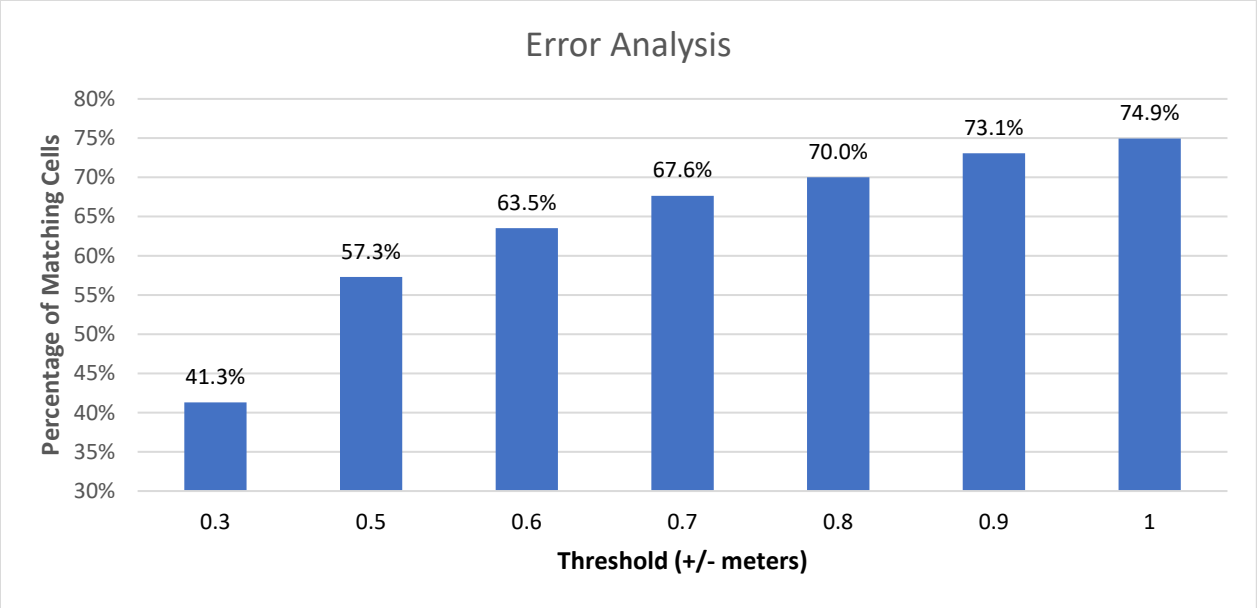

Figure 11. Hydric soil and water table error analysis results.

Cell-by-cell Groundwater Balance

The cell-by-cell groundwater balance residual map (Figure 12) indicates where recharge and discharge likely occur across the landscape. Negative values (brown cells) indicate groundwater recharge. Positive values (purple cells) indicate groundwater discharge. The cells of greatest interest are the dark purple cells adjacent to lake shorelines, as they indicate potential lake-bottom groundwater discharge. Four areas displayed strong discharge along accessible lakeshores (Figure 13).

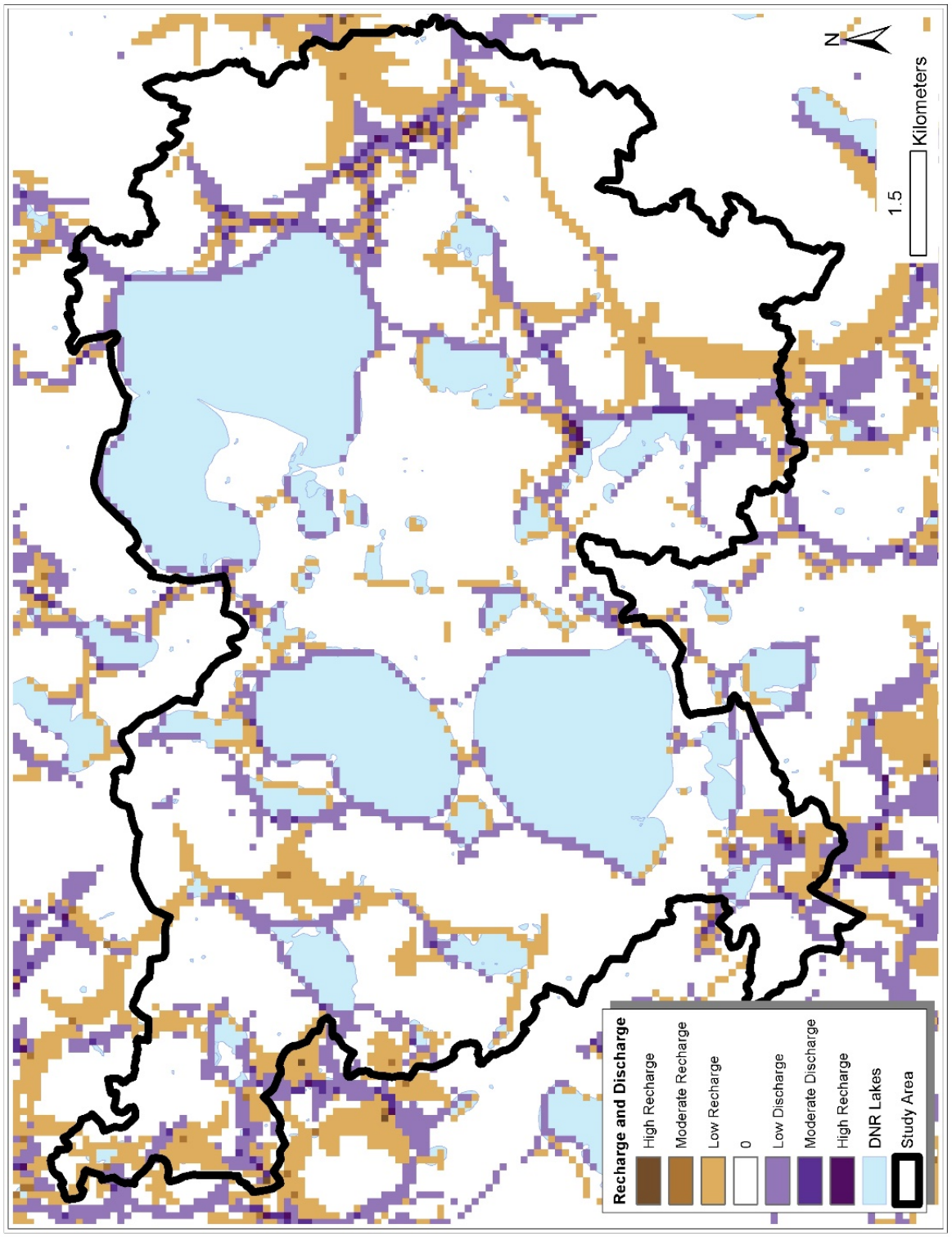

Figure 12. Groundwater recharge and discharge.

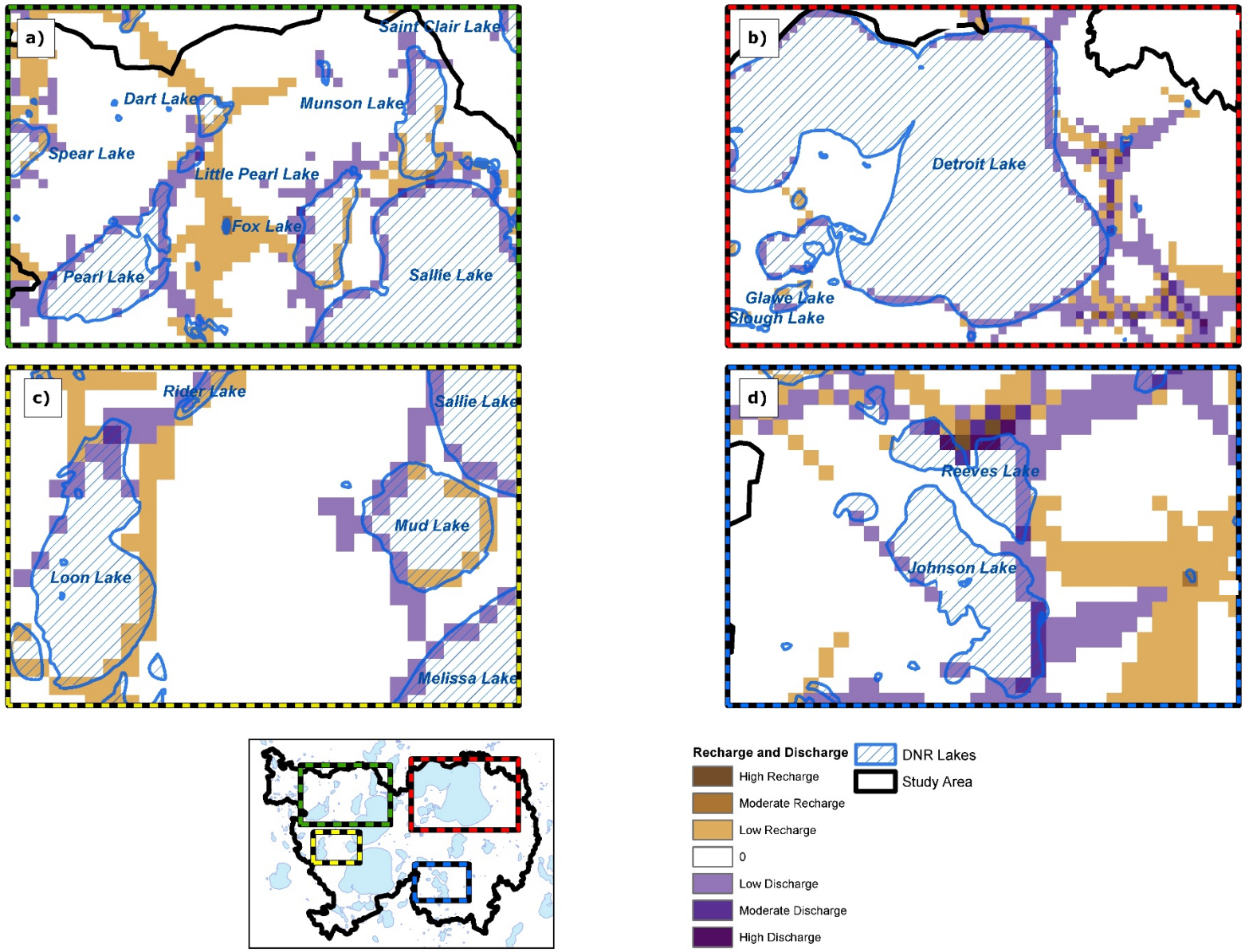

Figure 13. Areas of distinct shoreline groundwater discharge

Area 1 (Figure 13a) shows strong discharge on the north and west sides of several of the lakes. The western margin of Pearl and Little Pearl lakes shows moderate discharge, with two individual cells of strong discharge. Dart Lake has one moderate discharge cell on the northwest margin; however, much of the shoreline displays moderate recharge. Fox, Munson, and Sallie lakes have moderate to strong discharge occurring along the north and western margins. Moderate to high recharge zones occur on the eastern and southern margins.

Area 2 shows the eastern shore of Detroit Lake having moderate to strong discharge (Figure 13b). The strongest discharge cells are located where streams or wetlands are present.

Area 3 (Figure 13c) shows strong to moderate discharge along the north and western margins of Loon Lake, while Mud Lake displays moderate discharge along the western margin. Recharge occurs along the eastern margins of each waterbody.

Area 4 (Figure 13d) shows Reeves and Johnson lakes in detail. Reeves Lake has strong discharge along the northern margin, with recharge occurring in an isolated cell on the western end of the lake, which is adjacent to a large wetland. Johnson Lake has strong discharge occurring along the eastern margin. When water levels are high, the lakes can be connected by open water. Floating bogs are abundant in both lakes. At the time of the survey, lower water levels had allowed several of the floating bogs to become stuck in the shallow area between the two lakes, some taking root and making the channel impassable by watercraft.

Satellite Imagery

Relative temperature differences are observable across the three maps, and many locations stand out as areas of potential groundwater discharge zones needing further

investigation. It is important to note and discuss the several factors likely contributing to the locations of “cold” and “warm” water spots shown on the maps. Geologic, hydrologic, and data processing techniques all contribute to the apparent temperatures.

Locations of Interest

While viewing the images, it is important to note that the darkest colors within each individual waterbody could represent groundwater discharge. Shallower lakes are likely to have warmer overall temperatures than the larger, deeper lakes such as Detroit, Sallie, and Melissa. These larger lakes have a higher volume of water, which takes significantly longer to respond to air temperatures. Since groundwater most often discharges near the shoreline (John and Lock 1977; Lee 1977; Pfannkuch and Winter 1984; Winter and Pfannkuch 1984), cold plumes near the shoreline and in shallower regions of the lake may be an indication of groundwater discharge.

July 2006 Image. The most noticeable dark lake pixels in the July 2006 ASTER image are seen in Detroit, Sallie, and Melissa, and are predominantly located in the northern halves of each waterbody (Figure 14). These appear to correlate with the location of the Pelican River as it enters the waterbody. Examining the largest lakes in greater detail, thin lines of black (cold) pixels can be observed along the western and southern edges of Sallie and Melissa, as well as in the southern portions of Detroit. Several of these edges correspond to sharp changes in topographic relief, which often results in groundwater discharge.

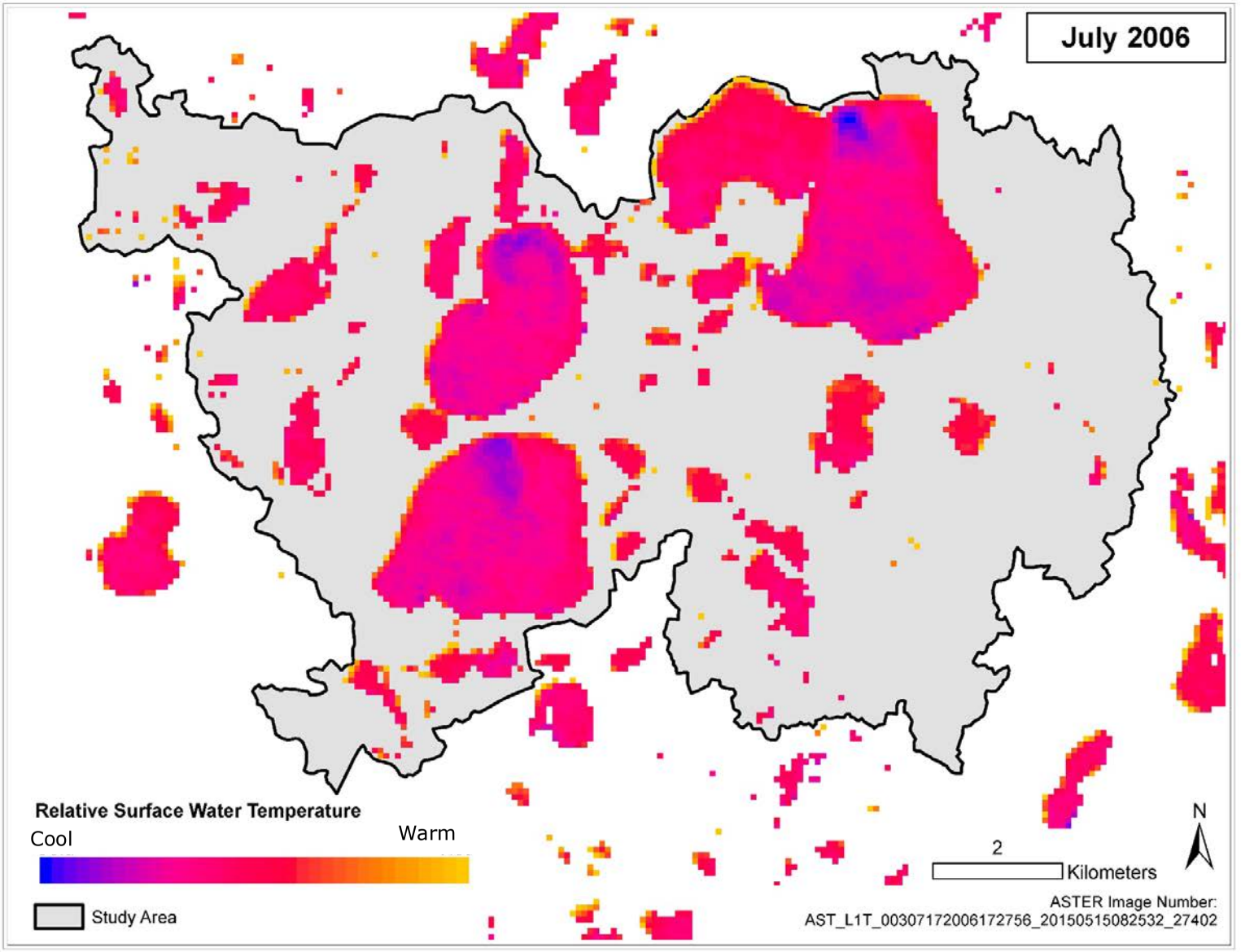

Figure 14. Relative surface water temperatures, July 2006 (ASTER).

August 2006. On the August 2006 image (Figure 15), Detroit Lake displays a very different pattern from July. The most evident dark pixels are located along the western shore of the largest lobe of the lake, with smaller areas located along the southern shore. These potential groundwater discharge zones are likely due to steep changes in groundwater gradient due to topography. The cool spot on the southeastern shore could be attributed to steep groundwater gradients. Lake Sallie has smaller areas of interest along the southeast and southwest shorelines, likely due to steep gradients. Interestingly, Mud Lake located just to the southwest of Lake Sallie shows a large influx of cool water originating from the southwest shore. Lake Melissa still shows a plume along the north that is likely the Pelican River. Prominent dark spots are also apparent along the eastern and west-central shores, and may indicate groundwater discharge.

September 2015. The September 2015 ASTER image shows a trend of cool temperatures along the western side of the watershed, with most of the warmest temperatures occurring in the western half (Figure 16). It is physically unlikely to have such a dramatic trend, and possible that the image data were not suitable due to unforeseen factors. Atmospheric influences not removed in the atmospheric correction step of image processing may have caused this apparent trend.

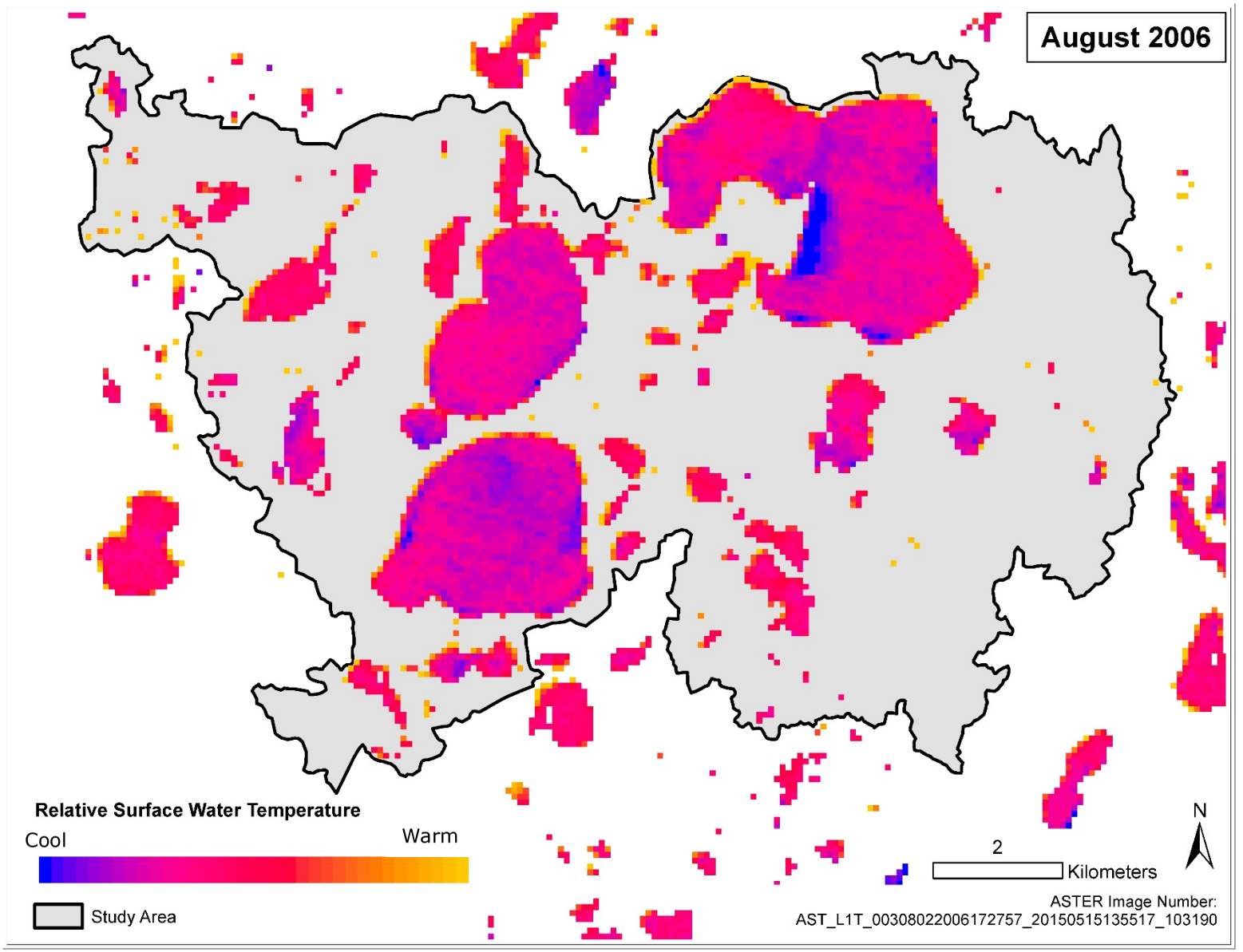

Figure 15. Relative surface water temperatures, August 2006 (ASTER).

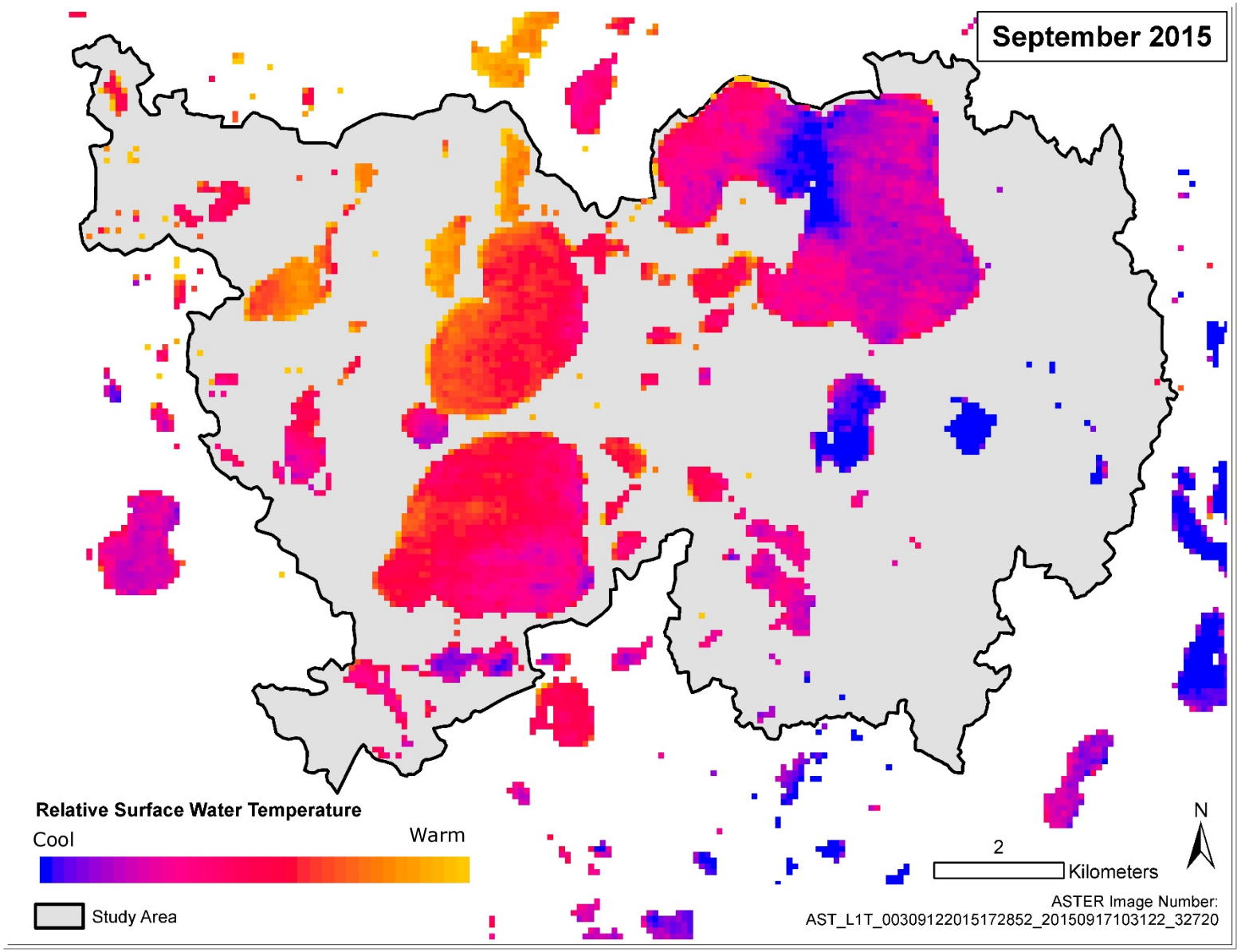

Figure 16. Relative surface water temperatures, September 2015 (ASTER).

UAV Imagery

This section describes the results obtained by examining individual thermal images for cool areas indicating springs or seeps. The following examples reveal the images where a strong surface water temperature was observed.

Locations of Interest

Location 1 (Figure 17 (46.782487°,-95.912245°)) is in the northwest corner of Fox Lake (Figure 13a) and corresponds closely to the northern-most strong discharge indicated by the discharge model (Figure 13a). Cool water appears to flow outward and toward the deeper center of the lake at several locations along the shoreline (Figure 17a). Cool water is also seen flowing outward from the shoreline to the left of the dock and indicates a potential seepage zone (Figure 17b).

Location 2 (Figure 18 (46.792860°, -95.925957°) is in Dart Lake in a location not predicted by the discharge map (Figure 10a). An area of diffuse cool water is clearly visible adjacent to fallen trees and a low, often wet area in a row crop field on the north side of the lake. The cell-by-cell flow model indicated seepage would be occurring near the northwest corner of Dart Lake; however, none is visible in the thermal imagery. It should be noted that although no groundwater discharge is visible, a wetland area that appears to connect to the lake during high water levels is present in that location.

Location 3 (Figure 19 (46.775417°, -95.910901°) is along the west side of Fox Lake and shows focused flow coming from an adjacent wetland. The RGB imagery indicates the presence

of thick aquatic vegetation along the flow path, which contrasts with the apparently unvegetated lake bottom around it.

Location 4 (Figure 20 (46.737819°, -95.836986°) is on the southeastern edge of the peninsula between Reeves and Johnson lakes. Focused discharge originates from a pipe emerging from the hillside at the shoreline. This flows into the shallow, thickly vegetated lake margin where the signature is almost immediately lost.

Location 5 (Figure 21 (46.774296°, -95.807123°) shows the cool water of Sucker Creek discharging into Detroit Lake and flowing north-northeast.

Location 6 (Figure 22 (46.805120°, -95.815195°) shows a spring or culvert draining into Detroit Lake near the northeastern public boat launch. Iron staining on the rocks along the shoreline is visible at the discharge point in the RGB imagery.

Location 7 (Figure 23) is an example of how floating bogs appear cool in temperature, and should not be mistaken for groundwater point discharge. The bogs are pushed around the lake by the wind, sometimes becoming anchored to the lake bottom during low lake water levels. Floating bogs pushed up against the shoreline several lakes, obscuring the water temperature adjacent to the shoreline in those locations.

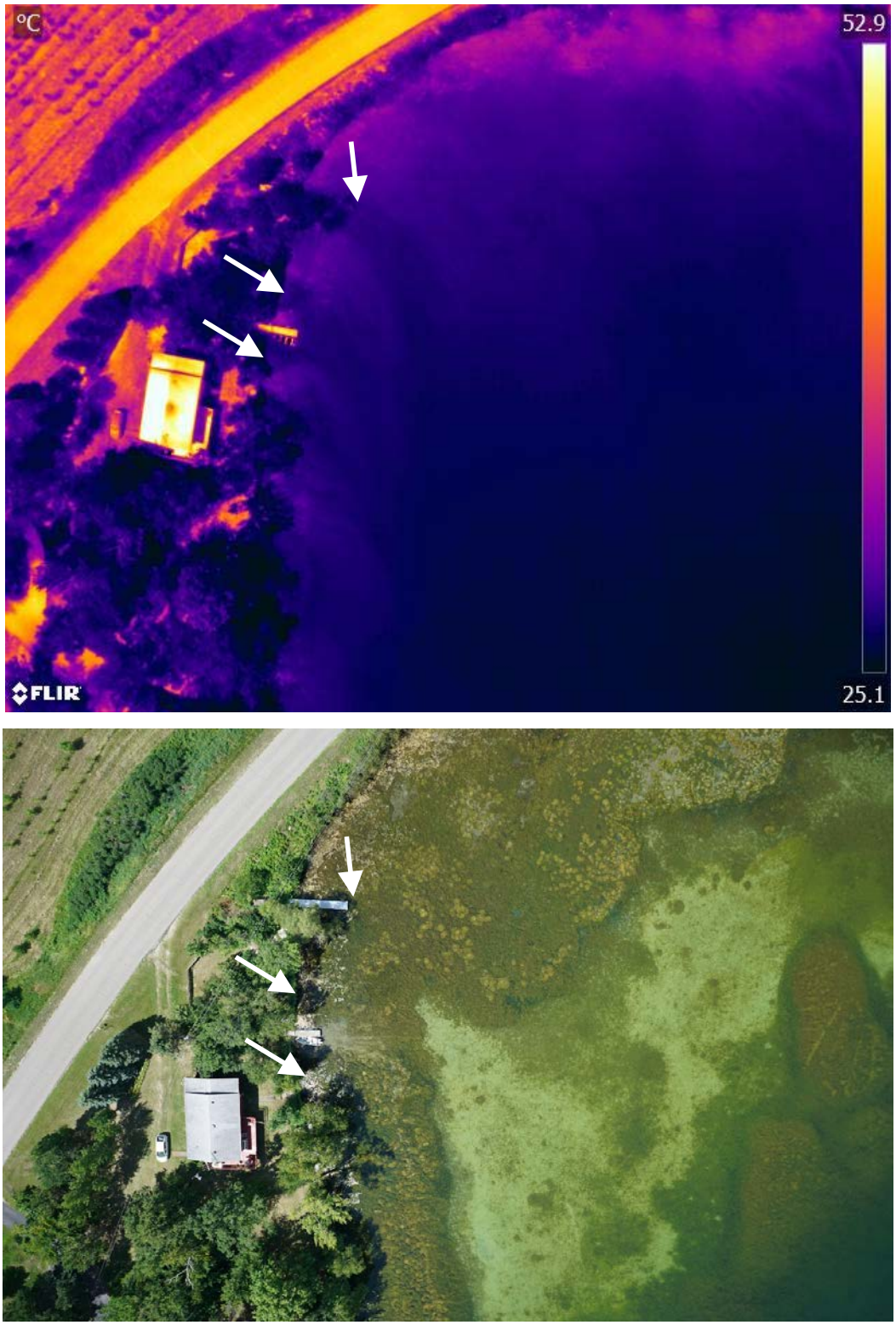

Figure 17a. Potential springs or seeps on Fox Lake. Cool (dark) streaks originating from shadowed shoreline areas.

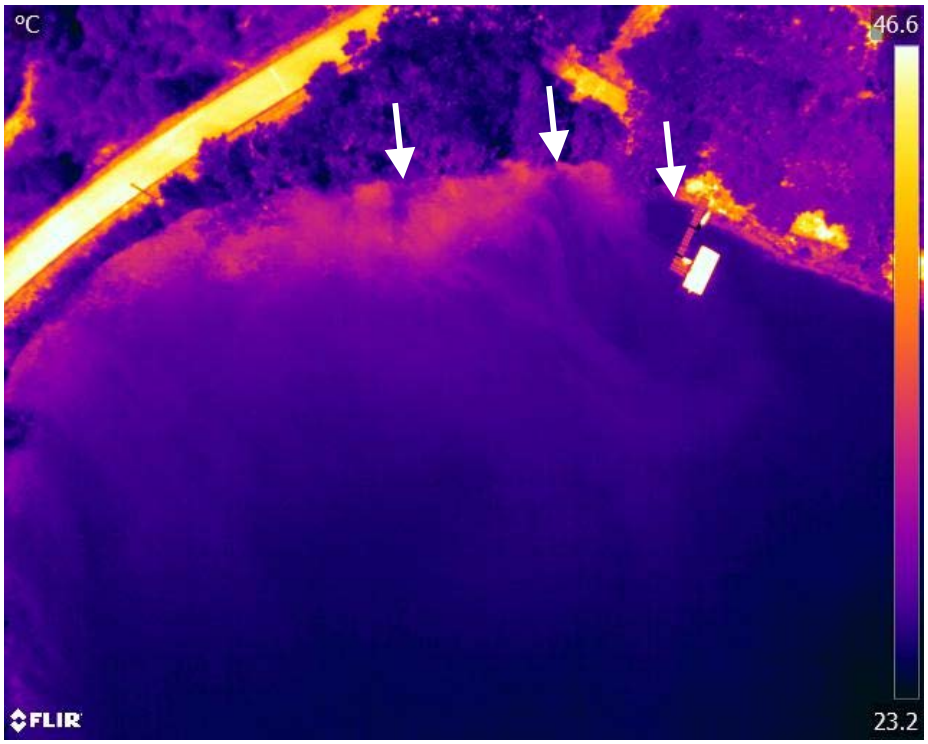

Figure 17b. Potential springs or seeps on Fox Lake.

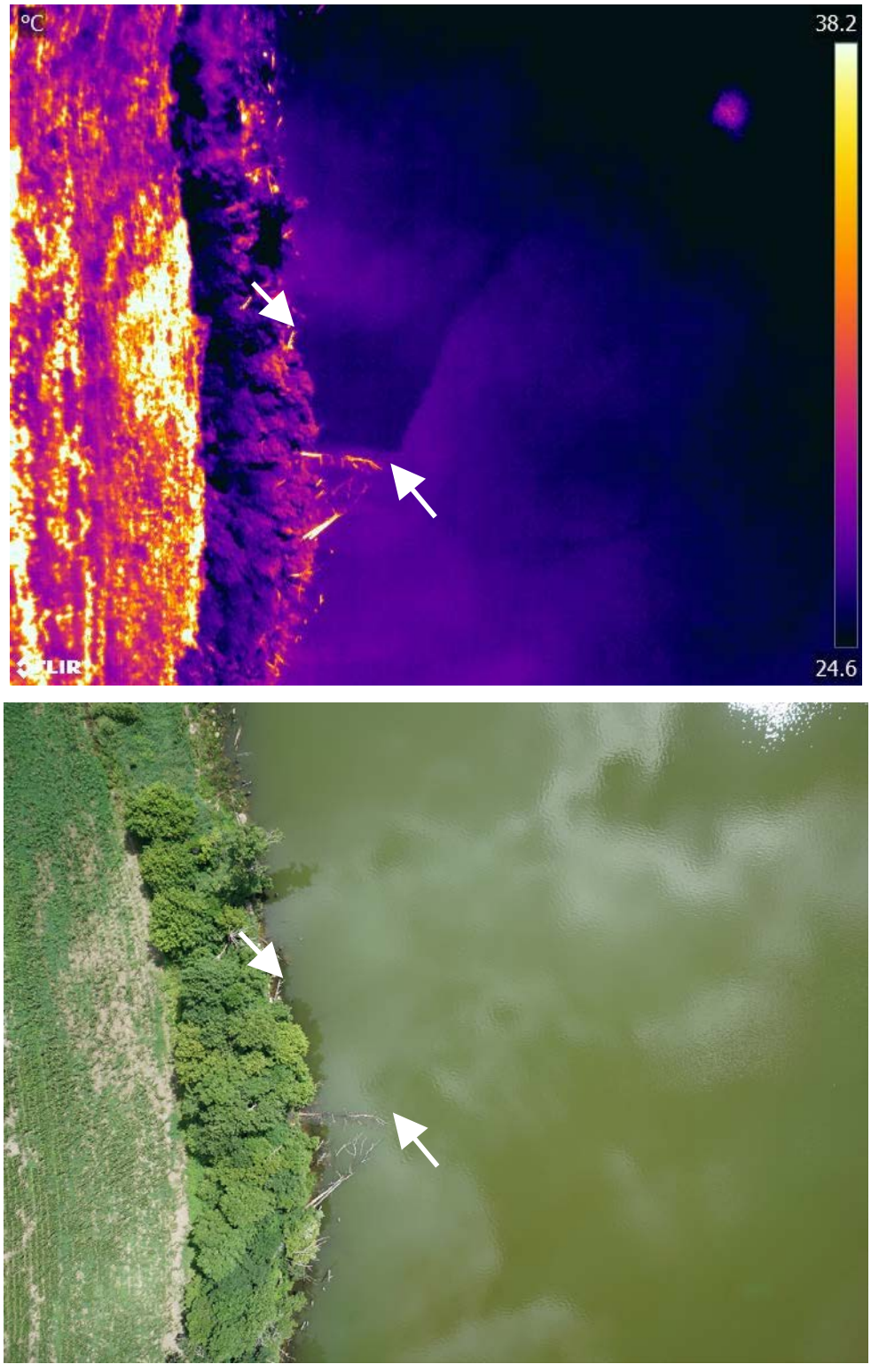

Figure 18. Seep on Dart Lake.

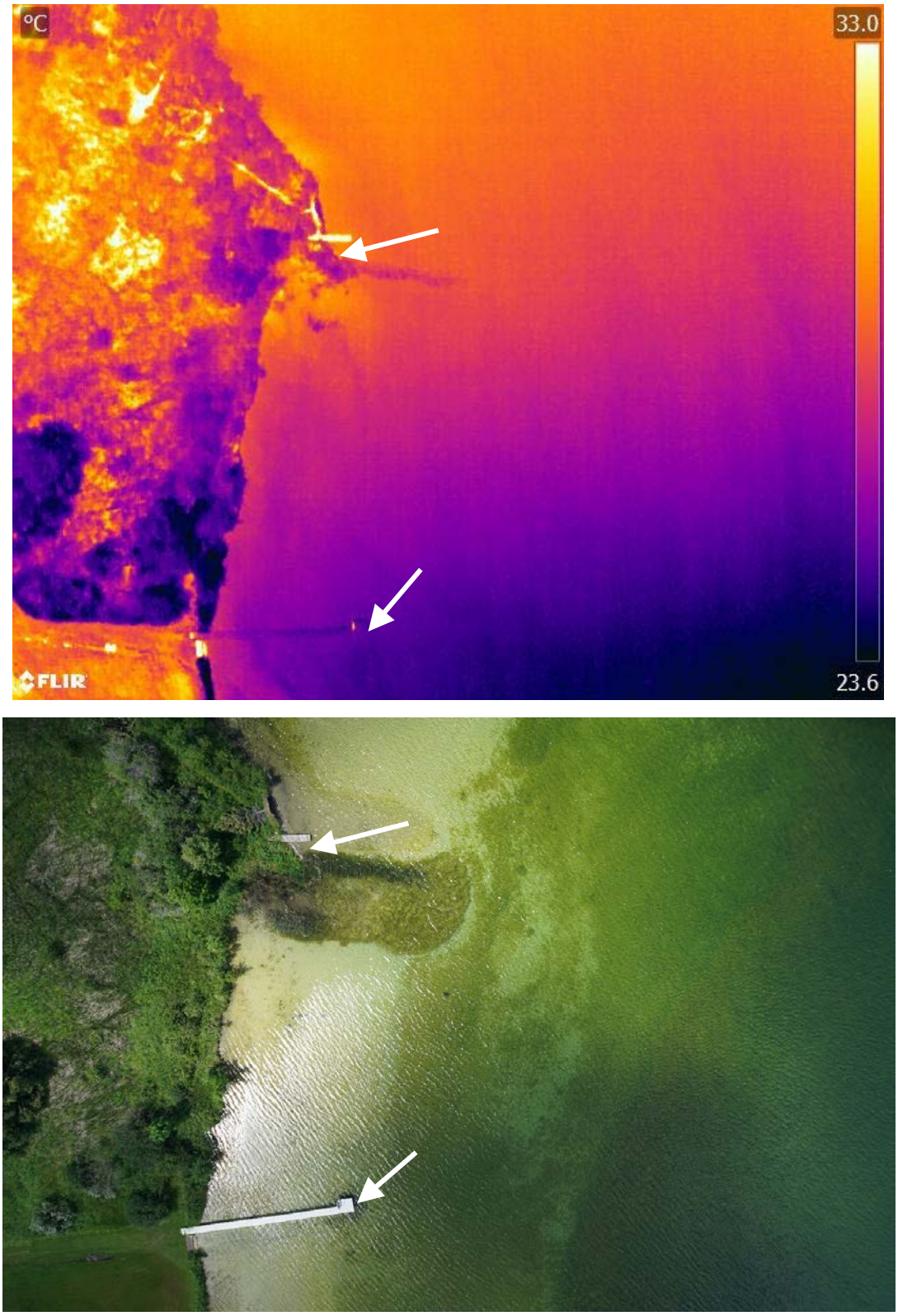

Figure 19. Surface water drainage from wetland adjacent to Fox Lake.

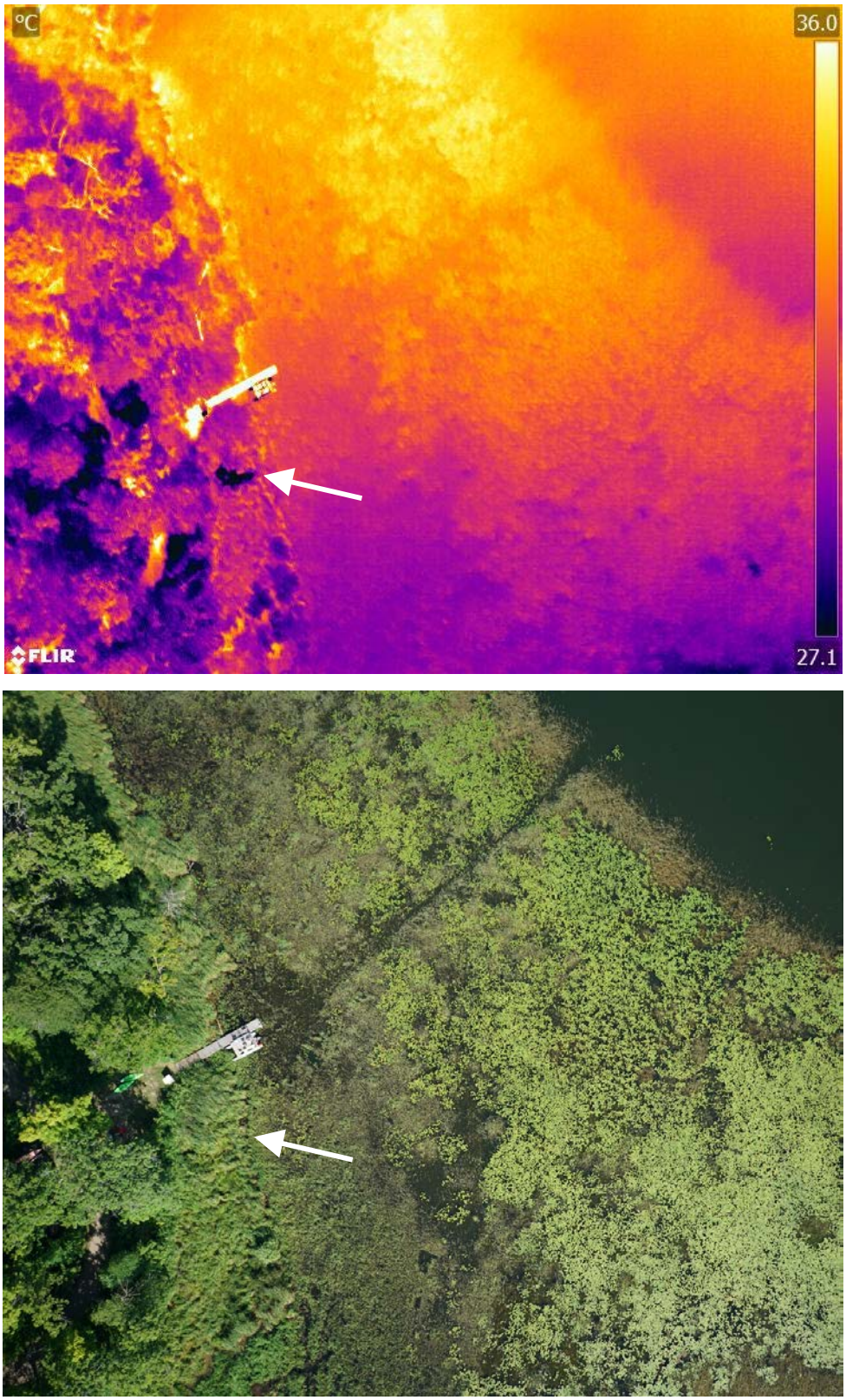

Figure 20. Spring emerging from pipe near shoreline on Johnson Lake.

Figure 21. Sucker Creek entering Detroit Lake.

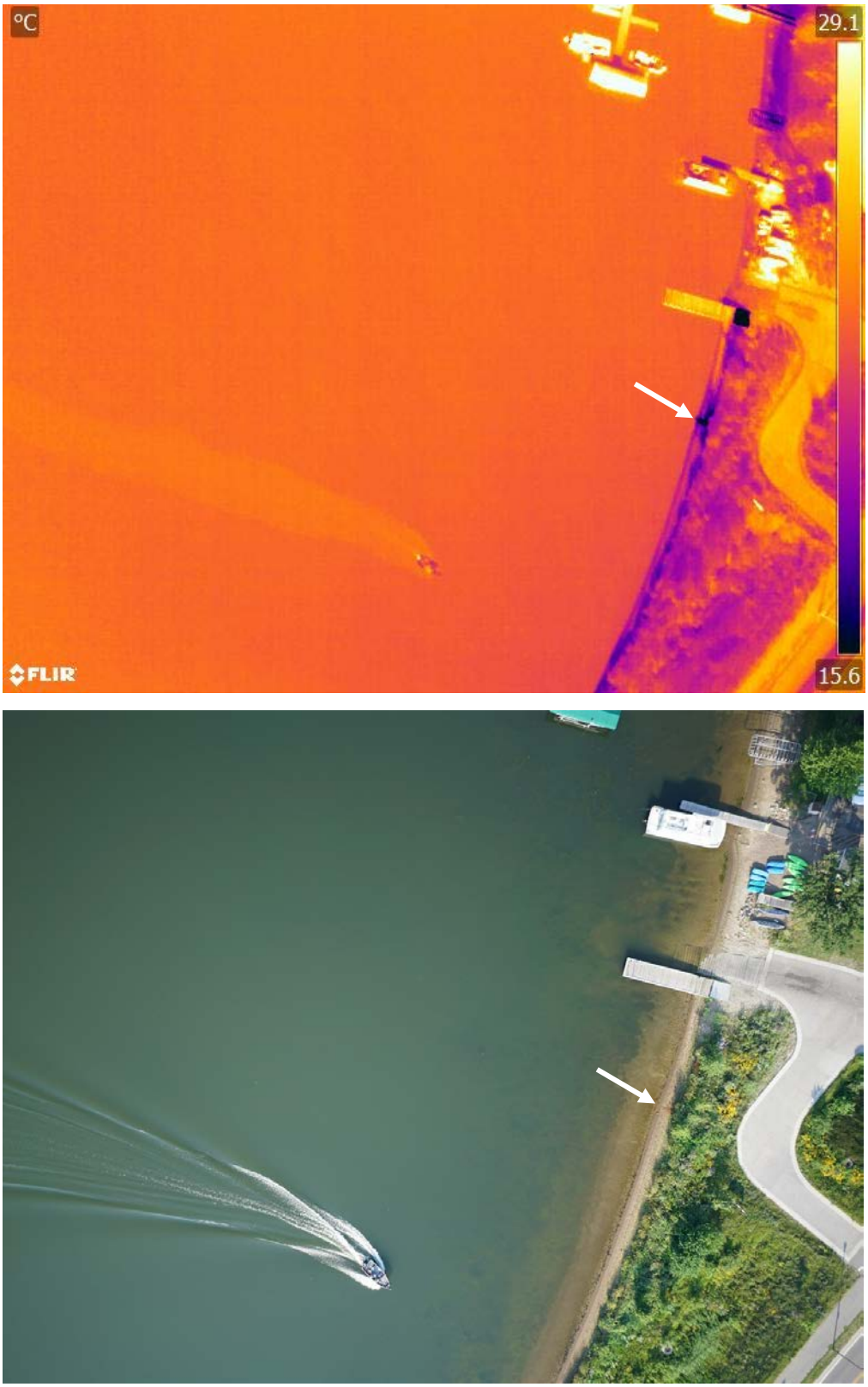

Figure 22. Spring or culvert entering Detroit Lake.

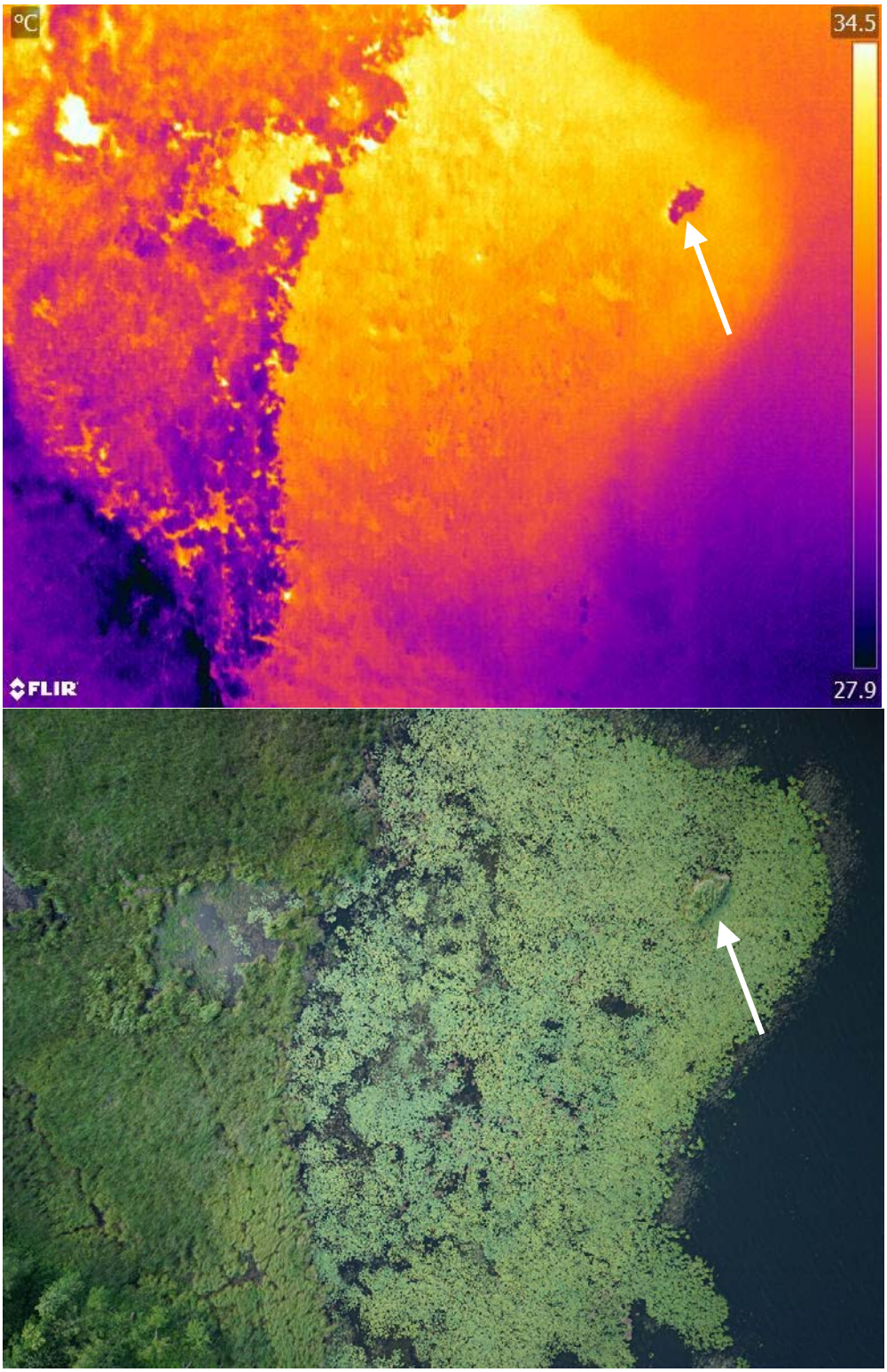

Figure 23. Floating bog on Johnson Lake.

Ground Calibration

The observed ground calibration temperatures for air and water provided a reference for temperatures recorded by the UAV thermal imagery. Diurnal fluctuations in air temperature during the two days of surveying revealed that the average maximum was 35℃, the average minimum was 14℃, with an average temperature of 23℃. Diurnal fluctuations in surface water temperatures during the two days of surveying revealed that the average maximum was 32℃, the average minimum was 22℃, with an average temperature of 26℃. Surface water temperatures for each lake and air temperatures for three sites are shown in graphs (Appendix F).

Temperatures recorded by water thermistors were compared with temperatures indicated by UAV thermal imagery by visually estimating the locations of the thermistors in the thermal images (Appendix G). Overall, UAV temperatures failed to reliably report surface water temperatures. At best, the UAV was within 0.2℃. At worst, the UAV thermal sensor recorded a temperature that was as much as 29℃ different from one recorded by the thermistor. The standard deviation of UAV temperature from the thermistor temperature was 7℃.

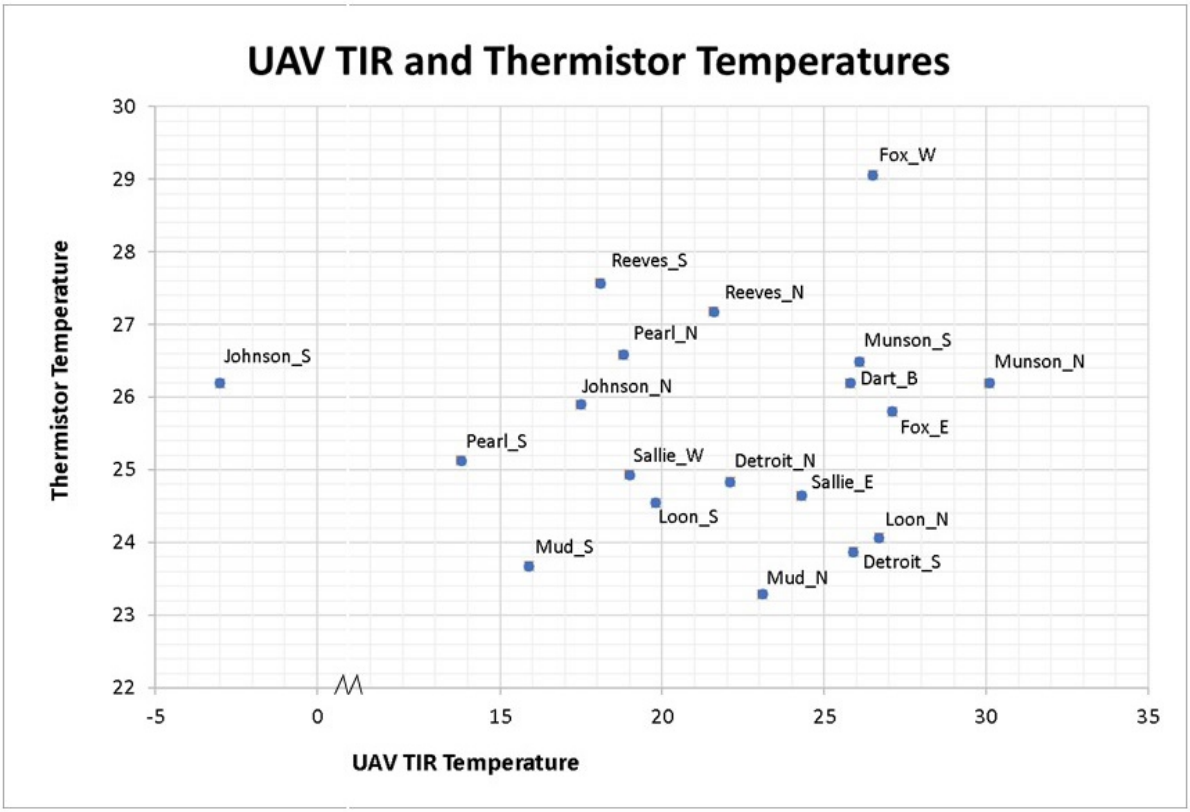

Figure 24. Comparison of surface water temperatures recorded by thermistors and UAV imagery at each thermistor location.

CHAPTER IV

DISCUSSION

Water Table Estimation and Darcy Flow Model

The model of the water table functioned reasonably well, matching the 75% of the hydric cells matched within 1 m, which is likely within the typical range for the annual rise and fall of the water table in the area. The steepest slopes of the water table (Figure 9) do not always coincide with changes in surficial geology (Figure 3). These larger slopes may be the result of an abrupt change in recharge and or hydraulic conductivity. Where the relatively low-permeability sediments of the three moraines meet the outwash plain, steeper slopes are observed with lower hydraulic conductivity the likely cause. Smaller areas of steeper slopes, located adjacent to Fox Lake and south of Buck Lake, could be attributed to higher recharge rates, as they are located entirely within the outwash plain. Further study of the surficial geology in the area would be necessary to obtain a definitive answer.

Incorporating more data points in the form of consistently saturated National Wetland Inventory (NWI) wetlands would likely improve the water table model without requiring much field work or time. Wetlands belonging to non-tidal wetland water regime classes F, G, and H of the new Cowardin classification system should be used, as they indicate semi-permanently flooded, intermittently exposed, and permanently flooded areas. Other water regime classes are not saturated as regularly, and may not provide a reliable indicator of the water table.

The error analysis using the hydric soil elevations demonstrated agreement with 75% of elevations falling within the 1 m threshold. It is important to note that hydric soils can form as a result of a perched water table, and therefore may not reflect closely the elevation of the water table at all locations. When using this method for error analysis, it is necessary to review the elevations and landscape positions of the hydric soils to verify that they are likely connected to the water table.

Small-scale heterogeneities in sediments (>10 m) in and around the lakes influence groundwater flow paths (Winter 1999; Kishel and Gerla 2002), and were not accounted for in the model. These small-scale heterogeneities have not been mapped, and therefore could not be included.

Satellite Imagery Analysis

Satellite imagery largely failed to provide a meaningful way to identify springs and seeps within the study area. A disadvantage of satellite imagery, when compared to UAV imagery, is that is affected by atmospheric interference, and not all interference can be filtered out quickly and easily using existing tools. When processing the ASTER data, the gridded 90 m TIR pixels are clipped to the irregular shapes of the lakes. Pixels that cover both land and water surfaces have values that reflect both. Note that the edges of many of the lakes appear to be very warm. This is likely due to pixels covering the warm land surface and skewing to the warmer values, which is then reflected in the whole pixel value (Figure 20). To eliminate this issue, a 90 m buffer could be created along the shorelines; however, many small lakes and waterbodies could be removed as a result (Becker and Daw 2005).

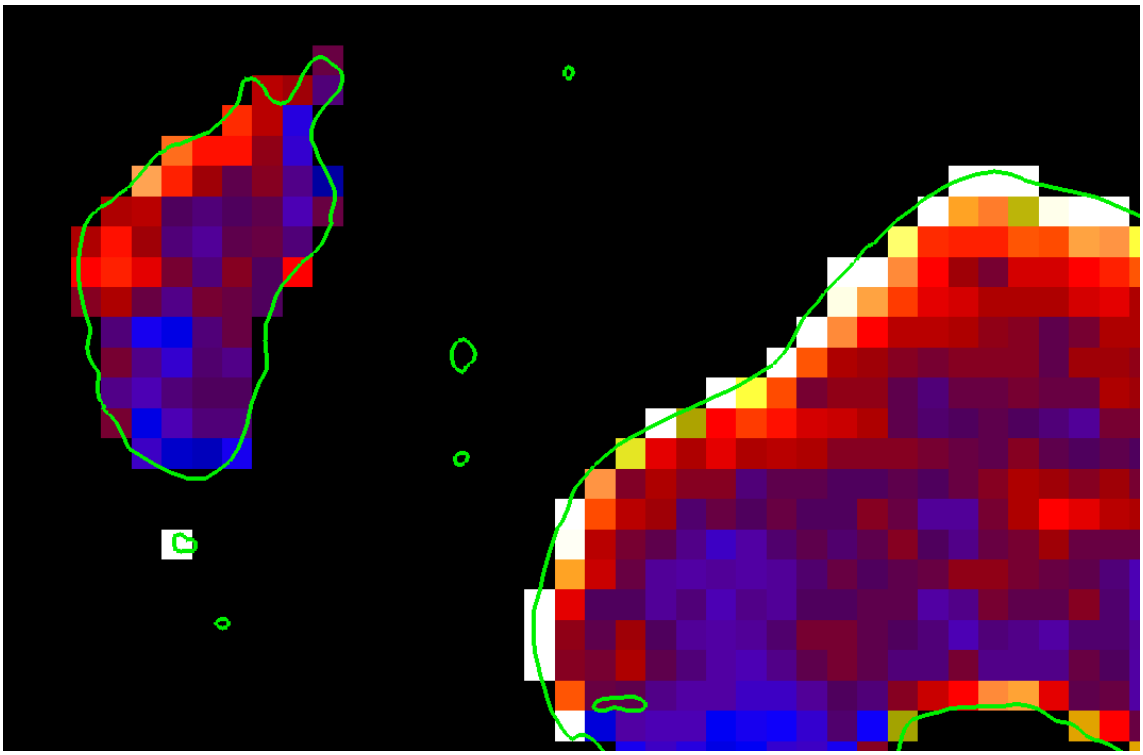

Figure 25. Lake boundaries and relative lake surface temperature (ASTER). Pixels that cover both land and water surface do not provide accurate temperatures for either surface.

UAV Imagery Analysis

Surface water flowing into the surveyed lakes was easily visible; however, diffuse discharge flowing into the lakes, if present, was not readily located. A few potential springs and several seeps were revealed in the thermal imagery. The method worked very well for identifying surface waters flowing from streams and wetlands into the lakes, which were located in or near discharge cells on the recharge and discharge map (Figures 12 and 13). Groundwater discharging subaerially was most easily seen, even through dense vegetation. For example, seeps on Fox and Dart lakes and the spring on Johnson Lake were strongly visible, and located within 300 m of discharge cells indicated by the recharge and discharge maps (Figures 12 and 13).

Other shoreline locations mapped as discharge zones did not reveal visible groundwater in the thermal imagery. Groundwater discharge rates may be too low to create a large enough temperature difference when mixed with surface water. Another possibility is that the groundwater is discharging deeper into the lake, and is not seen because the colder, more dense water remains close to the bottom (Hare et al. 2015). This issue cannot be resolved with this method, as aerial thermal imagery only collects surface or skin temperatures. Vertical temperature probes would need to be used to determine the presence of deeper groundwater seeps (Hare et al. 2015).

An alternative explanation for not detecting many seeps may be that diffuse flow is not the most prevalent discharge pattern. If this is the case, it is likely that heterogeneities in the geologic substrate are playing a vital role in influence flow pathways.

Upon reviewing the RGB images alongside the thermal images, some cool zones in the surface water were attributed to shadowing from overhanging vegetation or structures, or the presence of dense floating bogs.

The sensor was not self-cooling, and therefore results were likely inconsistent because of instrumental drift. Additional heat was created at the sensor as a result of direct sun exposure and heat produced by the operation of the sensor itself (FLIR 2016). This resulted in the same object shown in two consecutively ordered photos taken 1 second apart to appear to have two different temperatures (Appendix G, Munson Lake South). Because of the difference in temperature for the same object, normalizing each image and then attempting to stitch overlapping images using Photoscan (Agisoft LLC, St. Petersburg, Russia) or Pix4Dmapper (Pix4D

S.A., Lausanne, Switzerland) did not provide useful or accurate results, even with the modest goal of comparing relative, not absolute, temperatures across the image. Another concern is that large-scale diffuse discharge will not be seen in one image when flying at lower altitudes, and may not be visible as a result of the relative temperature changing frame by frame. Further study could determine how much discharge needs to occur before it is visible with the thermal camera.

High-resolution imagery makes for very large files. Processing these images can be very time and processing power intensive. Imagery for 11 lakes was collected, producing 158 gigabytes of data. This requires a large amount of storage space.

Influencing Factors for All Thermal Imagery

Geologic factors

Outwash sand and gravel comprise most of the study area, while Pearl, Little Pearl, Dart, and part of Johnson lakes are underlain by clay till. Clay till is not as permeable as sand and gravel; therefore, groundwater discharge is less likely to occur into lakes underlain by clay till. Groundwater discharge is focused on the littoral zone of lakes (John and Lock 1977; Lee 1977; Pfannkuch and Winter 1984; Winter and Pfannkuch 1984; Kishel and Gerla 2002), which often have more abundant organic debris and heterogeneous sediments. This will alter the simple patterns of groundwater discharge into lakes that are predicted by water table gradients alone.

Hydrologic factors

Surface water flowing into lakes from streams could be a controlling factor, as previous groundwater flow models have shown that the Pelican River is a gaining stream (Miller, 1983),

meaning it receives groundwater discharge along its reach. Lake depth and volume relate directly to how quickly a body of water responds to changes in air temperature. Larger bodies of water take longer to gain and lose heat. Cold water sinks below warm water, and may not rise to the surface where the signature can be viewed with thermal imagery (Hare et al. 2015).

Weather factors

Wind speed and direction effect the mixing of the surface and groundwater, causing diffuse groundwater discharge to be masked by warmer temperatures. In addition, this mixing action plays a role in displacing cool groundwater plumes from the exact discharge location.

Ecological factors

Vegetation both on and in the water obscured origins and signatures of springs and seeps. Floating and emergent aquatic vegetation appeared to have a warming effect on the surface water skin temperature, potentially masking cooler groundwater. Trees overhanging the shorelines produced shadows and made it difficult or impossible to discover from the imagery alone whether the discharge zone could be attributed to a spring on the shoreline or a seep. Floating bogs tend to accumulate on lake margins according to wind direction, further obscuring the water near the shoreline.

CHAPTER V

CONCLUSIONS AND RECOMMENDATIONS

Modeling the water table using elevations of lakes and streams extracted from a DEM provided reasonable results. Select hydric soils provide a reasonable indicator of reliable water table presence for modeling in data-poor areas. Through an iterative process of including more water table elevation control points -wetlands and streams – a more accurate water table model can likely be achieved.

The large-scale imagery coupled with local thermal heterogeneity leads to limited information on groundwater discharge from satellite imagery.

Use of a UAV and collection of higher resolution imagery provides better results. Excessive drift and significant mismatch of temperatures among images suggest that better results may be achieved by using a self-cooling thermal camera that can maintain accurate temperature measurements from frame to frame. Collecting imagery at higher altitudes would increase the area included in a single frame, and may enable large diffuse zones of groundwater discharge to be more easily viewed. High-resolution RGB imagery should always be collected in conjunction with the thermal imagery to assist in identifying features. Thermal imagery collected at night would eliminate interference by shadows and reflections on the surface water.

Results suggest that large, well-defined springs and seeps can be identified with UAS imagery, but that slower and more diffuse groundwater seepage in shoreline areas is obscured by many factors, including differences in land cover, changing weather conditions, emergent vegetation, sediment characteristics, and shoreline development.

APPENDICES

Appendix A

Data Collection

- 1/3 arc-second (10 meter) Digital Elevation Model
    - USGS National Map Viewer: https://viewer.nationalmap.gov/basic/
- Subwatershed boundaries
    - Minnesota Department of Natural Resources: https://gisdata.mn.gov/dataset/geos-dnr-watersheds
- Generalized Lakes, Waterbodies, Rivers, and Streams
    - Minnesota Department of Natural Resources: https://gisdata.mn.gov/dataset/water-dnr-hydrography
    - USGS National Map Viewer: https://viewer.nationalmap.gov/basic/
- Minnesota state and county boundaries
    - Minnesota Geospatial Commons: https://gisdata.mn.gov/dataset/bdry-counties-in-minnesota
- Pelican River Watershed District Boundary
    - Pelican River Watershed District: www.prwd.org
- Surficial Geology
    - Minnesota Geological Survey: https://gisdata.mn.gov/dataset/geos-quaternary-geology-mn
- Soil
    - created by the NRCS, obtained from Becker County GIS: http://www.co.becker.mn.us/online_services/GIS_data.aspx

Appendix B

Water Table Interpolation

Alternative Method to Interpolate the Water Table by Dr. Phil Gerla, University of North Dakota

1. Download the 10m DEM and NHD lakes and streams coverage. (Data are available here: https://viewer.nationalmap.gov/basic/). UTM projection works best for our purpose.
2. Load the data into ArcMap and export the lakes and streams data from the gdb and into projected shape files. Note - there may be many other components of the gdb that are not needed. Toggle their view to make sure.

3. Use the Feature2Point tool to convert polygons (lakes) and lines (streams) to points, turn on the Inside option (checked) so that the point falls within the lake polygon. For streams, you may want to choose Feature Vertices2Points, although it may require a little editing to parse some of the vertices. On the other hand, Feature2Point may provide too few points for the streams.

4. Using the DEM, run the Extract Values2Points tool to find the elevations of the points for both files created in the previous step.

5. Join the lakes polygon file to the elevations associated with its point (i.e., create an elevation field for the lake features). Export or otherwise save the attribute file with the new elevation information. (Joins will not automatically save, so I exported the joined layer as a new shape file).

6. Create a nominal grid with the desired cell size using the Create Constant Raster tool. For simplicity, I selected a 100 m cell size and chose the bounding x-y coordinates in whole integral values to the nearest 100 m. Be certain to provide plenty of buffer around the area of interest.

7. Populate cells of this raster with the best-fit value for the water table elevation. Do this using the following steps:

a. Set the environment so that the output extent and snap raster are set to your nominal grid (step 6).

b. Use the lake points file, and stream points files that include the elevation field to find the best fit elevation for each cell. Use null for empty cells, which should be done automatically by ArcMap.

c. Do this by using the Polygon2Raster and Point2Raster tools. Be sure to set the environment to match the nominal grid!

d. Then use the Mosaic2NewRaster tool to combine the two rasters created in step 7c together.

8. Convert the mosaic grid into a point shape file so it can be interpolated. Use the Raster2Point tool

9. Edit the output to eliminate any points that seem way out of whack (usually stream cells or spots where there might be a perched water table).

10. The points should then be ready to interpolate into a grid. Again, use the nominal grid's properties to do this. Natural Neighbor seems to be the easiest to use and is designed for clustered data.

Appendix C

ASTER TIR Instrument Characteristics (NASA 2017)

Characteristic	TIR
Spectral Range	Band 10: 8.125 - 8.475 µm
	Band 11: 8.475 - 8.825 µm
	Band 12: 8.925 - 9.275 µm
	Band 13: 10.25 - 10.95 µm
	Band 14: 10.95 - 11.65 µm
Ground Resolution	90m
Data Rate (Mbits/sec)	4.2
Cross-track Pointing (deg.)	±8.55
Cross-track Pointing (km)	±116
Swath Width (km)	60
Detector Type	HgCdTe
Quantization (bits)	12

Appendix D

ASTER TIR Processing

The following steps (Yale University 2016), were completed to convert raw TIR imagery into Kelvin.

1. From the Toolbox select Radiometric Correction | Radiometric Calibration and select the five-band TIR file. Make sure the Calibration Type is Radiance, enter a new filename, and click OK.

2. From the Toolbox select Radiometric Correction | Thermal Atmospheric Correction and select as input the file created in Step 1. In the dialog window take all defaults and enter an output filename to create the input to the Emissivity Normalization process.

3. Again from the Toolbox, select Radiometric Correction | Emissivity Normalization and select the Thermal Correction file just created in Step 2. Take all defaults, make sure the Output Temperature Image is toggled to Yes and enter a filename for this.

The result is a brightness temperature file with units in Kelvin.

Once the Kelvin temperature file was created for the entire image, the DNR 24k lakes shapefile was used to create a mask to block out the land surface, allowing the focus and scaling to be exclusively on the waterbodies.

The mask was generated by using the following steps:

1. In ENVI under Tools, open Raster management >Masking and select Build Mask.

2. Choose Select EVF > then select the desired shapefile. In this case it was DNR 24k Lakes.shp. Choose the temperature image as your Target image. This creates a .tif file that assigns value of 0 to land surface, and 1 to lakes.

3. In band math, multiply the temperature image by the lake mask raster. Land surface temperature values become 0, and lake surface values stay the same. The result is a masked image showing surface temperatures only for the lakes.

An appropriate color ramp was then selected to display the relative temperatures of the lakes. The resulting images show relative temperature across each individual image. Dark colors represent cool temperatures, while lighter colors represent warmer colors. See the appendix for the Relative Surface Temperatures of Lakes maps.

Appendix E

Historical Lake Water Levels
(Minnesota Department of Natural Resources)

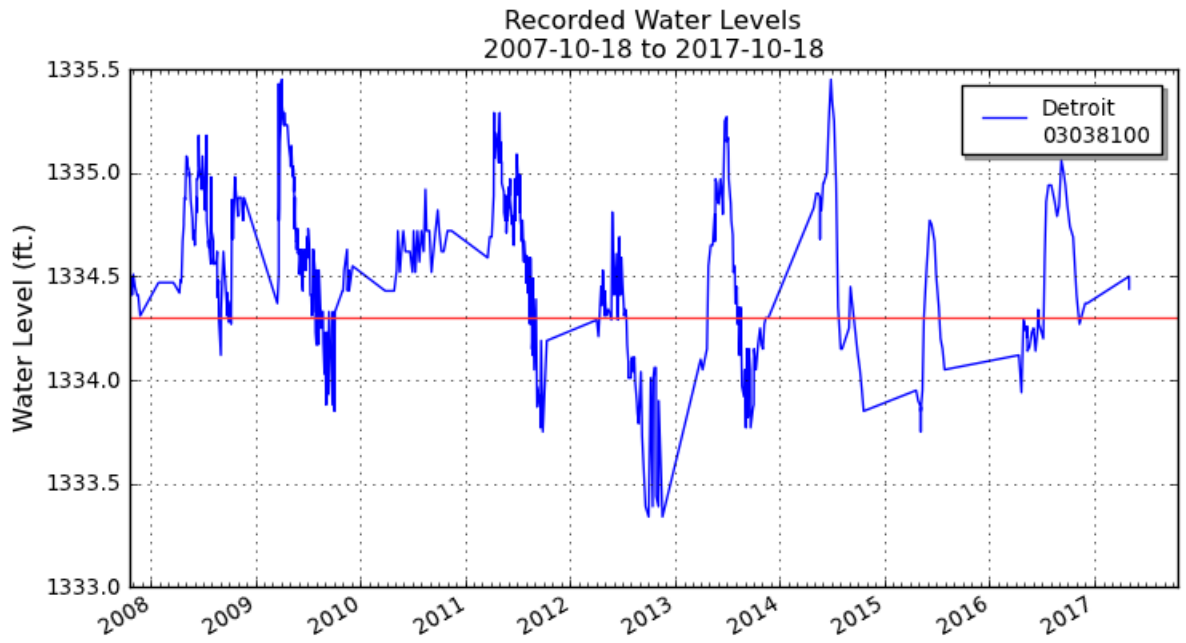

Lake name: Detroit

Water Level Data

Period of record: 08/25/1943 to 05/02/2017

# of readings: 4181

Highest recorded: 1335.78 ft (06/28/1998)

Lowest recorded: 1333.34 ft (10/01/2012)

Recorded range: 2.44 ft

Last reading: 1334.44 ft (05/02/2017)

Ordinary High Water Level (OHW) elevation: 1334.3 ft

Datum: NGVD 29 (ft)

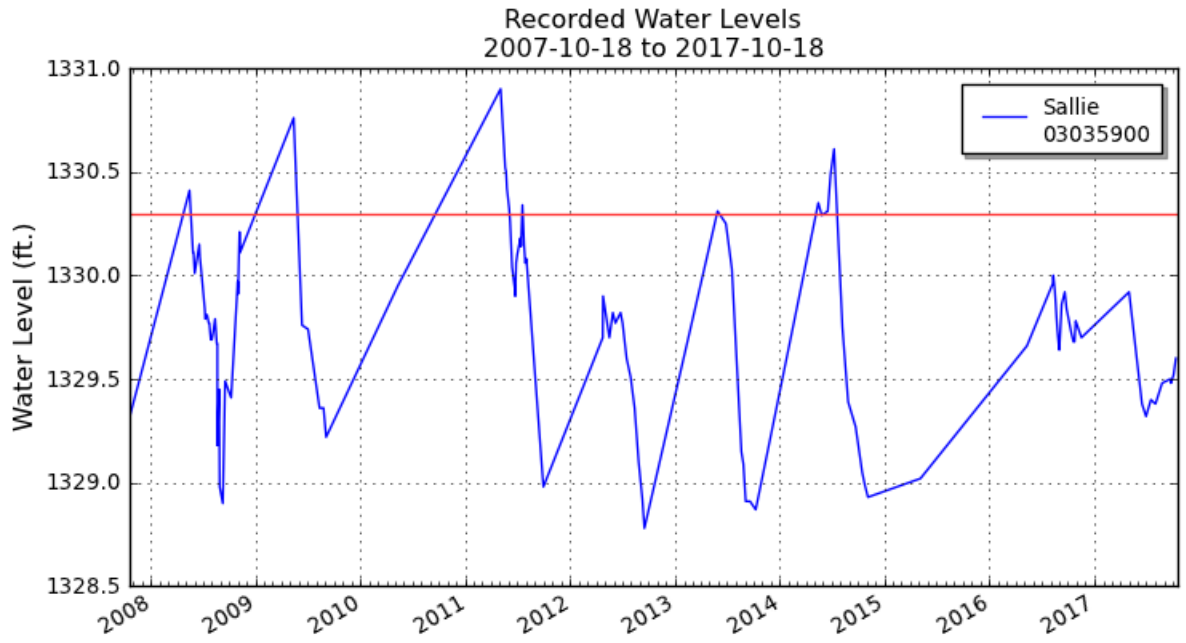

Lake name: Sallie

Water Level Data

Period of record: 01/03/1935 to 10/12/2017

# of readings: 1870

Highest recorded: 1331 ft (08/09/1993)

Lowest recorded: 1325.42 ft (07/25/1936)

Recorded range: 5.58 ft

Last reading: 1329.6 ft (10/12/2017)

Ordinary High Water Level (OHW) elevation: 1330.3 ft

Datum: NGVD 29 (ft)

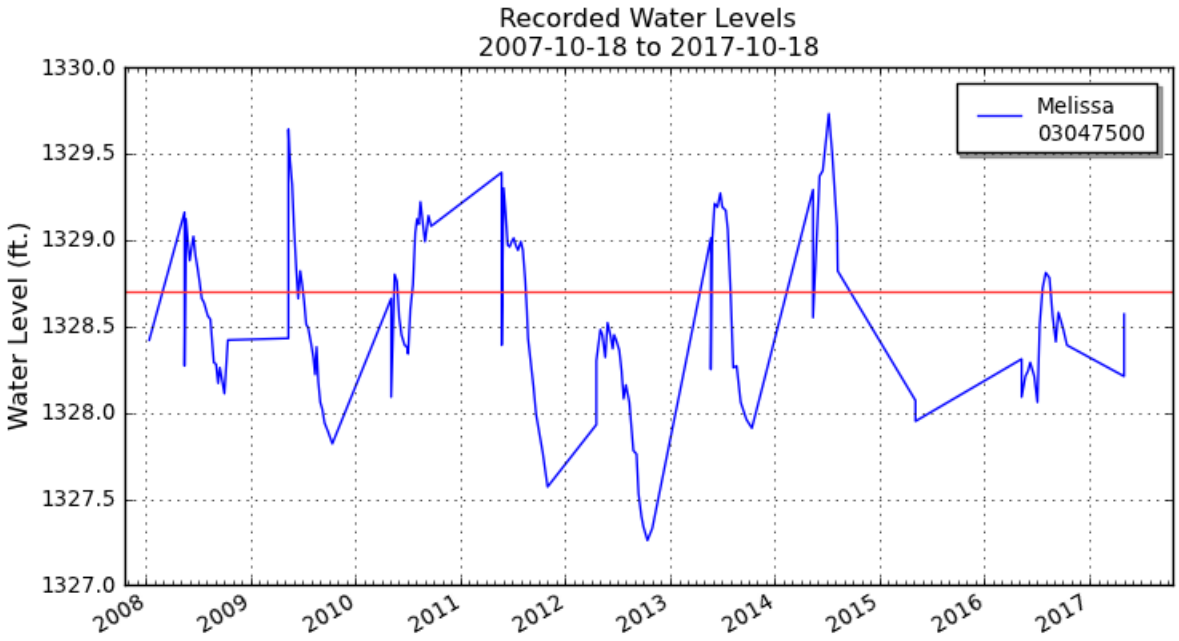

Lake name: Melissa

Water Level Data

Period of record: 04/27/1937 to 05/02/2017

# of readings: 1845

Highest recorded: 1329.88 ft (07/10/2000)

Lowest recorded: 1323.58 ft (05/14/1937)

Recorded range: 6.3 ft

Last reading: 1328.21 ft (05/02/2017)

Ordinary High Water Level (OHW) elevation: 1328.7 ft

Datum: NGVD 29 (ft)

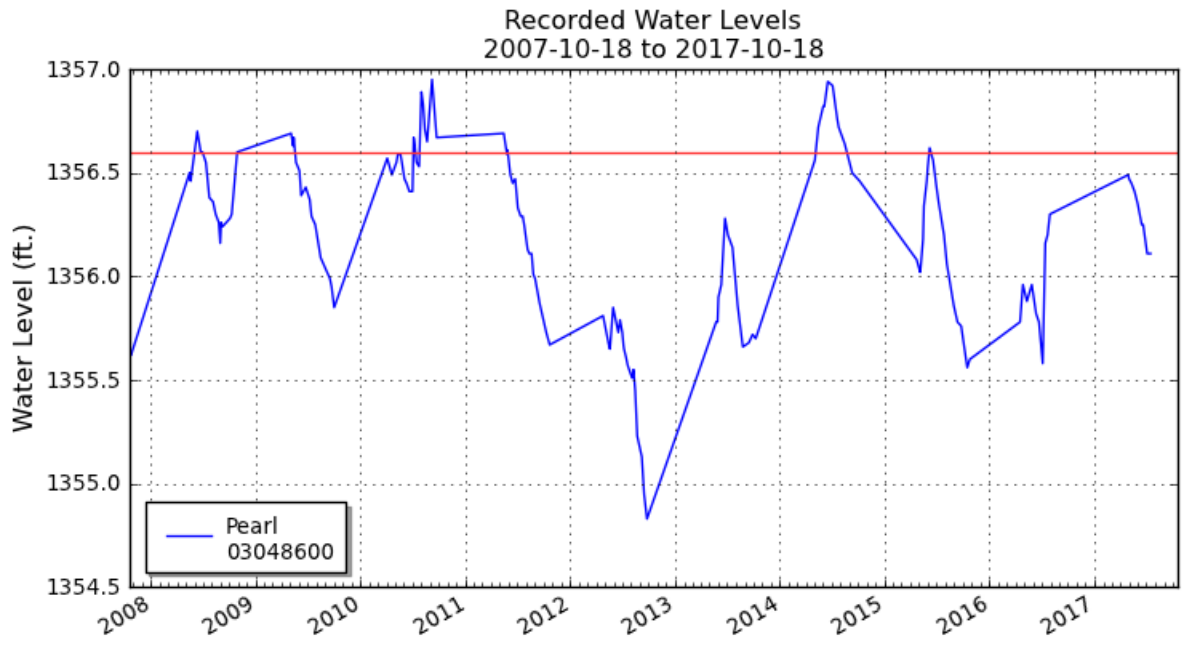

Lake name: Pearl

Water Level Data

Period of record: 05/23/1996 to 07/16/2017

# of readings: 266

Highest recorded: 1358.24 ft (07/08/2002)

Lowest recorded: 1354.83 ft (09/25/2012)

Recorded range: 3.41 ft

Last reading: 1356.11 ft (07/16/2017)

Ordinary High Water Level (OHW) elevation: 1356.6 ft

Datum: NGVD 29 (ft)

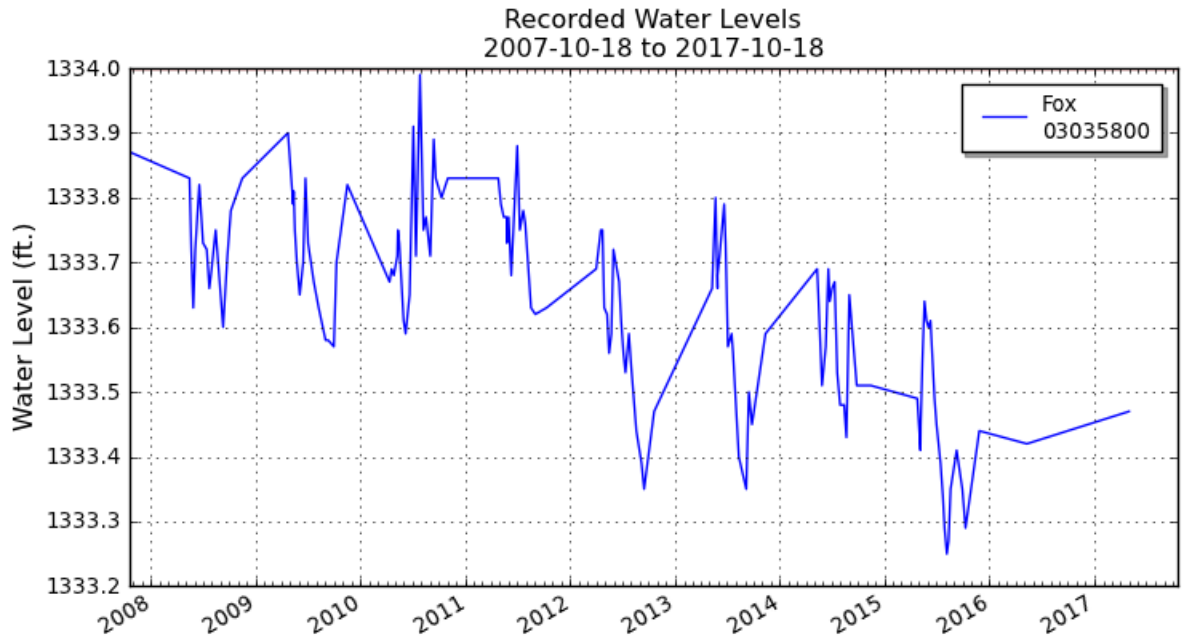

Lake name: Fox

Water Level Data

Period of record: 05/06/1992 to 05/02/2017

# of readings: 351

Highest recorded: 1334.17 ft (07/07/1998)

Lowest recorded: 1333.25 ft (08/06/2015)

Recorded range: 0.92 ft

Last reading: 1333.47 ft (05/02/2017)

Ordinary High Water Level (OHW) elevation: 1334 ft

Datum: NGVD 29 (ft)

Appendix F

Ground Calibration Temperature Plots

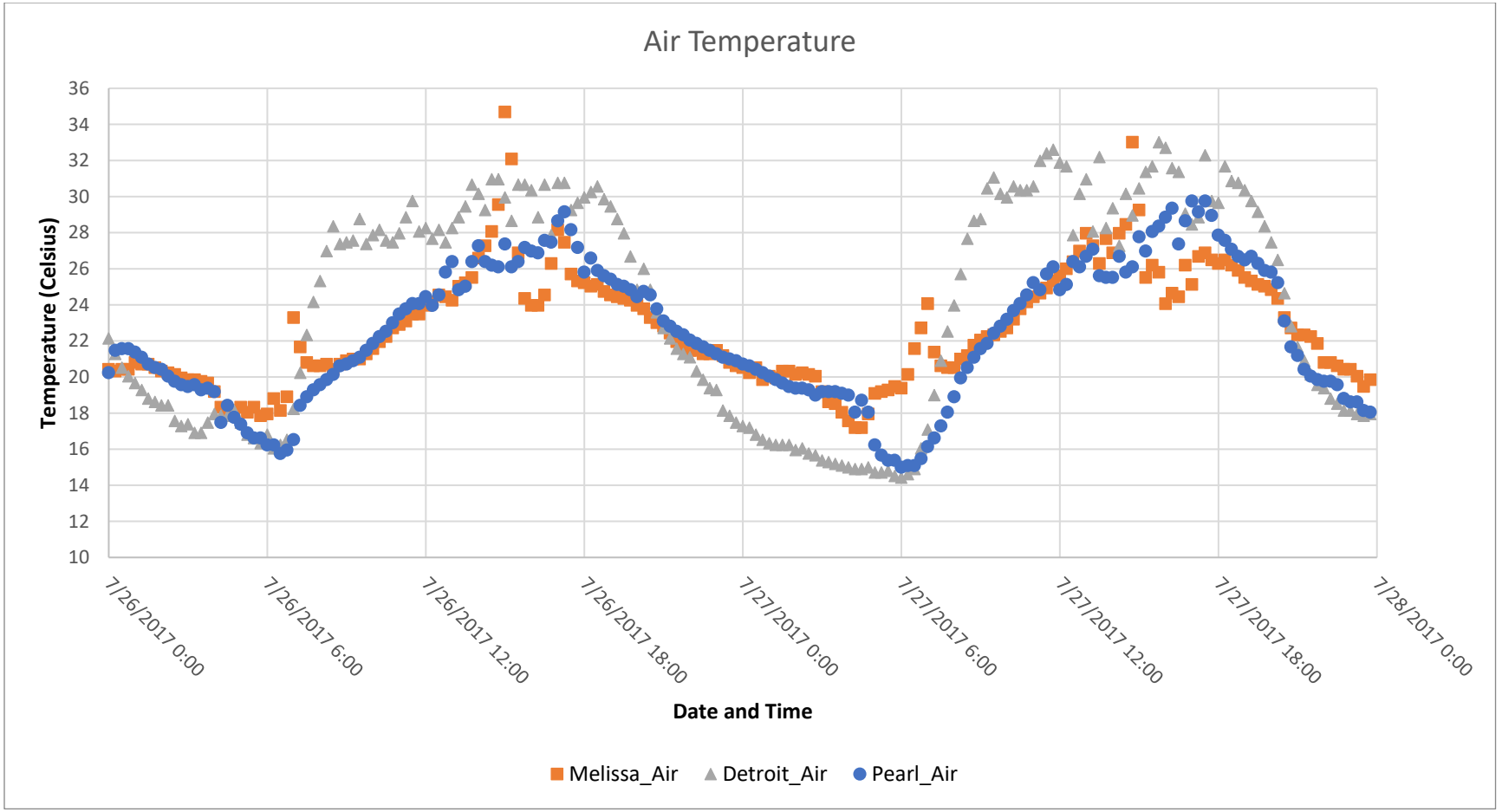

Air temperatures recorded for study area. Lake Melissa air temperatures spike at 7am and 3pm daily due to sprinklers hitting the thermistor.

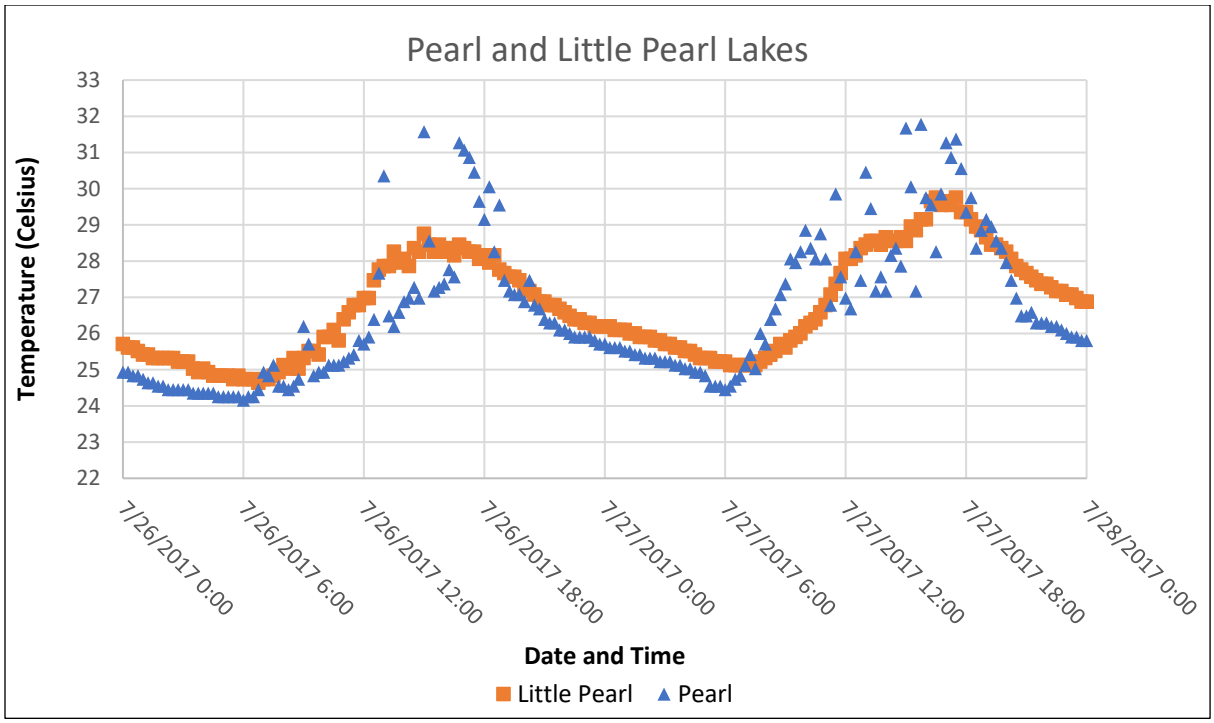
Pearl and Little Pearl Lakes
Temperature (Celsius)
33
32
31
30
29
28
27
26
25
24
23
22
7/26/2017 0:00
7/26/2017 6:00
7/26/2017 12:00
7/26/2017 18:00
7/27/2017 0:00
7/27/2017 6:00
7/27/2017 12:00
7/27/2017 18:00
7/28/2017 0:00
Date and Time
Little Pearl
Pearl

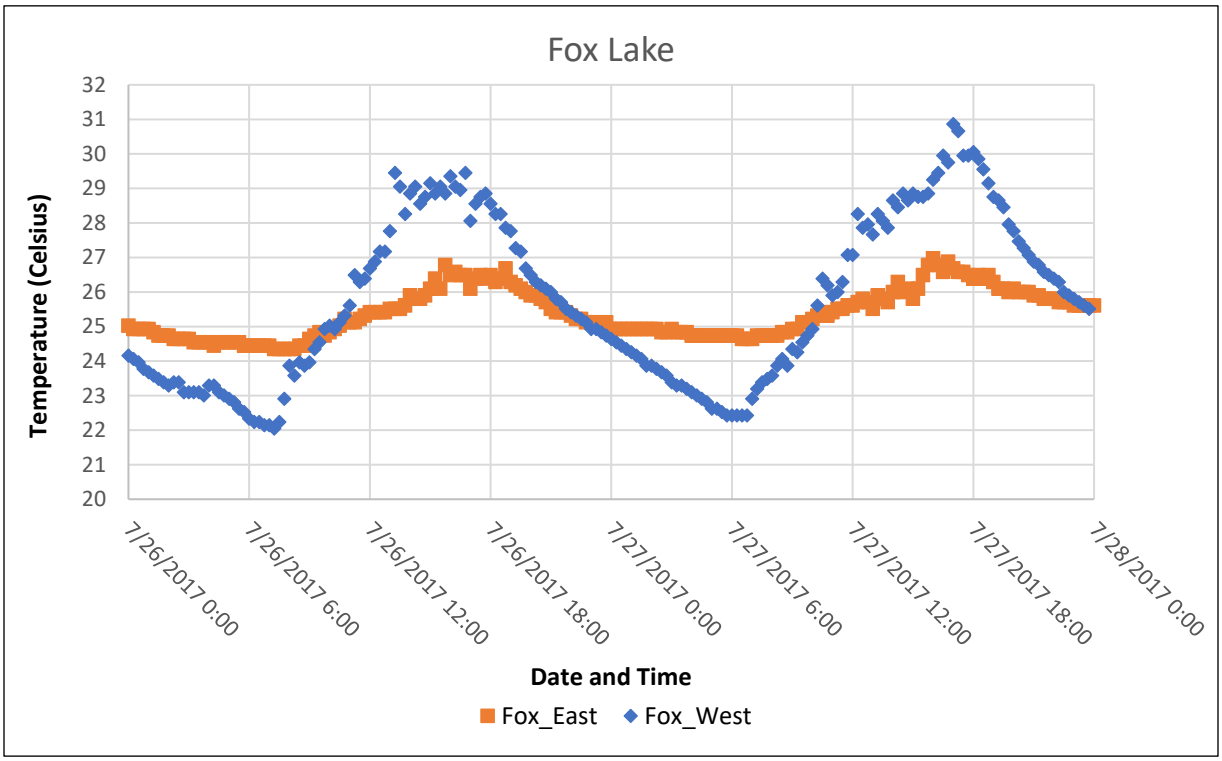
Fox Lake
Temperature (Celsius)
32
31
30
29
28
27
26
25
24
23
22
21
20
7/26/2017 0:00
7/26/2017 6:00
7/26/2017 12:00
7/26/2017 18:00
7/27/2017 0:00
7/27/2017 6:00
7/27/2017 12:00
7/27/2017 18:00
7/28/2017 0:00
Date and Time
Fox_East
Fox_West

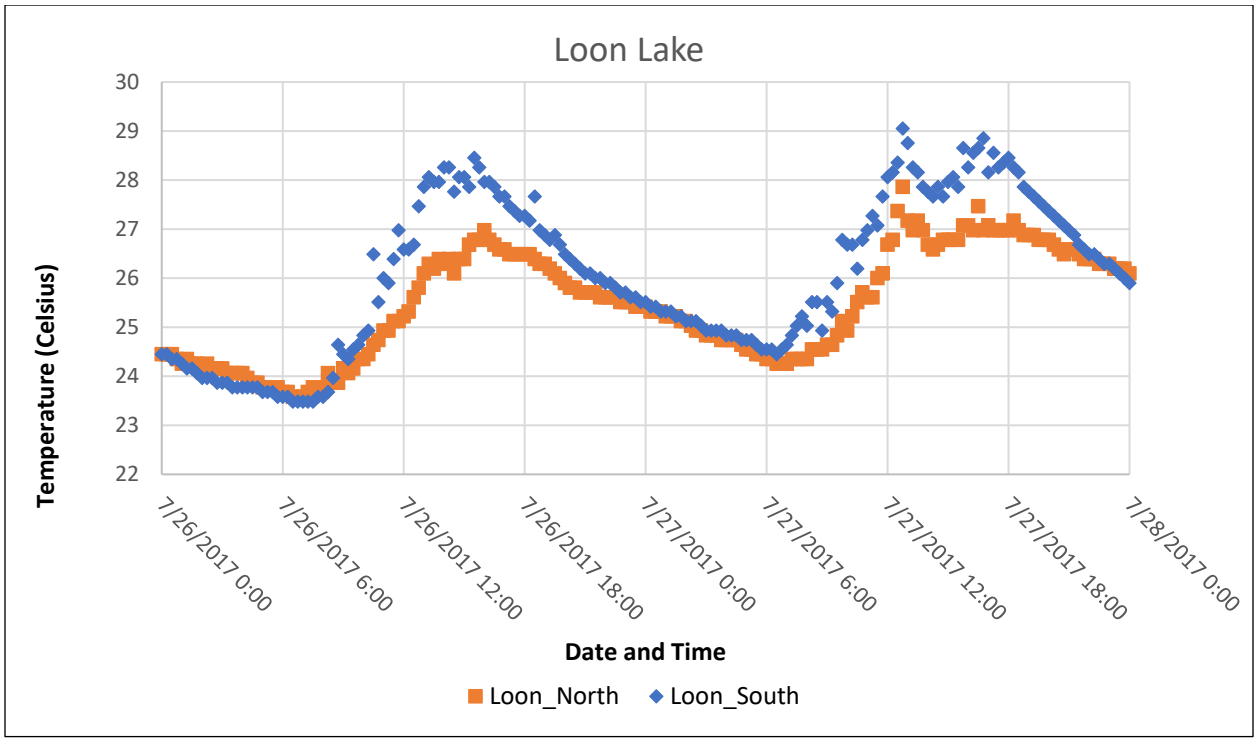
Loon Lake
Temperature (Celsius)
30
29
28
27
26
25
24
23
22
7/26/2017 0:00
7/26/2017 6:00
7/26/2017 12:00
7/26/2017 18:00
7/27/2017 0:00
7/27/2017 6:00
7/27/2017 12:00
7/27/2017 18:00
7/28/2017 0:00
Date and Time
Loon_North
Loon_South

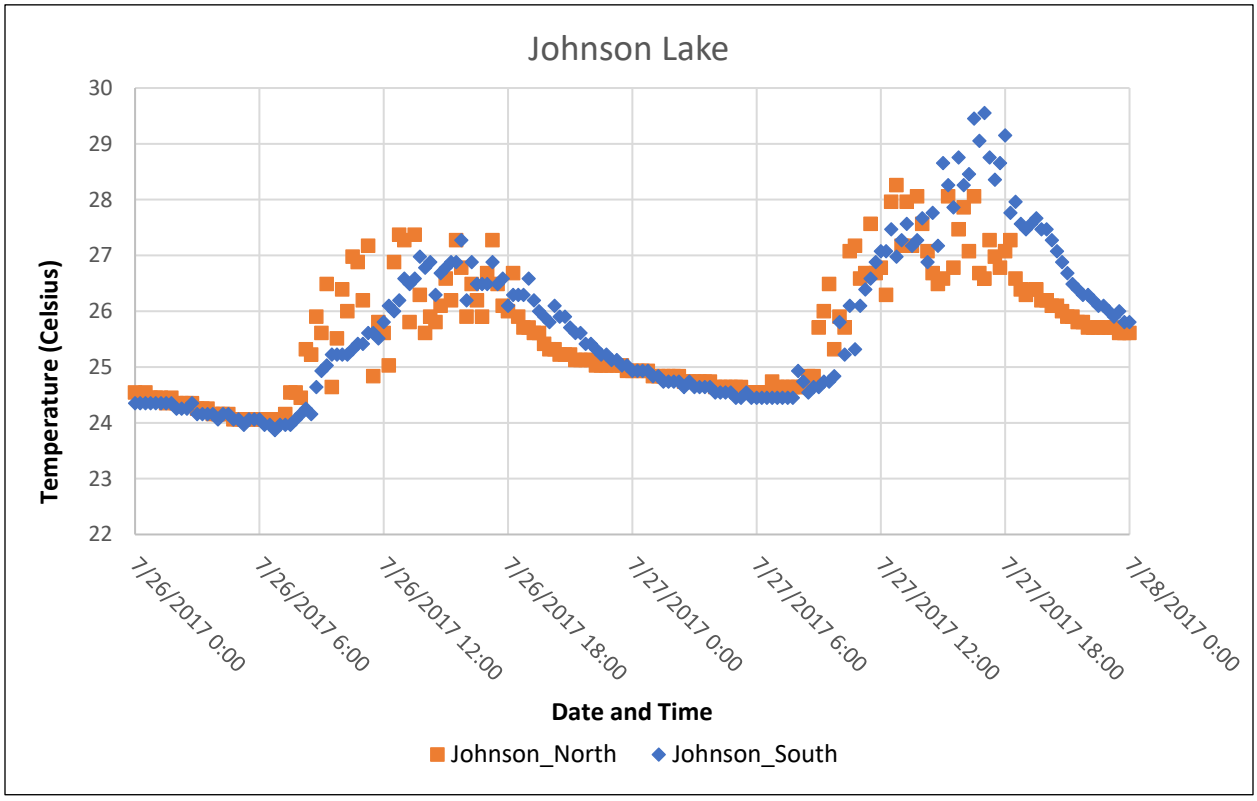
Johnson Lake
Temperature (Celsius)
30
29
28
27
26
25
24
23
22
7/26/2017 0:00
7/26/2017 6:00
7/26/2017 12:00
7/26/2017 18:00
7/27/2017 0:00
7/27/2017 6:00
7/27/2017 12:00
7/27/2017 18:00
7/28/2017 0:00
Date and Time
Johnson_North
Johnson_South

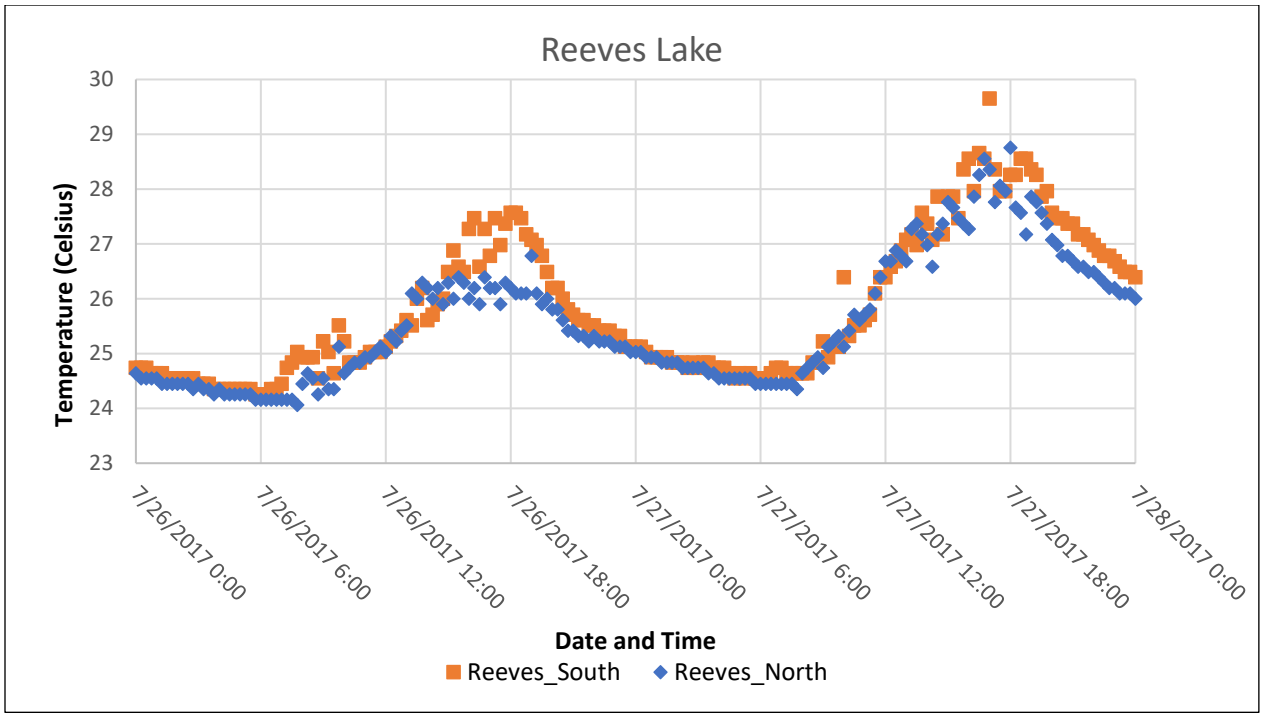
Reeves Lake
Temperature (Celsius)
30
29
28
27
26
25
24
23
7/26/2017 0:00
7/26/2017 6:00
7/26/2017 12:00
7/26/2017 18:00
7/27/2017 0:00
7/27/2017 6:00
7/27/2017 12:00
7/27/2017 18:00
7/28/2017 0:00
Date and Time
Reeves_South
Reeves_North

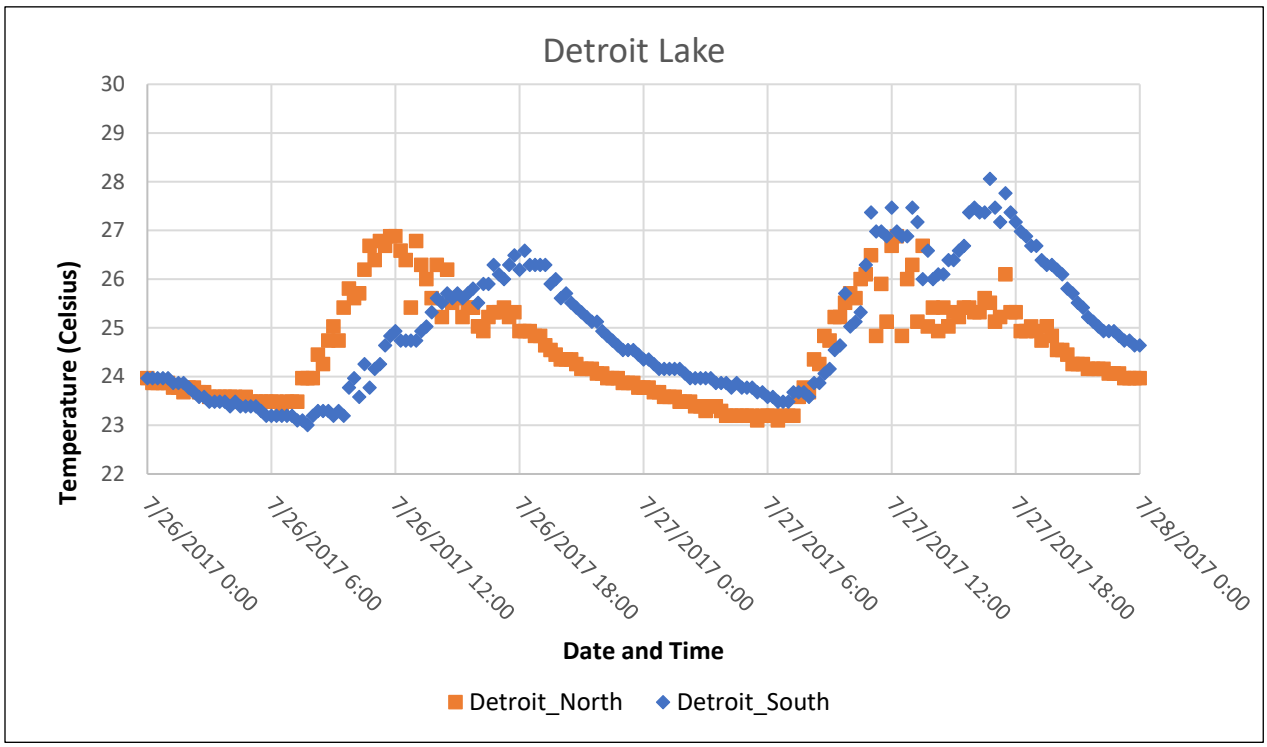
Detroit Lake
Temperature (Celsius)
30
29
28
27
26
25
24
23
22
7/26/2017 0:00
7/26/2017 6:00
7/26/2017 12:00
7/26/2017 18:00
7/27/2017 0:00
7/27/2017 6:00
7/27/2017 12:00
7/27/2017 18:00
7/28/2017 0:00
Date and Time
Detroit_North
Detroit_South

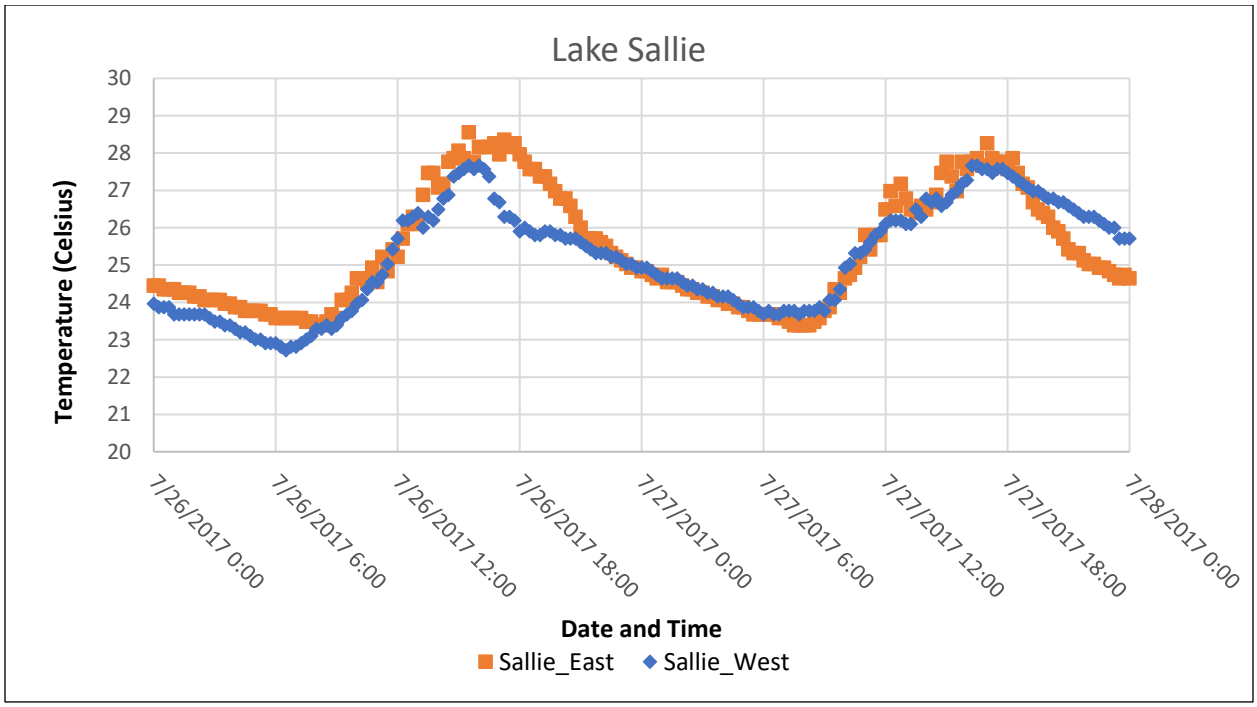
Lake Sallie
Temperature (Celsius)
30
29
28
27
26
25
24
23
22
21
20
7/26/2017 0:00
7/26/2017 6:00
7/26/2017 12:00
7/26/2017 18:00
7/27/2017 0:00
7/27/2017 6:00
7/27/2017 12:00
7/27/2017 18:00
7/28/2017 0:00
Date and Time
Sallie_East
Sallie_West

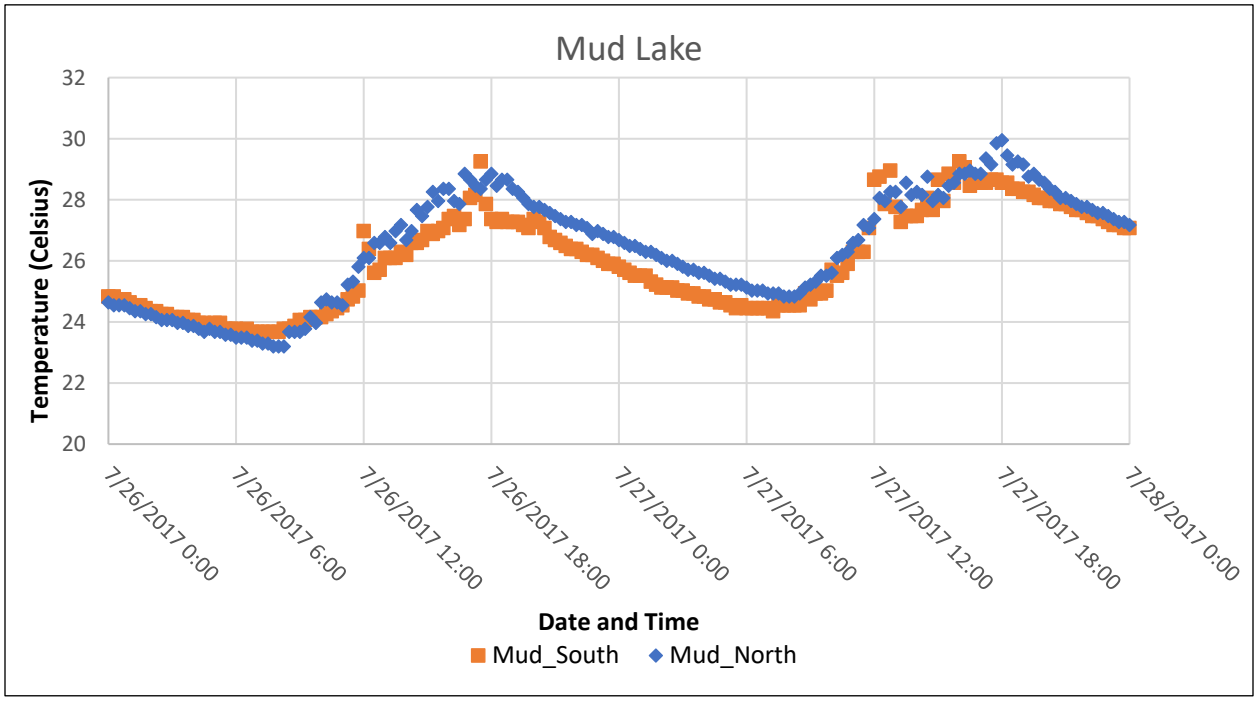
Mud Lake
Temperature (Celsius)
32
30
28
26
24
22
20
7/26/2017 0:00
7/26/2017 6:00
7/26/2017 12:00
7/26/2017 18:00
7/27/2017 0:00
7/27/2017 6:00
7/27/2017 12:00
7/27/2017 18:00
7/28/2017 0:00
Date and Time
Mud_South
Mud_North

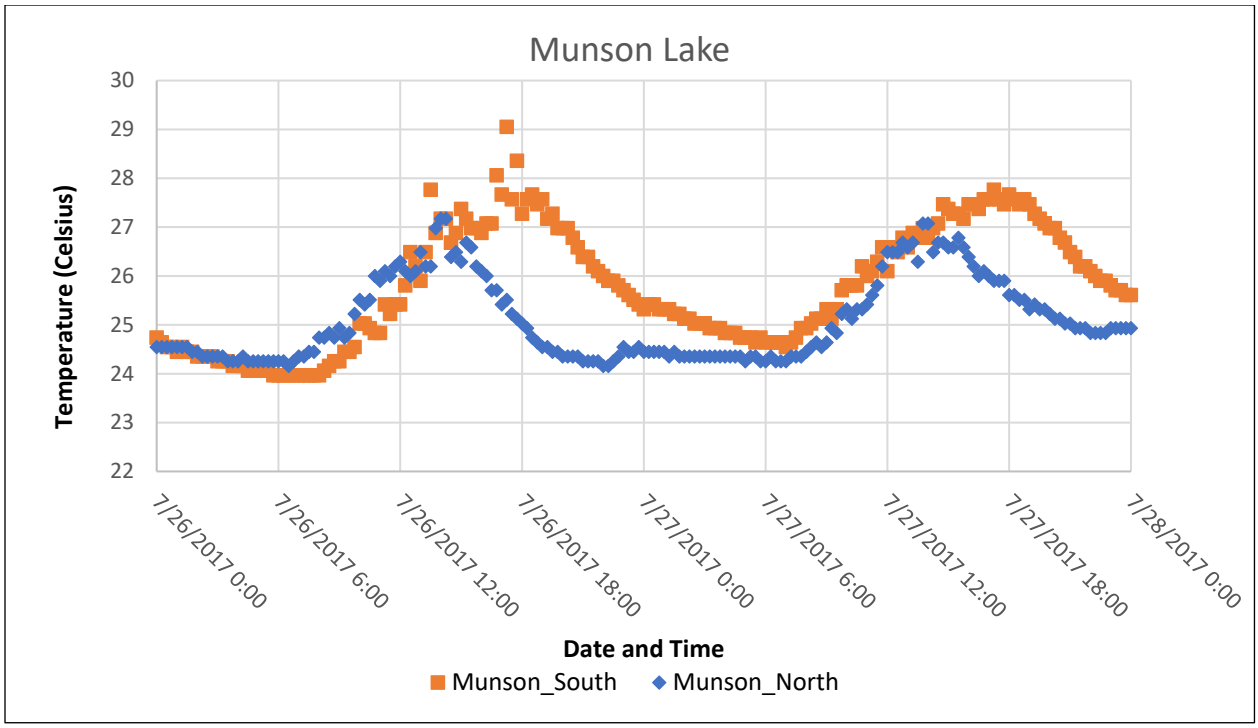
Munson Lake
Temperature (Celsius)
30
29
28
27
26
25
24
23
22
7/26/2017 0:00
7/26/2017 6:00
7/26/2017 12:00
7/26/2017 18:00
7/27/2017 0:00
7/27/2017 6:00
7/27/2017 12:00
7/27/2017 18:00
7/28/2017 0:00
Date and Time
Munson_South
Munson_North

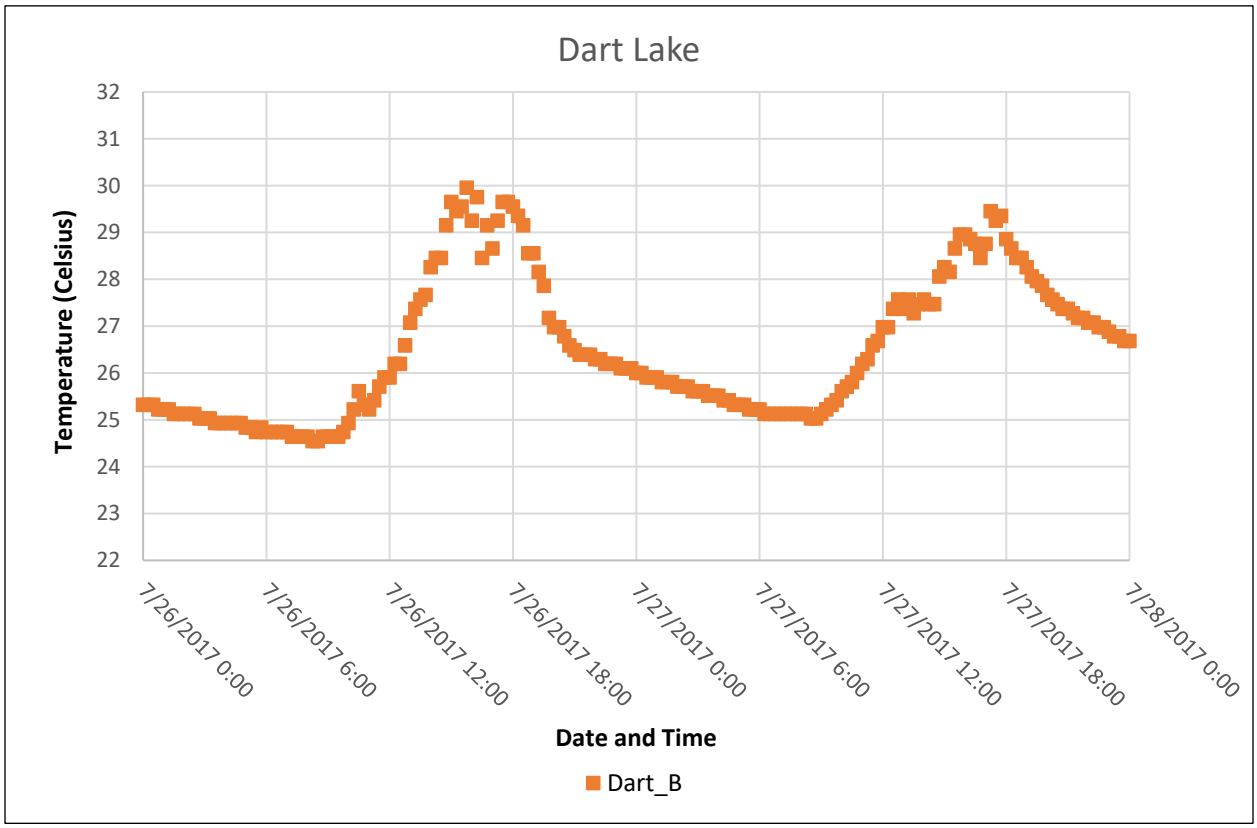
Dart Lake
Temperature (Celsius)
32
31
30
29
28
27
26
25
24
23
22
7/26/2017 0:00
7/26/2017 6:00
7/26/2017 12:00
7/26/2017 18:00
7/27/2017 0:00
7/27/2017 6:00
7/27/2017 12:00
7/27/2017 18:00
7/28/2017 0:00
Date and Time
Dart_B

Appendix G

Ground Calibration Thermistor Locations on UAV Imagery

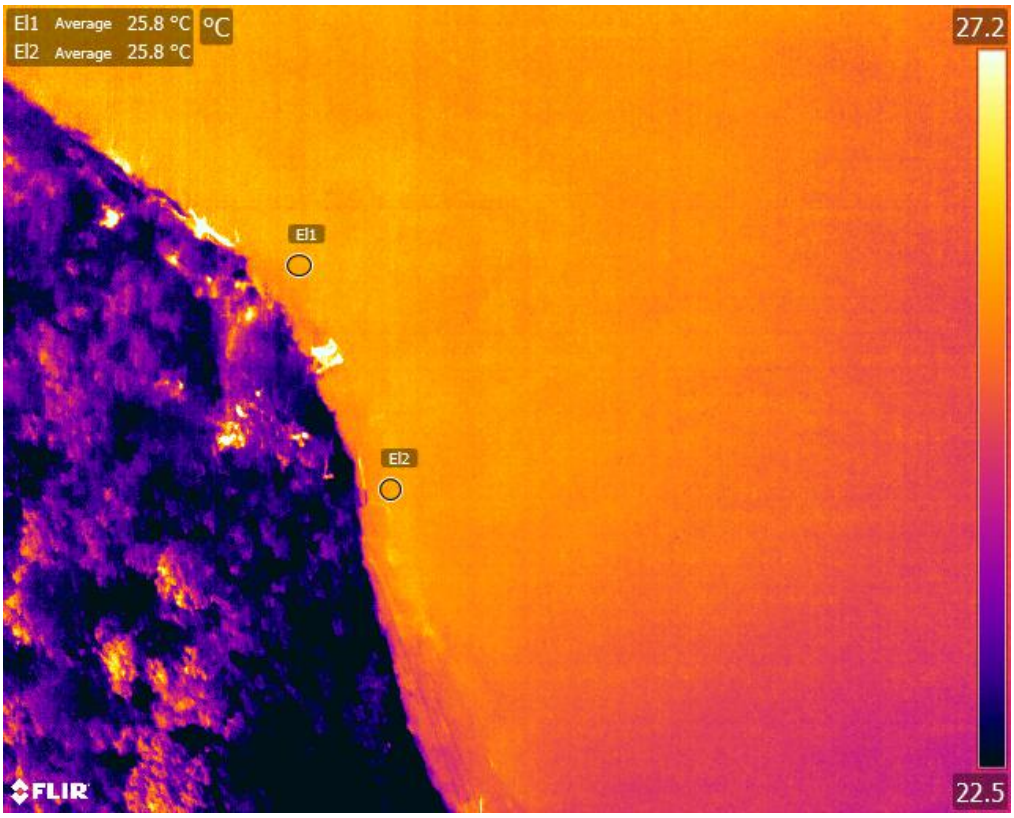

Dart Lake Thermistor Locations

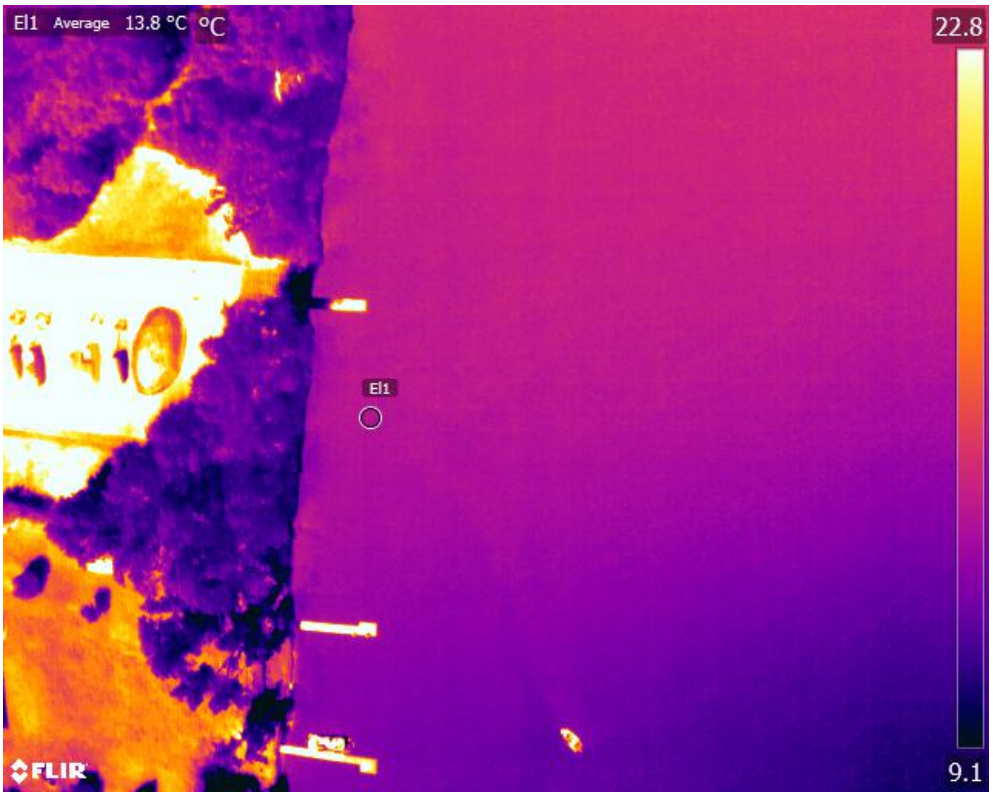

Pearl Lake South Thermistor Location

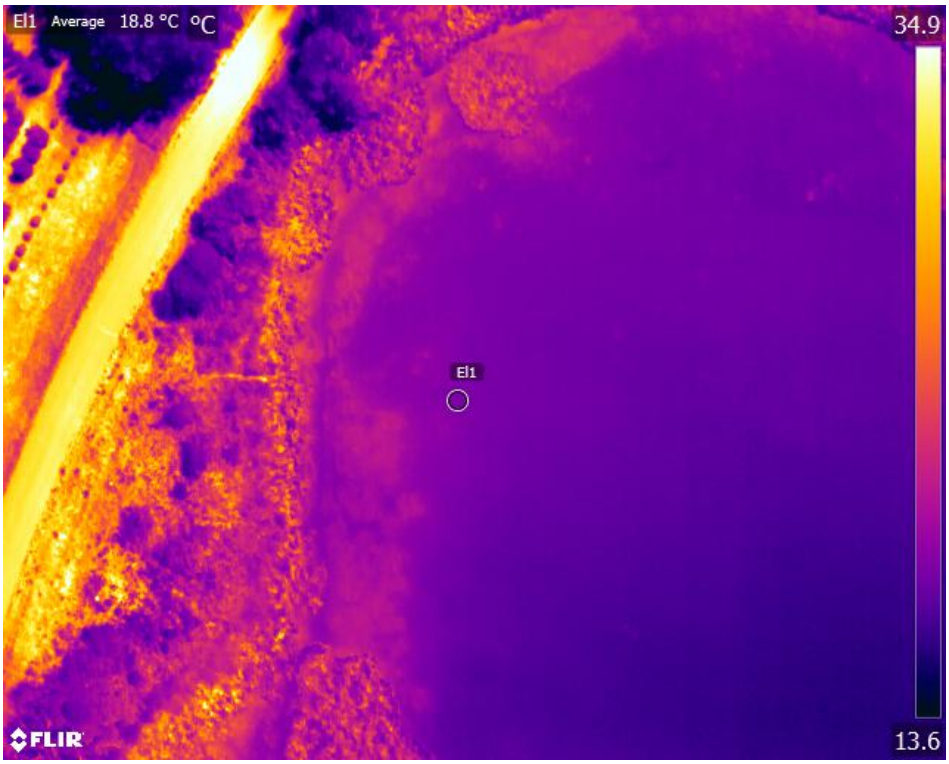

Little Pearl Lake (Pearl Lake North) Thermistor Location

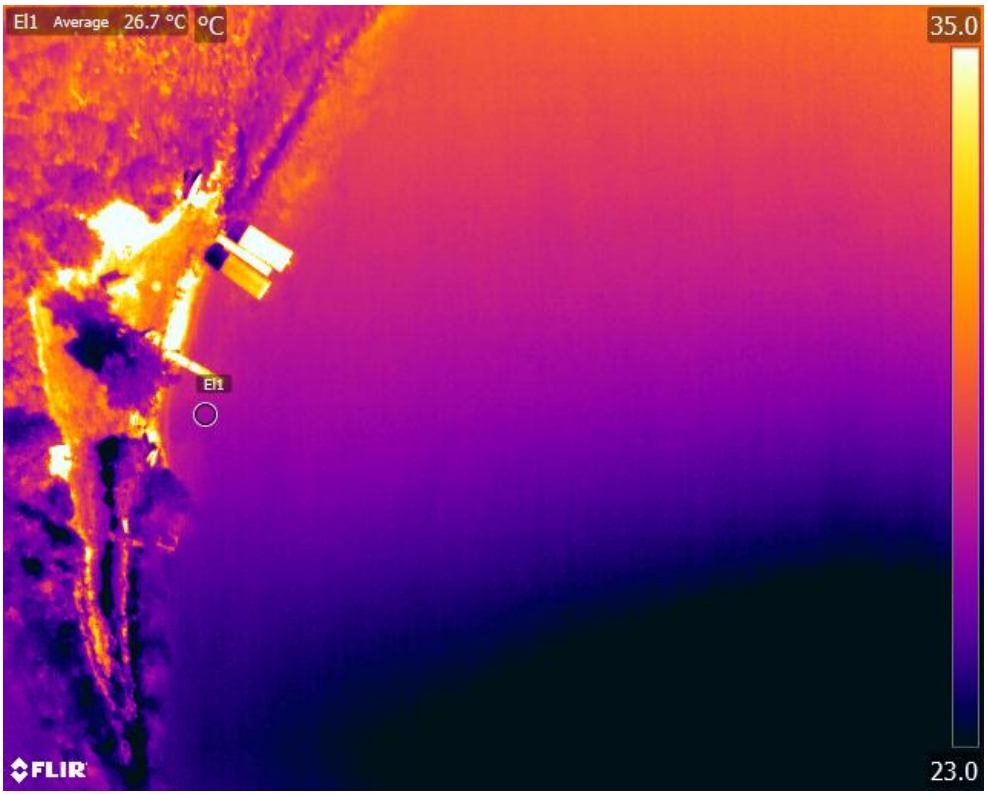

Loon Lake North Thermistor Location

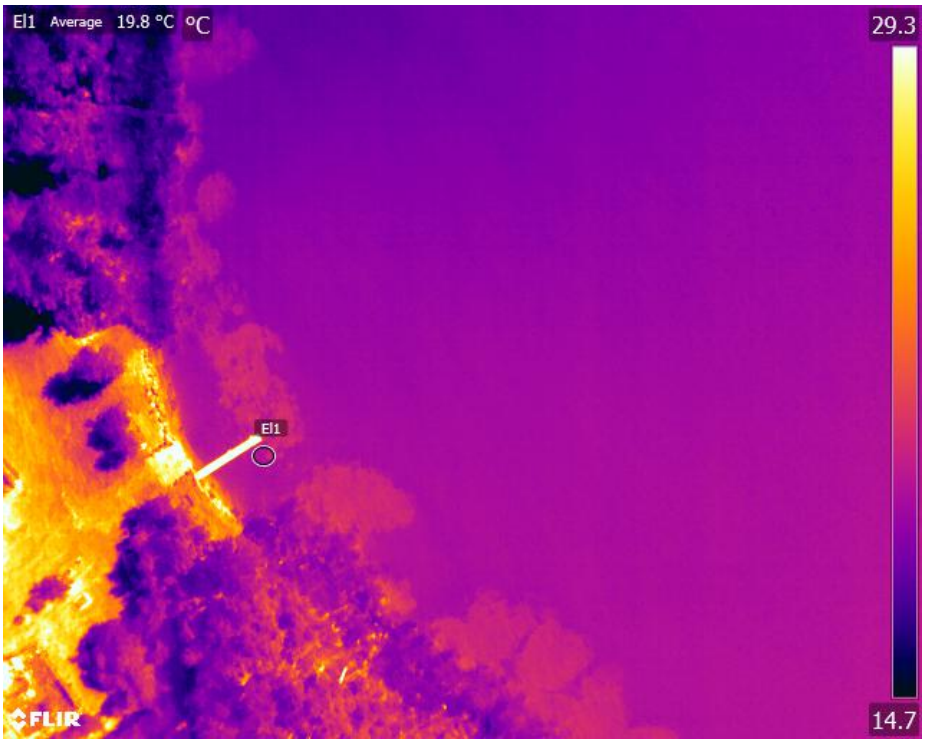

Loon Lake South Thermistor Location

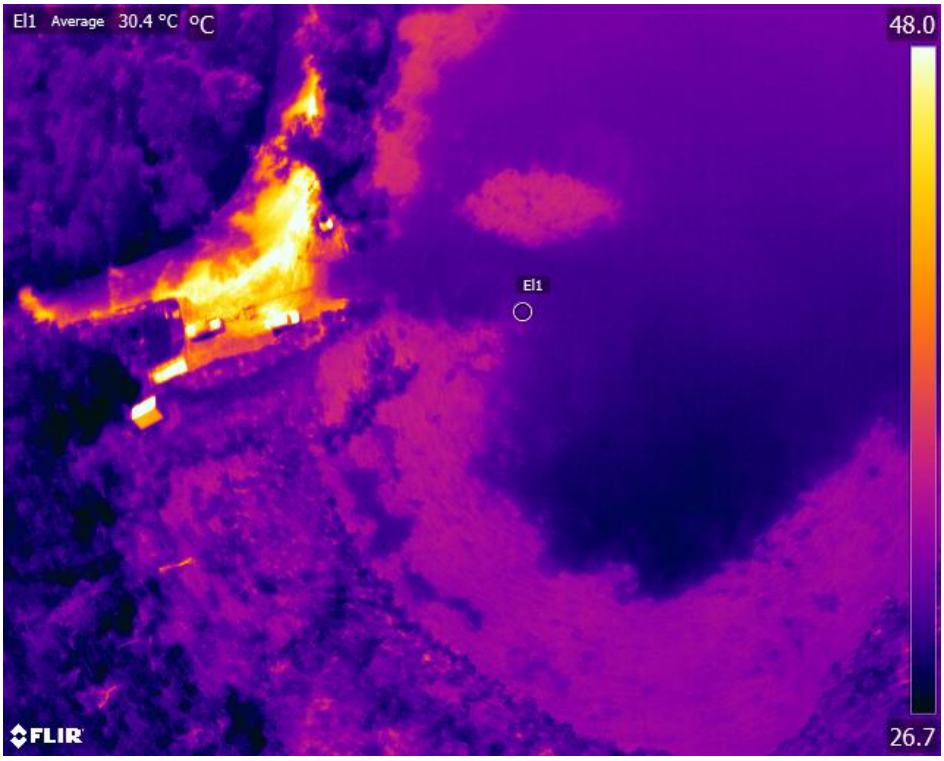

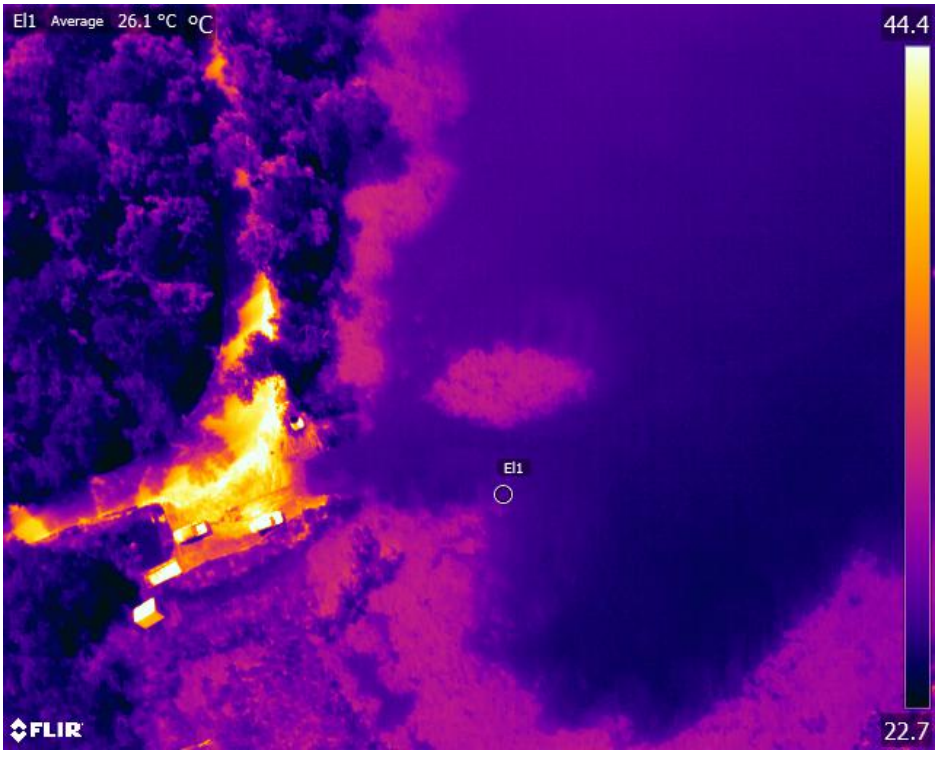

Munson Lake South Thermistor Location. Both thermal images collected at 1:08pm.

Munson Lake South Thermistor Location

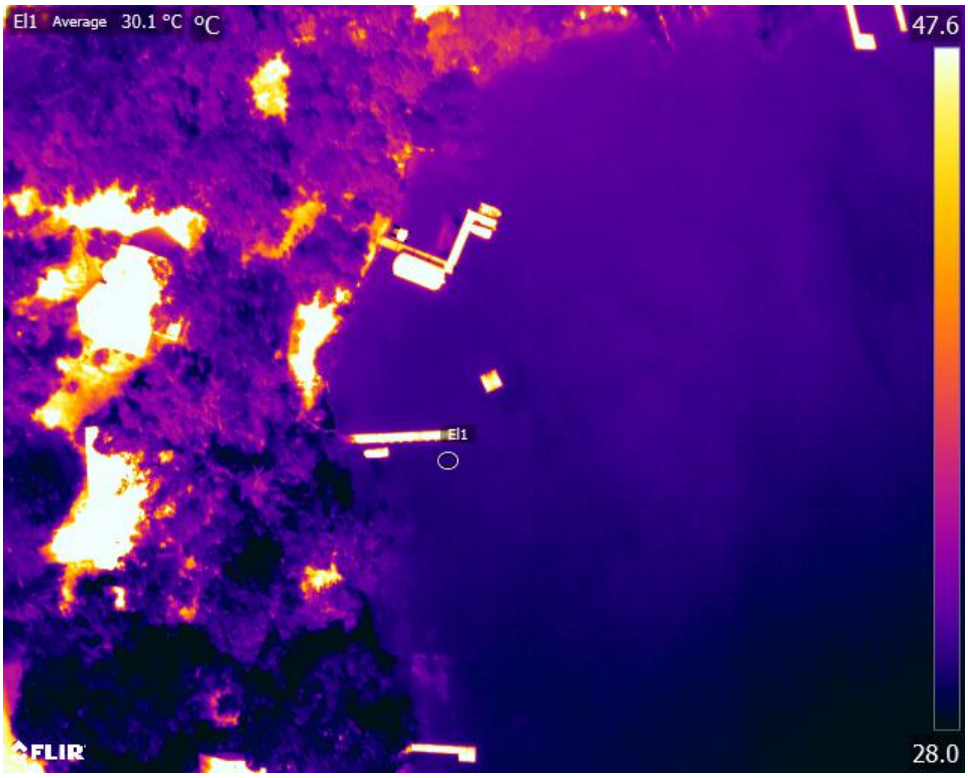

Munson Lake North Thermistor Location

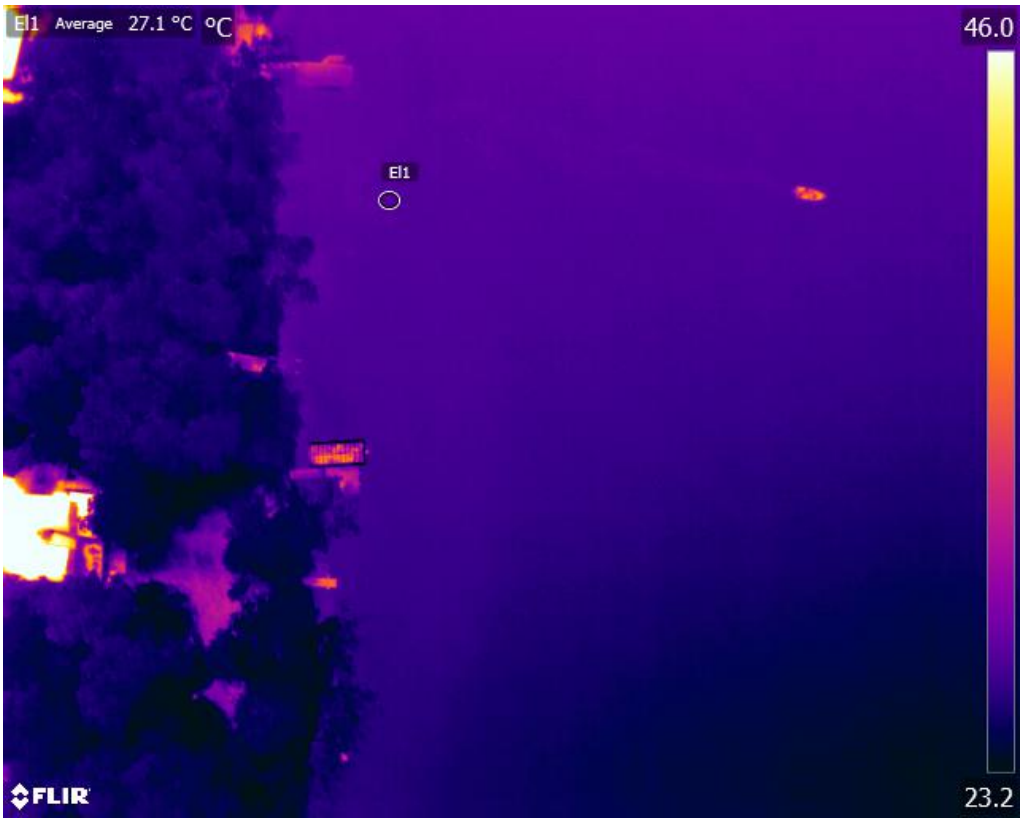

Fox Lake East Thermistor Location

Lake Sallie East Thermistor

Lake Sallie West Thermistor Location

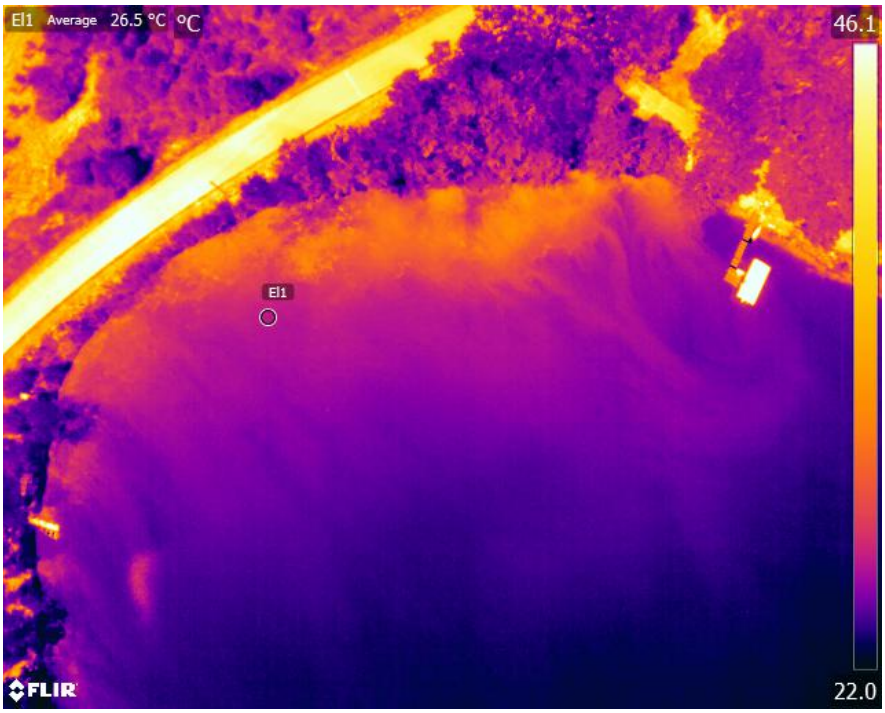

Fox Lake West Thermistor Location

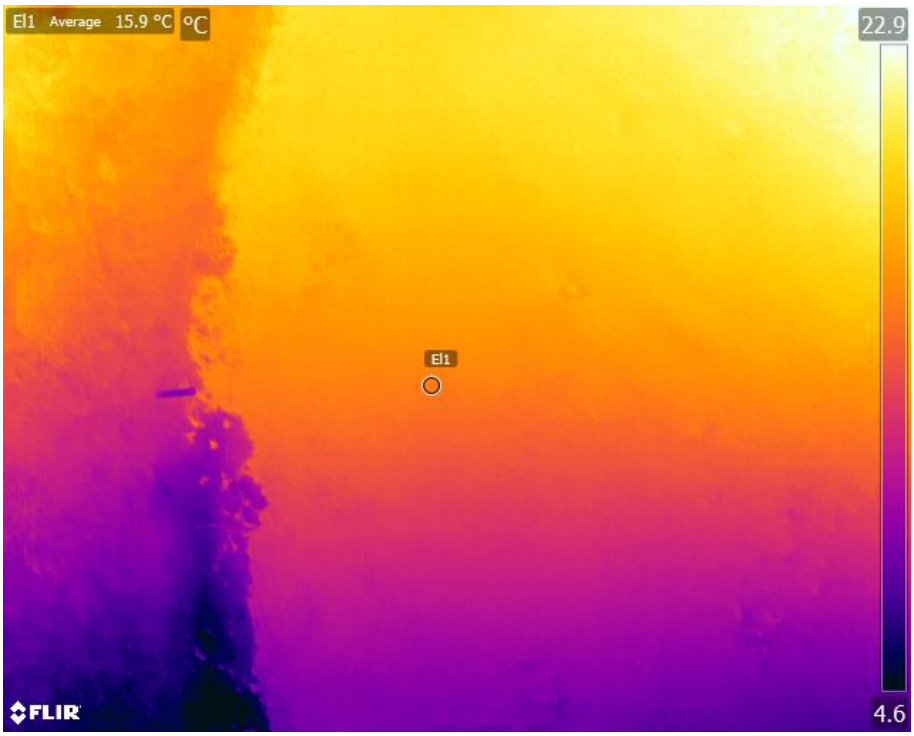

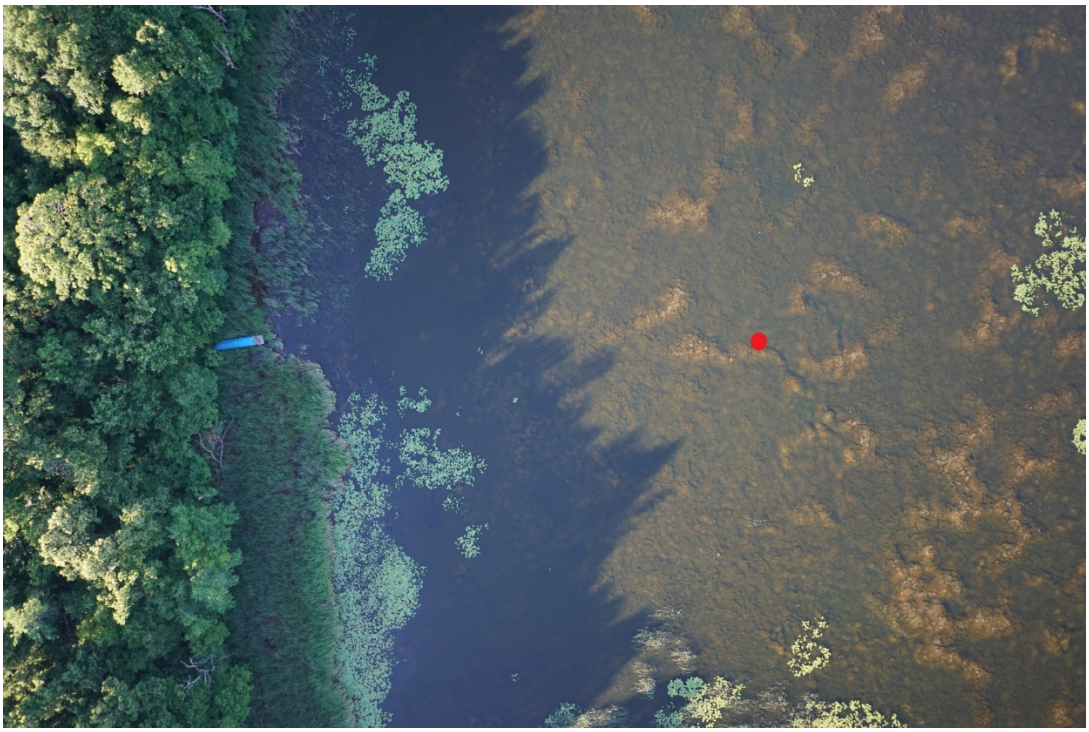

Mud Lake South Thermistor

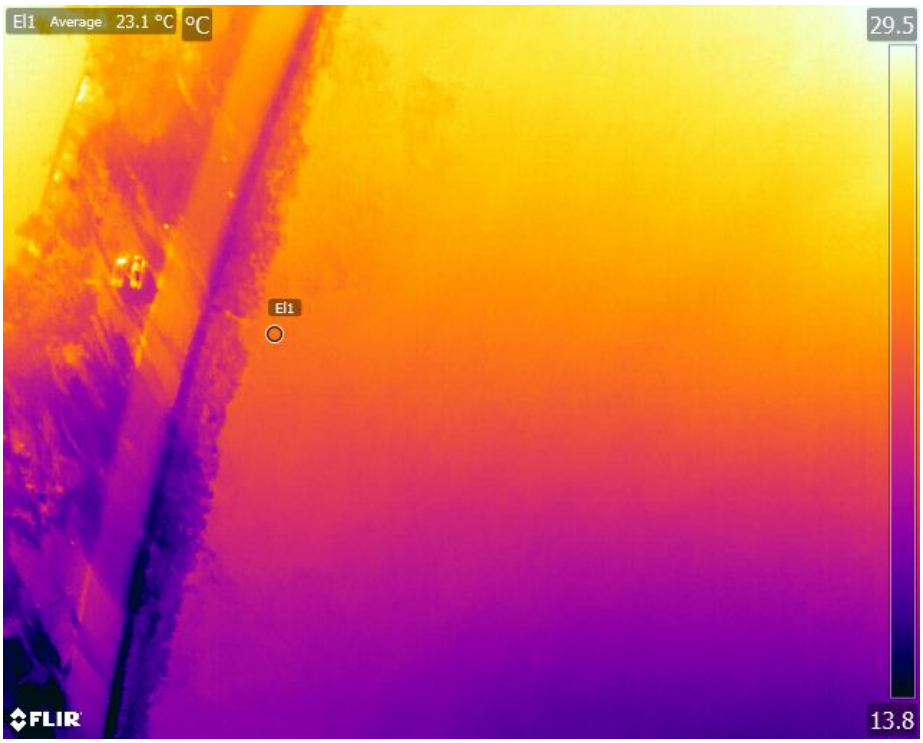

Mud Lake North Thermistor Location

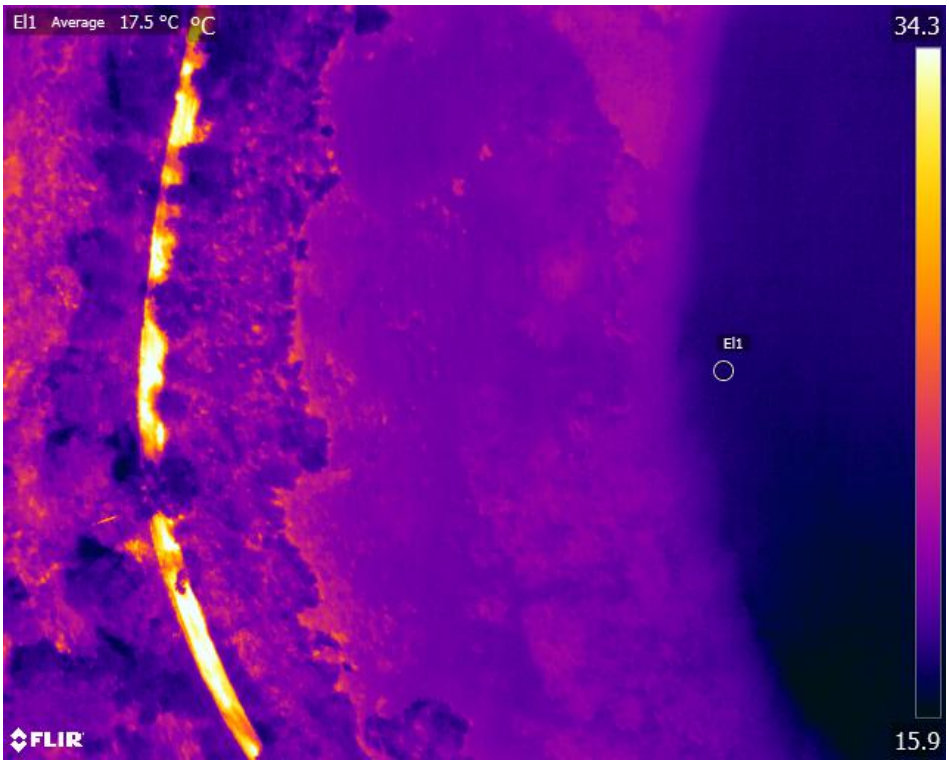

Johnson Lake North Thermistor Location

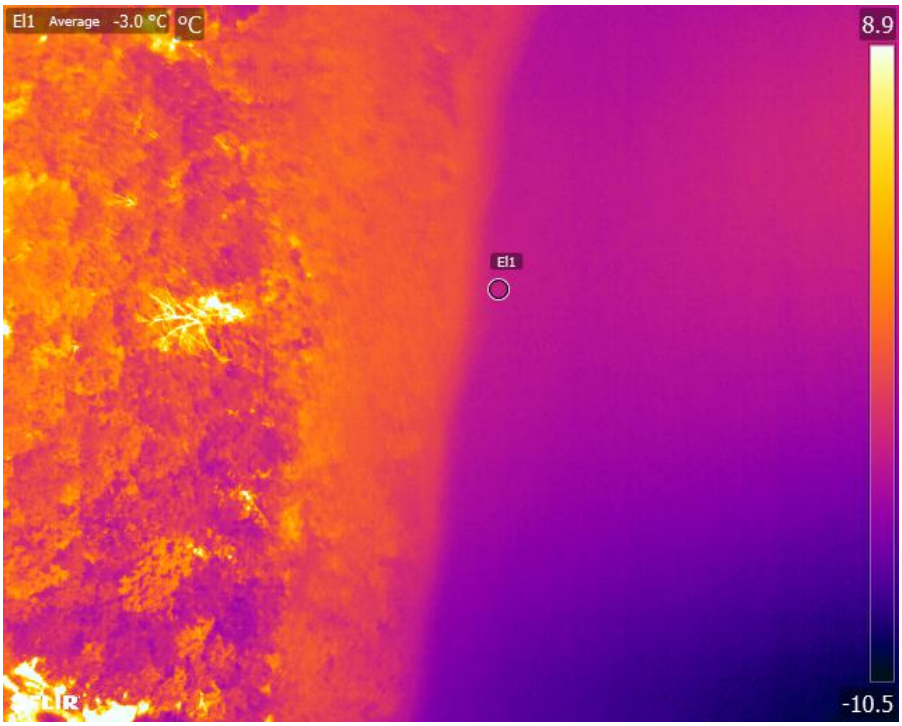

Johnson Lake South Thermistor Location

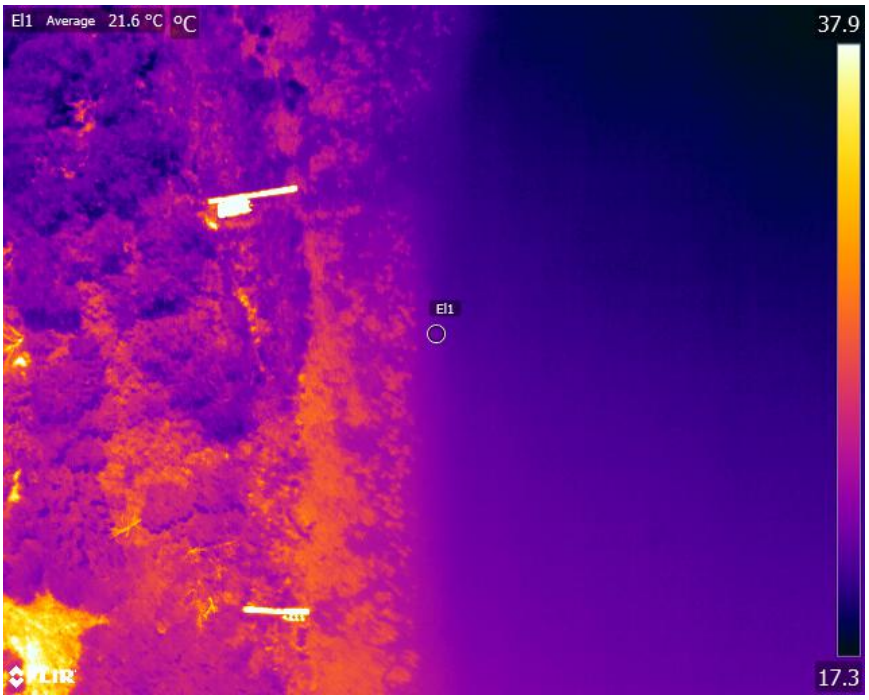

Reeves Lake North Thermistor Location

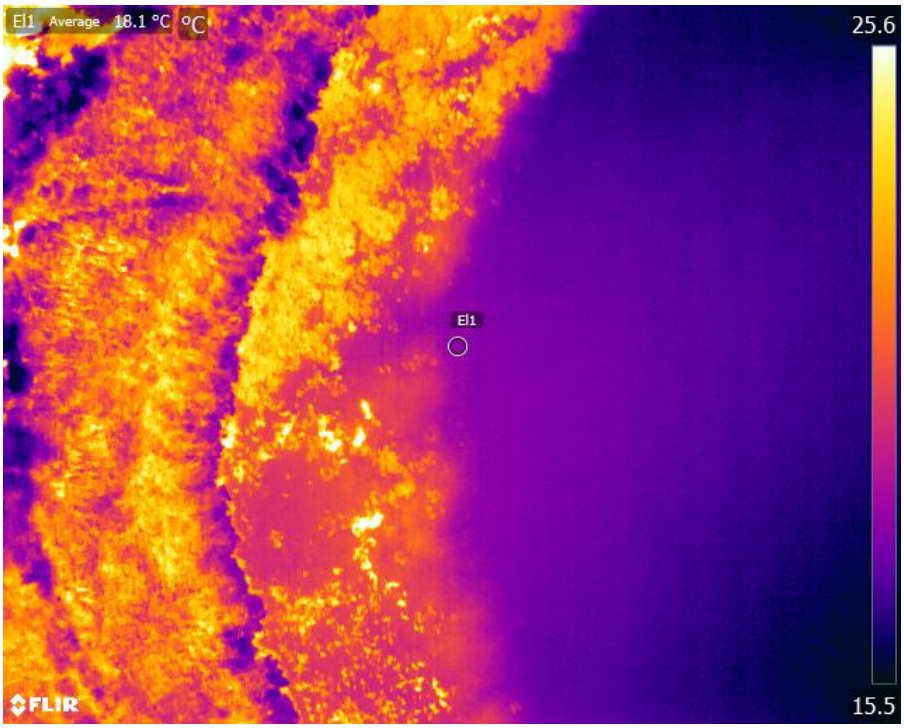

Reeves Lake South Thermistor Location

Detroit Lake South Thermistor Location

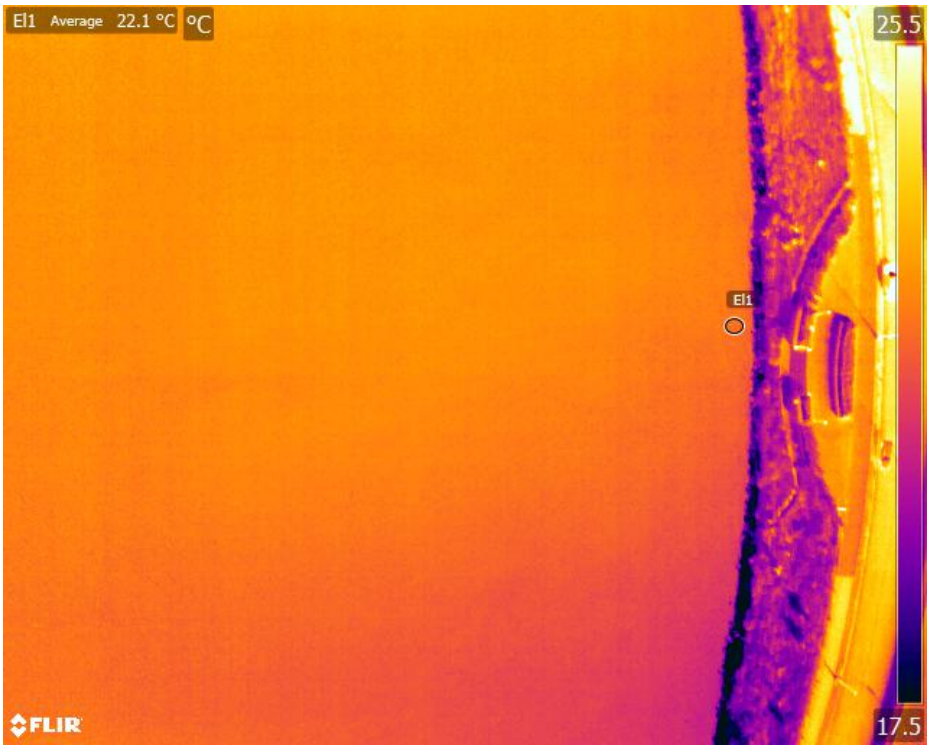

Detroit Lake North Thermistor Location

REFERENCES

Agisoft LLC (2012) Photoscan Professional Edition. Version 1.2.4, http://www.agisoft.com/. Cited 4 December 2017

Aicardi I, Chiabrando F, Lingua AM, et al (2016) A methodology for acquisition and processing of thermal data acquired by UAVs: a test about subfluvial springs' investigations. Geomatics, Nat Hazards Risk 5705:1–13. doi: 10.1080/19475705.2016.1225229

Anderson MP (2005) Heat as a ground water tracer. Ground Water 43:951–968. doi: 10.1111/j.1745-6584.2005.00052.x

Anderson MP, Woessner WW, Hunt RJ (2015) Applied Groundwater Modeling: Simulation of Flow and Advective Transport, 2nd edn. El Sevier, San Diego

Banks WSL, Paylor RL, Hughes WB (1996) Using thermal-infrared imagery to delineate ground-water discharge. Ground Water 34:434–443.

Barnett B, Townley LR, Post V, Evans RE, Hunt RJ, Peeters L, Richardson S, Werner AD, Knapton A and Boronkay A, (2012) Australian groundwater modelling guidelines, Waterlines report, National Water Commission, Canberra

Becker MW, Daw A (2005) Influence of lake morphology and clarity on water surface temperature as measured by EOS ASTER. Remote Sens Environ 99:288–294. doi: 10.1016/j.rse.2005.09.003

Becker MW (2006) Potential for satellite remote sensing of ground water. Ground Water 44:306–318. doi: 10.1111/j.1745-6584.2005.00123.x

Campbell JB, Wynne RH (2011) Introduction to Remote Sensing, 5th edn. Guilford Press, New York

ESRI (2015) ArcGIS for Desktop. Version 10.3.4, http://www.esri.com/products. Cited 4 December 2017

ESRI (2017) How Natural Neighbor Works. http://desktop.arcgis.com/en/arcmap/10.3/tools/spatial-analyst-toolbox/how-natural-neighbor-works.htm. Accessed 15 Jan 2017

ESRI (2017) What is Darcy flow analysis? In: ArcGIS Pro. http://pro.arcgis.com/en/pro-app/tool-reference/spatial-analyst/what-is-darcy-flow-analysis.htm. Accessed 10 May 2017

Fleming, AH (1994) The hydrogeology of Allen County, Indiana — A geologic and ground-water atlas: Indiana Geological Survey Special Report 57

FLIR (2016) Infrared Camera Accuracy and Uncertainty in Plain Language. In: FLIR Res. Sci. http://www.flir.com/science/blog/details/?ID=74935. Accessed 1 Sep 2017

Gerla PJ (1999) Estimating the ground-water contribution in wetlands using modeling and digital terrain analysis. Wetlands 19:394–402. doi: 10.1007/BF03161771

Haitjema HM, Mitchell-Bruker S (2005) Are water tables a subdued replica of the topography? Groundwater 43:781–786. doi: 10.1111/j.1745-6584.2005.00090.x

Hare DK, Briggs MA, Rosenberry DO, et al (2015) A comparison of thermal infrared to fiber-optic

distributed temperature sensing for evaluation of groundwater discharge to surface water. J Hydrol 530:153–166. doi: 10.1016/j.jhydrol.2015.09.059

Harris Geospatial (2017) Using ENVI. In: Harris Geospatial Docs Cent. http://www.harrisgeospatial.com/docs/routines-136.html. Accessed 1 Jan 2016

John PH, Lock MA (1977) The spatial distribution of groundwater discharge into the littoral zone of a New Zealand lake. J Hydrol 33:391–395.

Kishel HF, Gerla PJ (2002) Characteristics of preferential flow and groundwater discharge to Shingobee Lake, Minnesota, USA. Hydrol Process 16:1921–1934. doi: 10.1002/hyp.363

Lee DR (1972) Septic tank nutrients in groundwater entering Lake Sallie, Minnesota. MS Thesis. University of North Dakota

Lee DR (1977) A device for measuring seepage flux in lakes and estuaries. Limnol Oceanogr 22:140–147.

Lee DR (1985) Method for locating sediment anomalies in lakebeds that can be caused by groundwater flow. J Hydrol 79:187–193.

Lusardi B, Anderson F, Harris K (2005) Surficial Geology Units And Geomorphic Features Surficial Geology Of The Fargo-Moorhead Area. Minnesota Geological Survey and North Dakota Geological Survey Draft Map.

Midwest Regional Climate Center Cli-MATE Database. http://mrcc.isws.illinois.edu/CLIMATE/. Accessed 1 Jan 2017

Miller R (1982) Appraisal Of The Pelican River Sand-Plain Aquifer , Western Minnesota. USGS

Open-File Report 82-347, St. Paul, Minnesota.

Miller RT (1981) Hydrologic Data For The Pelican River Sand-Plain Aquifer, Western Minnesota. USGS Open File Report 80-695, St. Paul, Minnesota.

Minnesota Department of Natural Resources (2017) MN DNR LakeFinder. http://www.dnr.state.mn.us/lakefind/index.html. Accessed 1 Jan 2017

Minnesota Pollution Control Agency (2017) Minnesota's Impaired Waters List. In: Minnesota Pollut. Control website. https://www.pca.state.mn.us/water/minnesotas-impaired-waters-list. Accessed 10 Mar 2017

MN DNR (2016) Methods for Estimating Water-Table Elevation and Depth to Water Table. St. Paul

Moore GK (1982) Ground-Water Applications of Remote Sensing. USGS Open File Report 82-240, Sioux Falls, SD

NASA Jet Propulsion Laboratory (2004) ASTER Instrument Subsystems. In: ASTER. https://asterweb.jpl.nasa.gov/instrument.asp. Accessed 10 Mar 2017

NASA (2017) ASTER. In: Terra EOS Flagsh. https://terra.nasa.gov/about/terra-instruments/aster. Accessed 10 Mar 2017

Pfannkuch HO, Winter TC (1984) Effect of anisotropy and groundwater system geometry on seepage through lakesbeds. 1. Analog and dimensional analysis. J Hydrol 75:213–237.

Pix4D SA (2017) Pix4Dmapper. Version 4.0, https://pix4d.com/product/pix4dmapper-photogrammetry-software/. Cited 4 December 2017.

PRWD (2005) Pelican River Watershed District Revised Management Plan 2005 http://prwd.org/about-prwd/revised-mgt-plan/

Rundquist D, Murray G, Queen L (1985) Airborne thermal mapping of a “flow-through” lake in the Nebraska Sandhills. JAWRA J Am Water Resour Assoc 21:989–994. doi: 10.1111/j.1752-1688.1985.tb00193.x

Stoertz MW, Bradbury KR (1989) Mapping recharge areas using a groundwater-flow model - a case-study. Ground Water 27:220–228.

Tamborski JJ, Rogers AD, Bokuniewicz HJ, et al (2015) Identification and quantification of diffuse fresh submarine groundwater discharge via airborne thermal infrared remote sensing. Remote Sens Environ 171:202–217. doi: 10.1016/j.rse.2015.10.010

Tcherepanov EN, Zlotnik V a., Henebry GM (2005) Using Landsat thermal imagery and GIS for identification of groundwater discharge into shallow groundwater-dominated lakes. Int J Remote Sens 26:3649–3661. doi: 10.1080/01431160500177315

Waters P, Greenbaum D, Smart P, Osmaston H (1990) Applications of remote sensing to groundwater hydrology. Remote Sens Rev 4:223–264.

Winter TC (1999) Relation of streams, lakes, and wetlands to groundwater flow systems. Hydrogeol J 7:28–45. doi: 10.1007/s100400050178

Winter TC, Harvey JW, Franke OL, Alley WM (1998) Ground water and surface water – a single resource. US Geol Surv Circular 1139

Winter TC, Pfannkuch HO (1984) Effect of anisotropy and groundwater system geometry on

seepage through lakebeds. 2. Numerical simulation analysis. J Hydrol 75:239–253.

Yale University (2016) ASTER. In: Cent. Earth Obs. http://yceo.yale.edu/how-convert-aster-tir-brightness-temperature-degrees-kelvin. Accessed 1 Jan 2016